

REPORT DOCUMENTATION PAGE		Form Approved OMB No. 0704-0188
<p>Public reporting burden for this collection of information is estimated to average 1 hour per response, including the time for reviewing instructions, searching existing data sources, gathering and maintaining the data needed, and completing and reviewing the collection of information. Send comments regarding this burden estimate or any other aspect of this collection of information, including suggestions for reducing the burden, to Department of Defense, Washington Headquarters Services, Directorate for Information Operations and Reports (0704-0188), 1215 Jefferson Davis Highway, Suite 1204, Arlington, VA 22202-4302. Respondents should be aware that notwithstanding any other provision of law, no person shall be subject to any penalty for failing to comply with a collection of information if it does not display a currently valid OMB control number.</p> <p>PLEASE DO NOT RETURN YOUR FORM TO THE ABOVE ADDRESS.</p>		
1. REPORT DATE (DD-MM-YYYY) 05-10-2010	2. REPORT TYPE Final Report	3. DATES COVERED (From – To) 01-Sep-07 - 01-Sep-10
4. TITLE AND SUBTITLE Investigation of the surface filamentary discharge in focus of microwave radiation	5a. CONTRACT NUMBER ISTC Registration No: 3784	
	5b. GRANT NUMBER	
	5c. PROGRAM ELEMENT NUMBER	
6. AUTHOR(S) Dr. Kirill Victorovich Khodataev	5d. PROJECT NUMBER	
	5d. TASK NUMBER	
	5e. WORK UNIT NUMBER	
7. PERFORMING ORGANIZATION NAME(S) AND ADDRESS(ES) Federal State Unitary Firm 'MRTI' of RAS Warshavskoe shosse 132 Moscow 117519 Russia		8. PERFORMING ORGANIZATION REPORT NUMBER N/A
9. SPONSORING/MONITORING AGENCY NAME(S) AND ADDRESS(ES) EOARD Unit 4515 BOX 14 APO AE 09421	10. SPONSOR/MONITOR'S ACRONYM(S)	
	11. SPONSOR/MONITOR'S REPORT NUMBER(S) ISTC 07-7011	
12. DISTRIBUTION/AVAILABILITY STATEMENT Approved for public release; distribution is unlimited. (approval given by local Public Affairs Office)		
13. SUPPLEMENTARY NOTES		
14. ABSTRACT <p>This report results from a contract tasking Federal State Unitary Firm 'MRTI' of RAS as follows: Experimental investigations of gaseous electrical discharges in quasi-optical beams of electromagnetic (EM) radiation in microwave (MW) wavelength range showed that they are being realized in a streamer form at some definite range of gas parameters and radiation. Such discharge effectively absorbs radiation energy. It opens wide possibility for their applications.</p> <p>In frames of the Project #2820 we studied initiated MW discharge in EM beam focus in air both free localized electrodeless one and attached to initiator (EM vibrator). During these investigations we varied air pressure, amplitude of electric component of linearly polarized field exciting the discharge, radiation pulse duration, etc. Namely this wide set of experimental conditions has allowed to reveal typical discharge forms, realization areas of these discharge forms, spatial discharge structure formation velocity, maximum gas temperature T of discharge plasma in streamer channels, absorbing ability etc.</p> <p>In frames of the Project #2820 we have carried out also initial investigations of a MW discharge on surface of a dielectric plate located in linearly polarized quasi-optical beam. They have shown that undercritical MW discharge with developed streamer structure can be realized in this case. Experiments were undertaken in the case of transversal location of the dielectric plate (perpendicularly to wave vector of radiation) and in the case of longitudinal location (parallel to wave vector and electric field).</p> <p>Our experiments have shown that such discharge on the dielectric surface in both cases keeps its streamer type at a pressure higher than some definite value both in dead air and in its high-speed flow. This surface MW discharge feature opens wide possibility of its practical application even in comparison with MW streamer volumetric discharges, for example, for creation of controlling forces, combustion ignition and stabilization in systems of external combustion, etc. In its turn this stimulates works on fundamental investigations of its features.</p> <p>Surface MW discharge in quasi-optical beam features investigation by traditional methods is complicated. So investigations will be carried out by the way of wide variation of this discharge realization conditions. At that we will use equipment and experience collected at fulfillment of works on the #2820</p>		
15. SUBJECT TERMS EOARD, Physics, Plasma Physics and Magnetohydrodynamics		

16. SECURITY CLASSIFICATION OF:			17. LIMITATION OF ABSTRACT UL	18, NUMBER OF PAGES 99	19a. NAME OF RESPONSIBLE PERSON Stephanie Masoni, Maj, USAF
a. REPORT UNCLAS	b. ABSTRACT UNCLAS	c. THIS PAGE UNCLAS			19b. TELEPHONE NUMBER <i>(Include area code)</i> +44 (0)1895 616420

**Project ISTC # 3784p
(077011)**

**Investigation of the surface filamentary discharge in focus of
microwave radiation**


**Final Technical Report
on the work performed from September 01, 2007 to August 31, 2010**

**Federal State Unitary Enterprise “Moscow Radiotechnical Institute of the
Russian Academy of Sciences”**

Warshavskoe shosse 132, 117519, Moscow, Russia

**Project Manager Kirill V.Khodataev
Dr. Sci, professor**

**Director Boris A. Makarov
Ph.D.**




August 2010

This work is supported financially by European Office of Aerospace Research and
Development (EOARD) and performed under the contract to the International Science and
Technology Center (ISTC), Moscow

Title of the Project: Investigation of the surface filamentary discharge in focus of microwave radiation

Commencement Date: September 01, 2007

Duration: 36 months

Project manager: Khodataev Kirill Victorovich

Phone number: +7 495 315-24-97

Fax.number: +7 495 314-1053

E-mail address: K.V.K@home.ptt.ru

Leading Institute: Federal State Unitary Enterprise "Moscow Radiotechnical Institute of the Russian Academy of Sciences"
Warshavskoe shosse 132, 117519, Moscow, Russia
+7 495 314-31-11, mrti@mrtiran.ru

Participating Institutes: no

Foreign collaborators: no

Key words:

Microwave, diffuse, streamer, electrical discharge, surface discharge, high-speed flow, aerosol, humidity, two-phase medium, propane-air mixture.

Contents

1. Brief description of the work plan: objective, expected results, technical approach	5
1.1. Project goals.....	5
1.2. Expected results	5
1.3. Technical approach	6
2. Method, Experiments, Theory etc.	6
Chapter 1. Experimental basis	6
1.1. An installation with $\lambda = 8.9\text{cm}$	6
1.2. Set up with $\lambda = 2.5\text{cm}$	9
Chapter 2. Determination of air electric breakdown minimum field at presence of a dielectric plate with various dielectric properties and thickness in EM quasi-optical beam at a perpendicular and longitudinal location at wavelengths 8.9cm and 2.5cm (Tasks 1- 4)	11
2.1. Experiments at the wavelength 8.9cm.....	11
2.2. Experiments at the wavelength of 2.5cm	14
Chapter 3. Research of influence of a dielectric surface on subcritical and deeply subcritical surface transversal and longitudinal MW discharge initiation possibility by means of EM vibrators at wavelengths of 8.9cm and 2.5cm (Tasks 5-8).....	16
3.1. Experiments at the wavelength of 8.9 cm	16
3.2. Experiments at the wavelength 2.5 cm.....	21
Chapter 4. Determination of boundary transition pressure of transition of MW discharge diffuse form in air into a streamer one at perpendicular and longitudinal locations of a dielectric plate in EM beam at wavelengths of 8.9cm and 2.5cm (Tasks 9 and 10).....	26
4.1. Experiments at the wavelength of 8.9cm	26
4.2. Experiments at the wavelength 2.5cm.....	27
Chapter 5. Determination of boundary field separating a subcritical surface MW discharge with developed streamer structure from deeply subcritical surface MW discharge with streamer channels attached to an initiator (Tasks 12-15)	28
5.1. Transversal discharge	28
a) Transversal discharge in the installation with the wavelength of 8.9cm	28
b) The transversal discharge in the installation with a wavelength of 2.5cm	29
5.2. Longitudinal discharge	33
a) Longitudinal discharge in the installation with the wavelength of 8.9cm	33
b) Longitudinal discharge in the installation with the wavelength of 2.5cm	36
Chapter 6. Ability of the streamer subcritical and deeply subcritical MW discharge to remain a surface one with respect to angular position of a plate concerning Pointing vector of EM field (Task 16).....	38
6.1. Experiments at the radiation wavelength 8.9 cm	38
6.2. Experiments at the wavelength of 2.5 cm	42
Chapter 7. Determination of streamer channels growth rate when they form a developed structure of subcritical surface MW discharge, and speed of discharge front propagation over a surface of a dielectric in EM wave (Tasks 17 - 20)	44
7.1. Experiments with the wavelength of 8.9cm	44
7.2. Experiments with the wavelength of 2.5cm	46
Chapter 8. Influence of the form of a dielectric surface on propagation characteristics of surface subcritical SW discharge with developed streamer structure (Tasks 21 и 22).....	49
8.1. Experiments at the wavelength 8.9cm.....	49
8.2. Experiments at the wavelength of 2.5cm	50
a) Experiment with “transversal” placing of a tube	50
b) Experiment with the longitudinal placing of a tube.....	51

Chapter 9. Experimental investigation of the surface streamer MW discharge features in different conditions (Tasks 24 - 30)	52
9.1. Experimental estimation of air temperature T in streamer plasma channels of transversal and longitudinal subcritical and deeply subcritical surface MW discharge in EM beam with $\lambda = 8.9\text{cm}$ by means of discharge ignition in a flammable propane-air mixture. ..	52
9.2. Studying of the transversal and longitudinal surface discharge properties in EM beam with $\lambda = 8.9\text{cm}$ at discharge ignition in humid air	55
9.3. Studying of transversal and longitudinal surface discharge properties in EM beam with $\lambda = 8.9\text{cm}$ at discharge ignition in air containing water aerosol	57
9.4. Studying of subcritical and deeply subcritical surface discharge properties in EM beam with $\lambda = 2.5\text{cm}$ at discharge ignition in a high-speed air flow containing water aerosol	60
a) Transversal discharge	63
b) Longitudinal discharge	65
9.5. Studying of subcritical and deeply subcritical surface discharge properties in EM beam with $\lambda = 2.5\text{cm}$ flow of propane-air flammable mixture at their different percentage	66
9.6. Influence of dielectric material and thickness properties on surface streamer discharge.	68
Chapter 10. Experimental estimation of absorbing ability of the transversal and longitudinal subcritical and deeply subcritical surface discharges in MW radiation beam (Task 31)	69
10.1. Absorbed energy measuring method	69
10.2. Results of observations and their processing	71
Chapter 11. Theoretical support of experiments and creation of theoretical models of surface MW discharge in quasi-optical EM beam in various conditions (Tasks 11, 23, 32)	74
11.1. Theoretical support of experiments	74
11.2. Construction of theoretical model of a breakdown in the presence of a dielectric layer	75
11.3. Critical breakdown field in MW field calculations at middle and high gas pressures	76
11.4. Calculations of the streamer discharge propagation velocity	81
11.5. Determination of electrostatic effects influence on behavior of the surface MW discharge	86
11.5a. Influence of the induced surface charge on a streamer propagation at MW wave falling on a dielectric surface	86
11.5b. Influence of the induced surface charge on a streamer propagation over a surface of radiating dielectric antenna	93
Results	96
Conclusions	97
References	97
Comments	99
Attachments	99

1. Brief description of the work plan: objective, expected results, technical approach

1.1. Project goals

Experimental researches of gaseous pulse electric discharges in quasi-optical beams of electromagnetic (EM) radiation of microwave (MW) wavelengths range have shown, that in a certain range of gas pressure p and EM field value they are realized in a streamer form. Such a discharge effectively absorbs energy of MW radiation. This feature of MW discharges opens ample opportunities for their practical application.

Within the limits of the project #2820 the free localized electrodeless and EM vibrator initiated MW discharge in air in a focus of EM beam was studied. In the course of carrying out of these researches pressure of air, amplitude of electric component of linearly polarized EM field exciting the discharge, duration of EM of radiation etc. were varied. Namely such wide set of experimental conditions has allowed to reveal characteristic types of the EM discharge, areas of realization of these discharge types realization, speeds of the discharge spatial structure formation, the maximum gas temperature T of the streamer channels of the discharge plasma, absorbing ability, etc.

Within the limits of the Project #2820p initial researches of the MW discharge on a surface of the dielectric plate placed in the linearly polarized quasi-optical EM beam (the Task XI) are executed. They have shown, that in this case can be realized the subcritical streamer MW discharge with surface developed structure. Experiments were carried out with a transversal location of a dielectric plate (perpendicularly to the wave vector of MW radiation) and with the longitudinal one (in parallel to the wave vector and the electric field) one.

Experiments have shown, that in both cases the MW discharge on the dielectric surface at pressure above some value keeps its streamer character, both in motionless air, and in a high-speed stream of air. This feature of the surface MW discharge opens ample opportunities for its practical application even in comparison with MW streamer volumetric discharges, for example, for creation of operating forces, ignition of a mixture and stabilization of its burning in systems of external burning etc. In turn, it stimulates works on basic researches of its features.

Research of properties of the surface MW discharge in the quasi-optical EM beam is complicated using traditional methods, also as researches of discharges with volumetric structure. Therefore in the proposed works they can be carried out by a wide variation of realization conditions of this discharge, using an experience and the equipment applied at performance of works under the Project #2820.

1.2. Expected results

The project concerns basic researches.

Within the limits of the given proposal following works will be performed and following results will be obtained:

- Experimentally to determine an influence of the dielectric plate presence in electromagnetic (EM) field on a level of the boundary breakdown field depending on air pressure and on EM vibrator ability (when it placed on it) to initiate subcritical and deeply subcritical surface MW streamer discharge.
- Experimentally to study mutual EM influence of several EM vibrators (initiating the discharge) located on a dielectric surface.
- Experimentally to determine the boundaries separating various forms of the surface subcritical initiated MW discharge.

- Experimentally to determine average growth velocity of the streamer channels forming surface developed structure of the subcritical discharge and a speed of its front propagation on a dielectric surface.
- Experimentally to estimate the plasma channels temperature of subcritical and deeply subcritical MW discharges by means of their ignition in a stream of propane-air mixture.
- Experimentally to estimate an influence of air humidity of various levels and presence of water aerosol in air on characteristics of subcritical and deeply subcritical MW discharge.
- Experimentally to determine an influence of orientation, geometry and parameters of a dielectric layer on which the discharge is lighted on all listed above characteristics of the surface MW discharge.
- Experiments will be accompanied by theoretical researches. Their results will allow to construct adequate theoretical models of surface MW discharge in quasi-optical EM beam at various physical statements.

1.3. Technical approach

The basic experiments were carried out with a help of existing in MRTI installations with pulse generators of powerful MW radiation at wavelengths of 8.9cm and 2.5cm. At carrying out of definite experiments the installations were modernized and supplemented with necessary elements. They will be in detail described in corresponding sections of the present Report.

2. Method, Experiments, Theory etc.

Chapter 1. Experimental basis

Experiments were carried out with a help of two experimental installations identical under the basic scheme, but differing by the wavelength of MW radiation.

The detailed description of installations is represented in the annual report for the 1st year of performance of the project performance¹.

Parameters of the installations are represented in **Table 1.1**.

Table 1.1

Wavelength, cm	2.5	8.9
Radiation pike power, kW	100-150	1000-2000
Pulse duration, μ s	35	43
Maximal field in the focus, kV/cm	5	5.5-6

1.1. An installation with $\lambda = 8.9$ cm

Experiments with $\lambda = 8.9$ cm were carried out in the installation with the parameters: power of the generator in a pulse $P_{\text{gen}} \leq 2\text{MW}$, duration of the pulse $\tau = 43\mu\text{s}$, an operating mode - single pulses.

The installation general view is shown in a **Fig.1.1**.



Fig.1.1. General view of the installation with wavelength $\lambda = 8.9\text{cm}$

The MW generator through a waveguide feeds an antenna horn. The radio transparent lens forms a radiation with a flat phase front. The spherical metal mirror creates a focus of a MW beam.

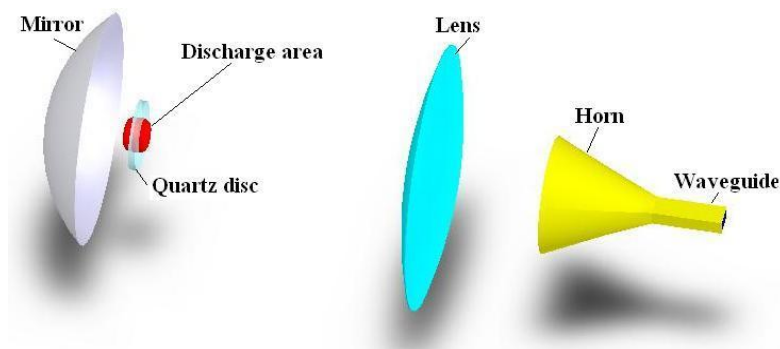


Fig.1.2. Elements of the electrodynamic system

A distribution of an electromagnetic field in a working zone was calculated with a help of program (code) CST MW STUDIO.

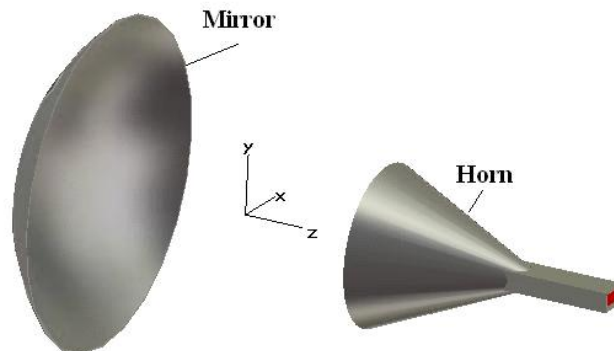


Fig.1.2. Model of MW system in the set up with $\lambda = 8.9\text{cm}$ accepted to MW field distribution calculation

Calculated distribution of the electric field amplitude for the model of MW system shown in Fig.1.2, represented in Fig.1.3.

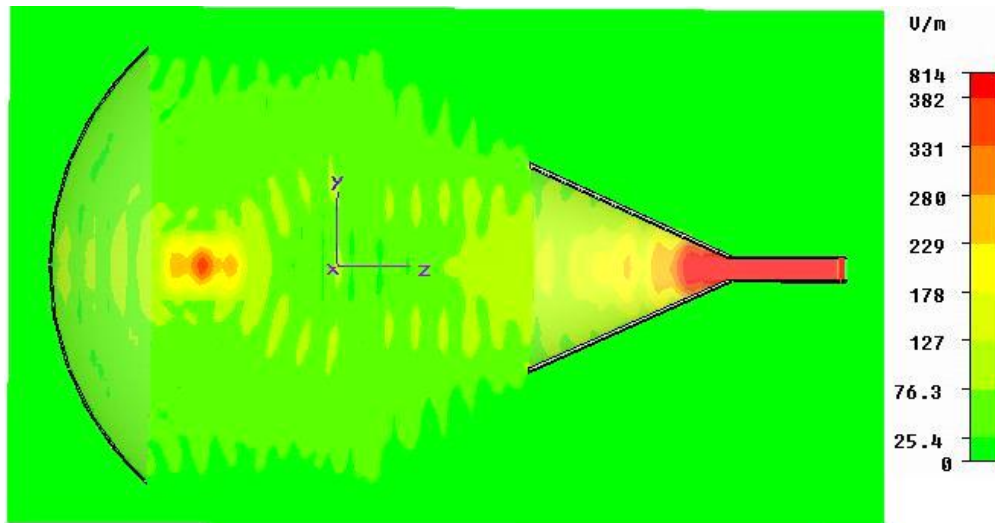


Fig.1.3. Electric field amplitude distribution at the set up with $\lambda=8.9\text{cm}$ at absence of a dielectric plate

Field level in the radiation focus depends on an attenuator position, included in feeding wave guide. In Fig.1.4 waveforms of electric field amplitude in the center of focus for four positions of the attenuator are shown, (a - the attenuator is opened, b - the attenuator is closed for 10mm, c - the attenuator is closed on 20mm, d - the attenuator is closed completely).

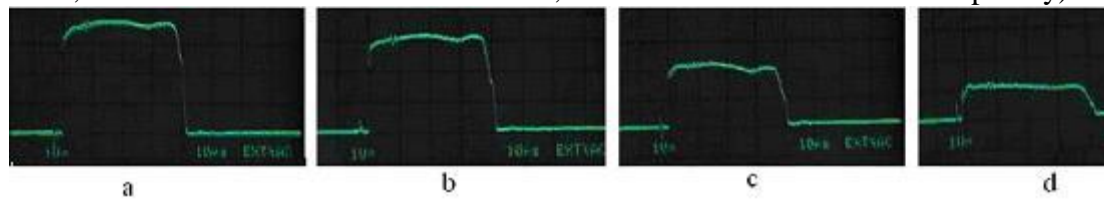


Fig.1.4. Field amplitude waveforms

In the installation with the wavelength $\lambda = 8.9\text{cm}$ calibration of electric field amplitude values in focus of radiation depending on the attenuator positions in the waveguide path is represented. Waveforms in a Fig.1.4 correspond to values of the electric field amplitude 4.7kV/cm, 3.7kV/cm, 2.3kV/cm, 1.2kV/cm.

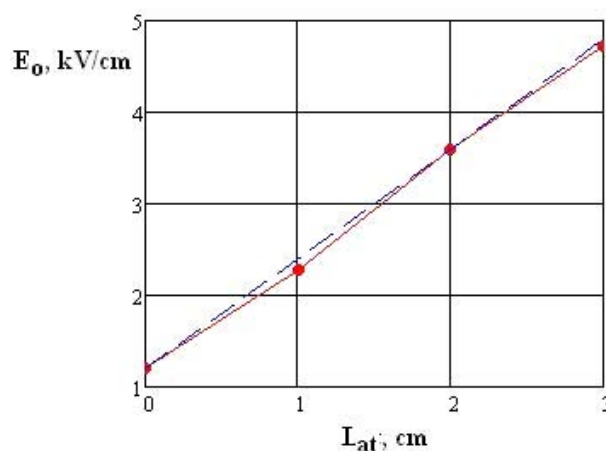


Fig.1.5. Dependence of electric field amplitude in focus of radiation via scale indications of the attenuator. Points - the measured values, a dotted line - the formula (1.1).

Calibration was made by determination of air breakdown pressure values both for absence of the initiator, and in the presence of a metal sphere of 0.5cm in diameter². Results of calibration are represented in **Fig.1.5**. The obtained dependence with satisfactory accuracy is approximated by the formula

$$E_{MW} = 1.2 \cdot 1 + L_{at} , \text{ kV/cm} \quad (1.1)$$

where E_{MW} is electric field amplitude in the focus, kV/cm, L_{at} readings of the attenuator scale, cm.

1.2. Set up with $\lambda = 2.5\text{cm}$

Experiments were carried out in the set up which scheme is represented in **Fig.1.6**.

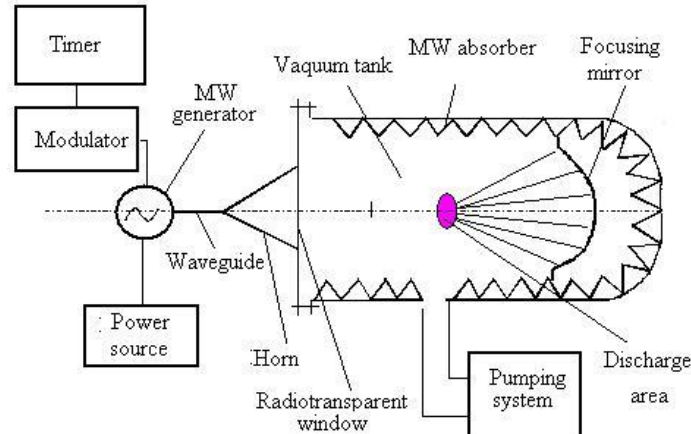


Fig. 1.6. A scheme of the set up on MW discharge investigation at $\lambda = 2.5\text{cm}$

General view of the set up is shown in **Fig.1.7**. One can see a vacuum chamber, a generator with a modulator and control post.



Fig.1.7. A general view of the set up on investigation of MW discharge at $\lambda = 2.5\text{cm}$

Experiments were carried out at the following parameters of the set up:
 outlet pulse power $P_{pul} = 100\text{kW}$.
 working mode – single pulses,
 pulse duration $\tau_{pul} = 30\mu\text{s}$.

A typical waveform of the MW pulse from the MW detector located in the outlet waveguide directly in front of the horn is represented in **Fig.1.8**.

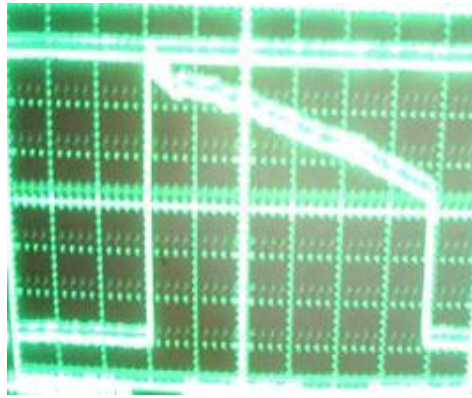


Fig.1.8. Typical MW pulse envelope waveform from the detector located in the outlet waveguide directly in front of the horn.

The rectangular waveguide of a cross section 8x17mm is connected with a generator exit. On its end is located the conjugation section to a round waveguide 20mm in diameter and a conic horn with an opening angle of 32° and the outlet diameter of 86mm. From an exit of the horn EM the EM wave is radiated into free space in a form of linearly, vertically polarized TEM wave. The horn is hermetically fixed over the centre of a motionless vertical flange. The horn opening is sealed with a help of flat radiotransparent plate. A waveguide system is filled with sulfur hexafluoride for prevention of undesirable electric breakdowns in it.

To the motionless flange with the radiating horn fixed to it the cylindrical vacuum chamber 37.5cm in diameter and 47.5cm length can be tightly connected. The chamber on the corresponding device of moving can be removed from the flange, releasing an access to the installation elements fixed to it. The internal surface of the chamber is covered by the radio absorbing material providing it «echo absence» in the MW range of λ . For visual registration of discharge processes the chamber has a horizontal window at the distance of 21.5cm from the chamber flange on the lateral surface at the level of the chamber axis. The window is executed in the form of a pipe with internal diameter of 60mm. At its free end face two optically transparent quartz glasses are tightly fixed, the cavity between which is filled with the distilled water.

The glow voltage of the MW generator was varied for change of the field amplitude. The field value was determined by the following method.

Into chosen point of the EM beam over its axis the metal ball of $2a = 0.2\text{cm}$ in diameter was located. The ball was fastened to the dielectric thread passed through a hole in it and tensed horizontally, perpendicularly to a direction of the beam propagation. The EM pulse with $\tau_{\text{pul}} = 30\mu\text{s}$ was radiated in the chamber. During the same time the ball surface was illuminated by ultra-violet radiation from the pulse source placed outside the EM beam. This radiation ensured presence of photo emission electrons near a surface of the ball. In various impulses Air pressure in the chamber was varied in various pulses and the maximum value at which the breakdown was still initiated was determined. Results of the field measurement are represented in **Table 1.2**.

Table 1.2

U_{glow} (V)	P_{max} (Torr)	E_{cr} (kV/cm)
115	72	1,7
130	156	3,2

Chapter 2. Determination of air electric breakdown minimum field at presence of a dielectric plate with various dielectric properties and thickness in EM quasi-optical beam at a perpendicular and longitudinal location at wavelengths 8.9cm and 2.5cm (Tasks 1- 4)

2.1. Experiments at the wavelength 8.9cm

Experiments with $\lambda = 8.9\text{cm}$ were carried out with a help of the set up with the following parameters:

Generator power in the pulse $P_{\text{gen}} \leq 1\text{MW}$.

Pulse duration $\tau = 43\mu\text{s}$.

Working mode - single pulses.

Amplitude of the electric field in the radiation focus had discrete values 4.8kV/cm, 3.9kV/cm, 2.3kV/cm, 1.2kV/cm. A scheme of radiation focus formation in the set up with $\lambda = 8.9\text{cm}$ is represented in **Fig.2.1**.

Dielectric plates are located in the radiation focus where the field is maximal. As dielectric plates we used a usual foil of polyethylene and a plate of quartz with a diameter of 20cm and thickness of 1cm. If necessary, metal half-wave thin vibrator was settled down on a surface of the plate turned to a mirror.

Models of MW system in the installation with $\lambda = 8.9\text{cm}$ at transversal and longitudinal placing of a dielectric layer (a quartz disk), used in calculation of an electromagnetic field distributions, are shown in **Fig.2.2**. Distributions of the electric field amplitude corresponding to them, calculated by means of the program MW SUITE, are shown in **Fig.2.3a** and **Fig.2.3b**.

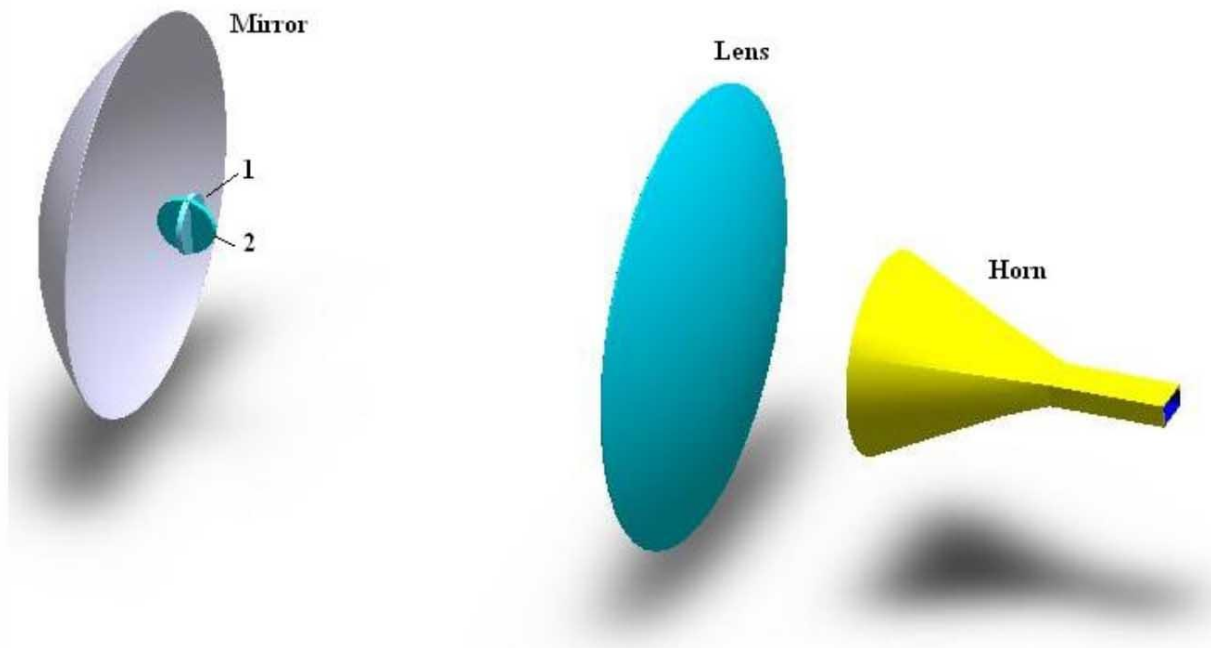


Fig.2.1. A scheme of the radiation focus formation in the installation with $\lambda = 8.9\text{cm}$ and variants of placing of dielectric samples placing: 1 - transversal placing, 2 - longitudinal placing

Measurements of the breakdown pressure values in the presence of a dielectric film or a quartz disk with a thickness of 1.0cm and 2.0cm, located in the radiation focus in the transversal plane are carried out.

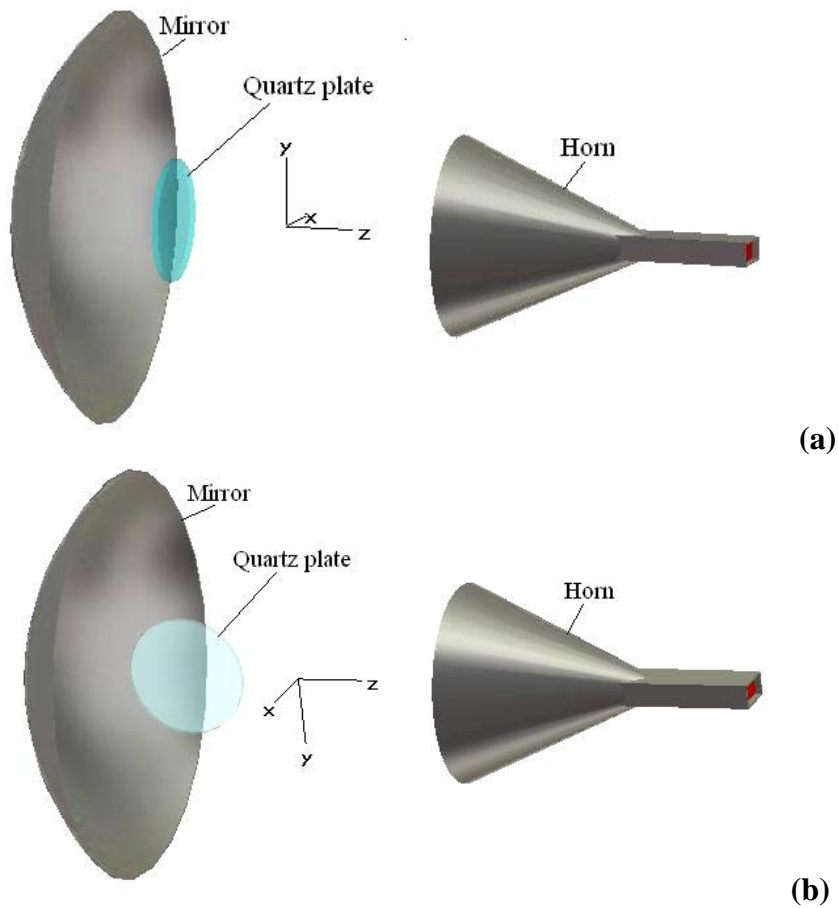


Fig.2.2. MW system in the installation with $\lambda = 8.9\text{cm}$ model at the transversal (a) and longitudinal (b) placing of the quartz disc accepted for the calculation of MW field distribution

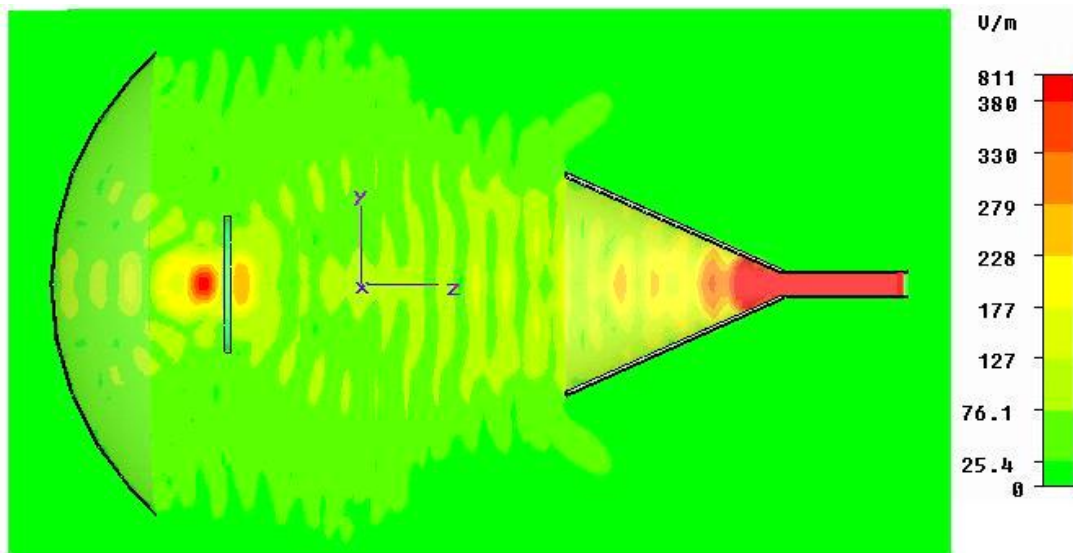


Fig.2.3a. Electric field amplitude distribution in the installation with $\lambda=8.9\text{cm}$ at presence of the quartz plate at its transversal placing

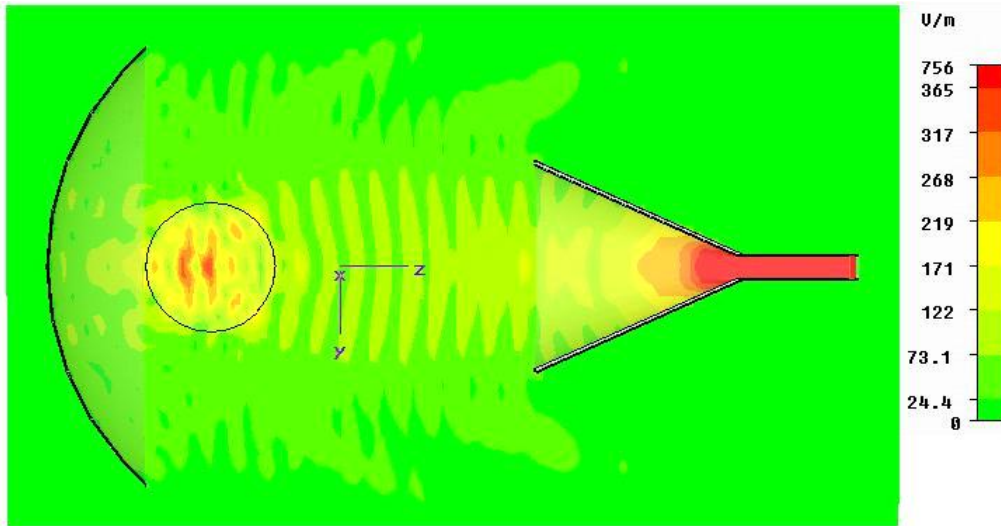


Fig.2.3b. Electric field amplitude distribution in the installation with $\lambda=8.9\text{cm}$ at presence of the quartz plate at its longitudinal placing

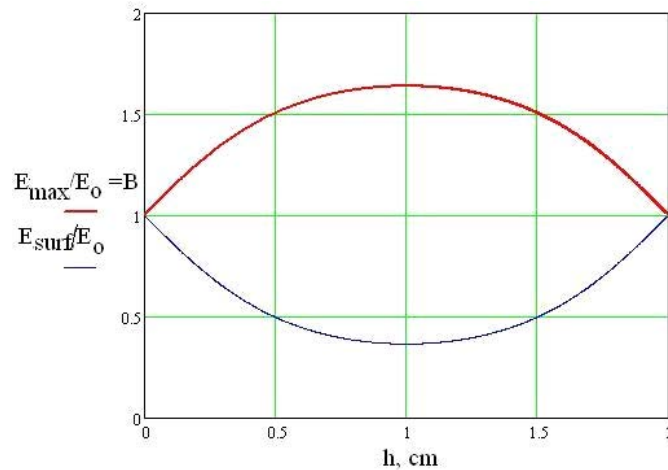


Fig.2.4. Relative amplitude on a plate surface ($\epsilon=4$) and maximal in the volume with respect to the plate thickness h

Measurements have shown that the dielectric plate without the initiator influences a breakdown threshold so far as its presence changes a maximum value of the electric field amplitude in the field of the beam propagation. The plate with the finite thickness h and dielectric permeability ϵ reflects a radiation part so the amplitude of the electric field component on a surface decreases, being equal to

$$|E_{surf}| = |E_0| - |E_1| \quad (2.1)$$

and the field at the distance of $\lambda/4$ from the plate rises

$$|E_{max}| = |E_0| + |E_1|, \quad (2.2)$$

where the second term in expressions depends on the plate thickness

$$E_1 h = E_0 \frac{\frac{1-\sqrt{\epsilon}}{1+\sqrt{\epsilon}} + \frac{\sqrt{\epsilon}-1}{\sqrt{\epsilon}+1} \exp -i2\sqrt{\epsilon}kh}{1 + \frac{1-\sqrt{\epsilon}}{1+\sqrt{\epsilon}} \frac{\sqrt{\epsilon}-1}{\sqrt{\epsilon}+1} \exp -i2\sqrt{\epsilon}kh}, \quad k = \frac{2\pi}{\lambda} \quad (2.3)$$

A dependence of relative amplitude on the plate surface with the permeability of $\epsilon=4$

$$B h = \frac{E_{surf}}{E_0} \quad (2.4)$$

via the plate thickness h at normal fall of the wave with $\lambda=8.9\text{cm}$ is shown in **Fig.2.4**.

Correspondingly the threshold breakdown field rises by 8 times.

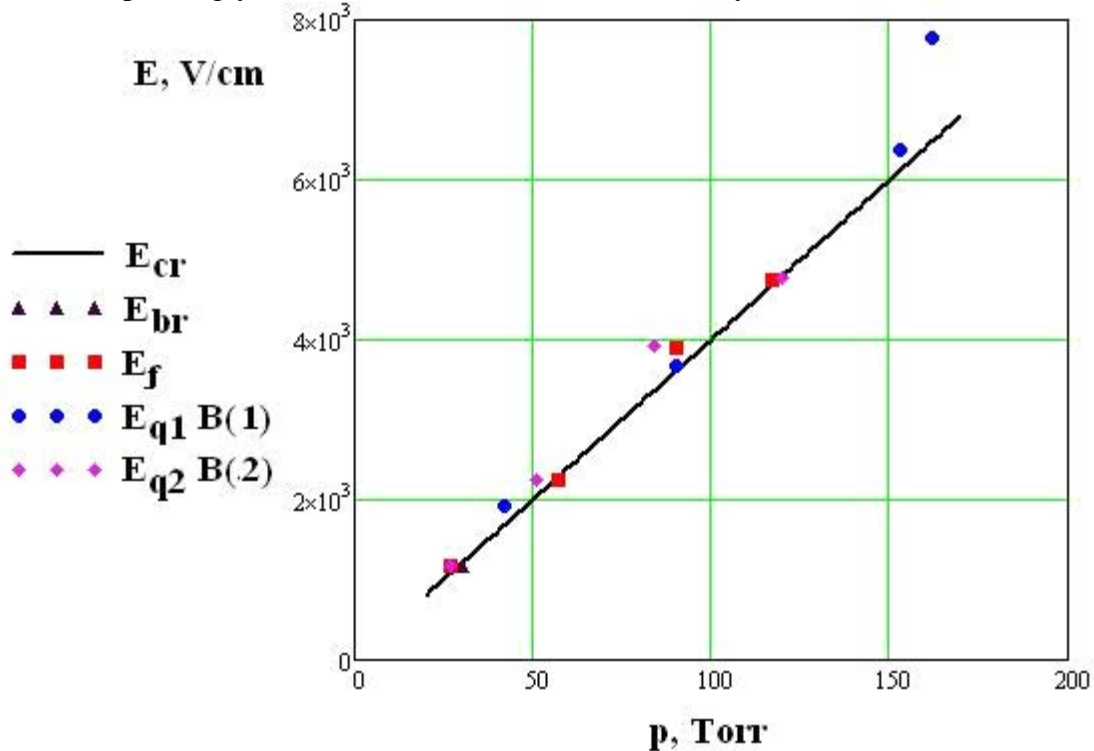


Fig.2.5. Electric field amplitude at the breakdown with respect to air pressure

Results of breakdown field amplitudes measurement are presented in Fig.2.5.

Measurements confidently show, that the surface itself surface does not influence the breakdown processes. The measured values of breakdown amplitude of the electric field coincide with the critical values for free space.

So, it is found that the dielectric plate influences a breakdown threshold since its presence changes the maximum value of the electric field amplitude in the area of MW radiation beam propagation. Change of the field amplitude is determined by the reflection coefficient from a plate. Generally the discharge has a volumetric character.

Experiments have shown, also as in the case of transversal placing, presence of a dielectric plate at the longitudinal placing influences a value of the breakdown voltage only so far as the presence of a dielectric changes an electric field distribution in comparison with the case of its absence. Accordingly, the thin dielectric film does not influence the breakdown intensity of the electric field.

2.2. Experiments at the wavelength of 2.5cm

A system of electromagnetic radiation focused beam formation is shown in Fig.2.6.

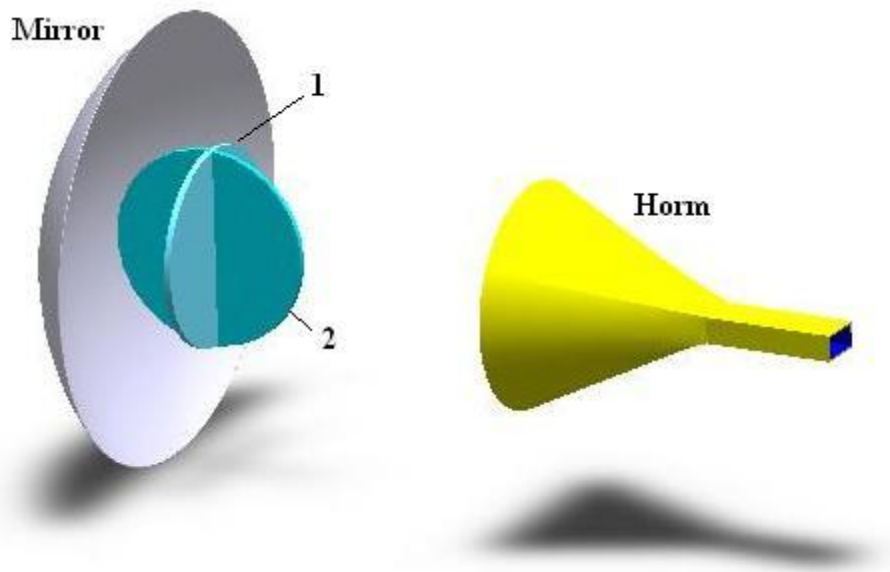


Fig.2.6. A scheme of the radiation focus formation in the installation with $\lambda = 2.5\text{cm}$ and variants of placing of dielectric samples: 1 - transversal placing, 2 - longitudinal placing (the model accepted to calculation)

On the wavelength $\lambda = 2.5\text{cm}$ in the range of air pressure the minimum field of electric air breakdown E_{cr} was experimentally determined at presence of a dielectric plate in EM quasi-optical beam with various values of the thickness parallel to vector E and perpendicular or parallel to the wave vector k (position 1 or 2 in Fig.2.6 accordingly).

Experiments at the wavelength $\lambda = 2.5\text{cm}$ have completely confirmed a conclusion that presence of a dielectric body influences a breakdown threshold only at the expense of redistribution of the electromagnetic field because of its presence. Surface presence itself does not influence a breakdown threshold value. This fact is most obviously shown in the case of the negligibly thin dielectric plate (in particular, a film) which influence on field distribution is small, and surface effects can be shown in full strength. In **Tables 2.1-2.2** the data showing with high accuracy an independence of the breakdown threshold on presence or absence of a dielectric film are represented. In them the following designations are used:

p – maximal air pressure value at which the breakdown did not appear,

U – readings of the MW pulse amplitude sensor.

In **Table 2.1** results of repeated measurements of threshold pressure in the case of absence of a dielectric film in the radiation focus, in **Table 2.2** - the same in presence of a film in the focus are represented.

Table 2.1

p, Torr	U, mV	$\langle U \rangle$, mV	$\langle p \rangle$, Torr
25,5	320	319.2	24.2
25,5	332		
24	316		
21,9	308		
24	320		

Table 2.2

p, Torr	U, mV	<U>, mV	<p>, Torr
25,5	348	332.8	24.3
24	332		
22,5	316		
24	336		
24	328		
24	332		
24	332		
24	324		
24	348		
24	332		

The gas pressure value at which the discharge in the presence of a film and without it changes within 1% that is essentially smaller the accuracy of measurements.

Chapter 3. Research of influence of a dielectric surface on subcritical and deeply subcritical surface transversal and longitudinal MW discharge initiation possibility by means of EM vibrators at wavelengths of 8.9cm and 2.5cm (Tasks 5-8)

3.1. Experiments at the wavelength of 8.9 cm

At the wavelength of $\lambda = 8.9\text{cm}$ the discharge initiated by the vibrator, located on a surface of a thin dielectric plate is experimentally obtained. At a transversal arrangement of a dielectric layer the discharge initiated by the vibrator, placed on a surface of a layer on a horn side, the streamer discharge develops exclusively on the layer surface. In **Fig.3.1** the discharge photos in a profile (**Fig.3.1 (a)** - the discharge on a film, **Fig.3.1 (b)** - the discharge on a quartz plate with a thickness of 1cm) are represented.

E=3.7 kV/cm

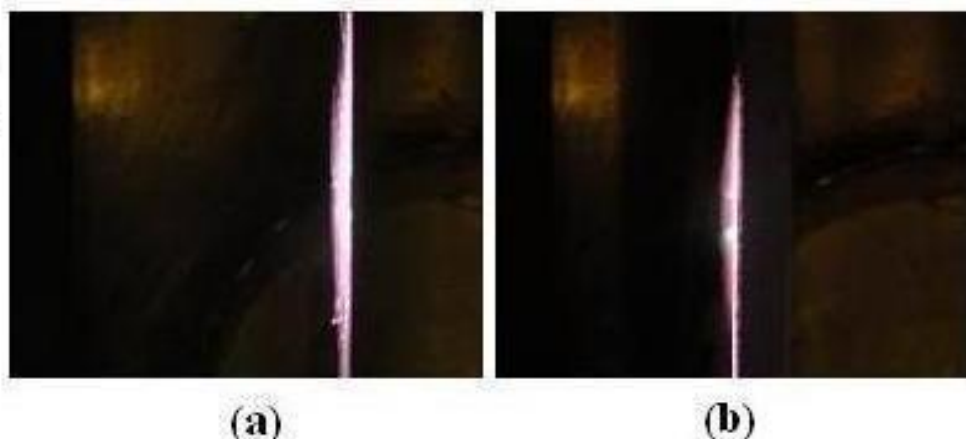


Fig.3.1. Surface discharge at the electric field amplitude of 3.7kV/cm: (a) – the film, (b) – the quartz disc of 1cm thickness

At an arrangement of the vibrator from a mirror side the streamer discharge depending on air pressure and electric field intensity can develop exclusively on a surface of a dielectric layer, or either over a surface, or in the volume. In **a Fig.3.2** photos of the initiated

"transversal" discharge are shown at the electric field strength of 3.7kV/cm and air pressure of 200Torr (above) and 150Torr (below).

In Fig.3.3 photos of the mixed discharge type, made are shown at different values of the electric field strength (for the dielectric film - (a) and the quartz disk of 1cm thickness - (b)) are shown.

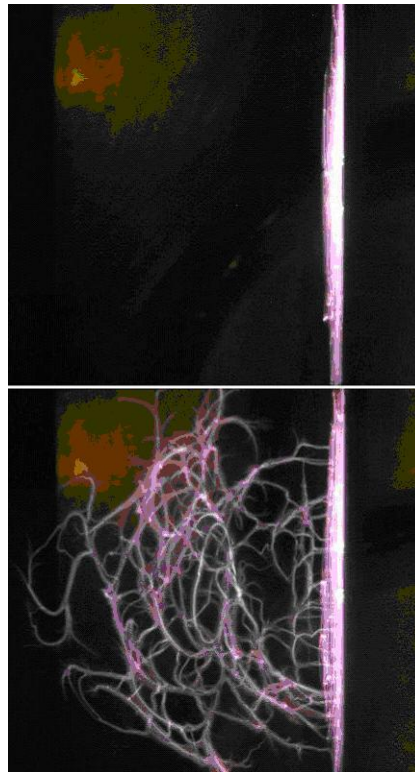


Fig.3.2. A photo of initiated "transversal" discharge on a polyethylene film at the electric field strength of 3.7kV/cm and air pressure of 200Torr (above) and 150Torr (below)

The boundary (in co-ordinates electric field - pressure) between the surface and surface-volumetric discharges (E_i – a red line in Fig.3.4) lies between a line of the critical field (E_{cr} and E_{br} - a black line in Fig.3.4) and the boundary of the attached discharge (E_s - a blue line in Fig.3.4). Purely surface discharge lies in the area between the lines E_s and E_i .

Photos in a Fig.3.3 are made at air pressure a little above the boundary E_i in Fig.3.4.

The phenomenon of the discharge separation from the surface of transversally located layer at placing of the initiator from the side of the focusing device is necessary for considering at discussion of possible variants of surface discharges use.

At initiation of the streamer discharge the initiator on a surface of a dielectric layer at its longitudinal placing the discharge always develops over a surface. The photo of the initiated "longitudinal" surface discharge on a quartz disk of 20cm in diameter and 2cm thickness is shown in Fig.3.5a. The "longitudinal" discharge on the surface of a textolite plate of 0.1cm thickness in the same conditions is shown in Fig.3.5b. The type of a dielectric material does not visibly influence the size of the discharge cells and a diameter of channels. However, the sizes of the discharge area are little wider.

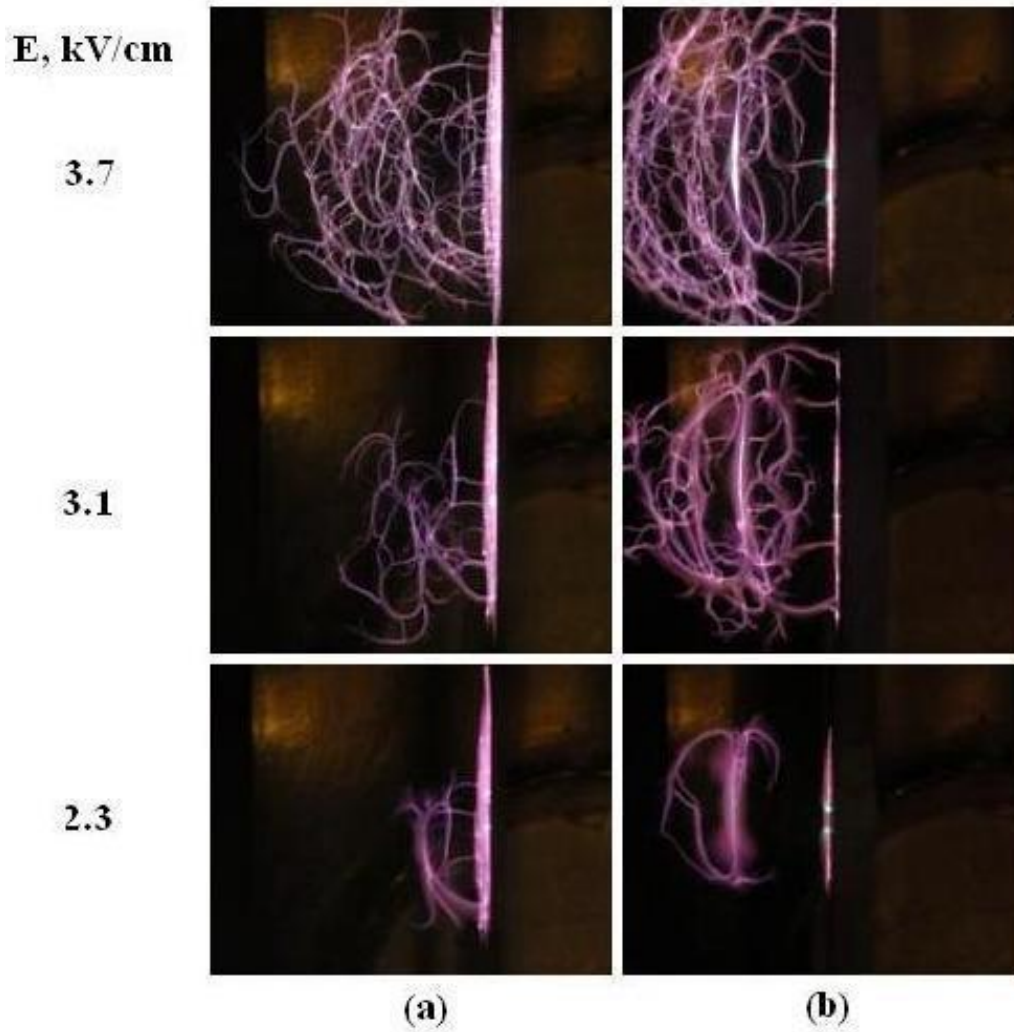


Fig.3.3. Surface-volumetric discharge at different values of the electric field strength: (a) – the film, (b) – the quartz disc of 1cm thickness

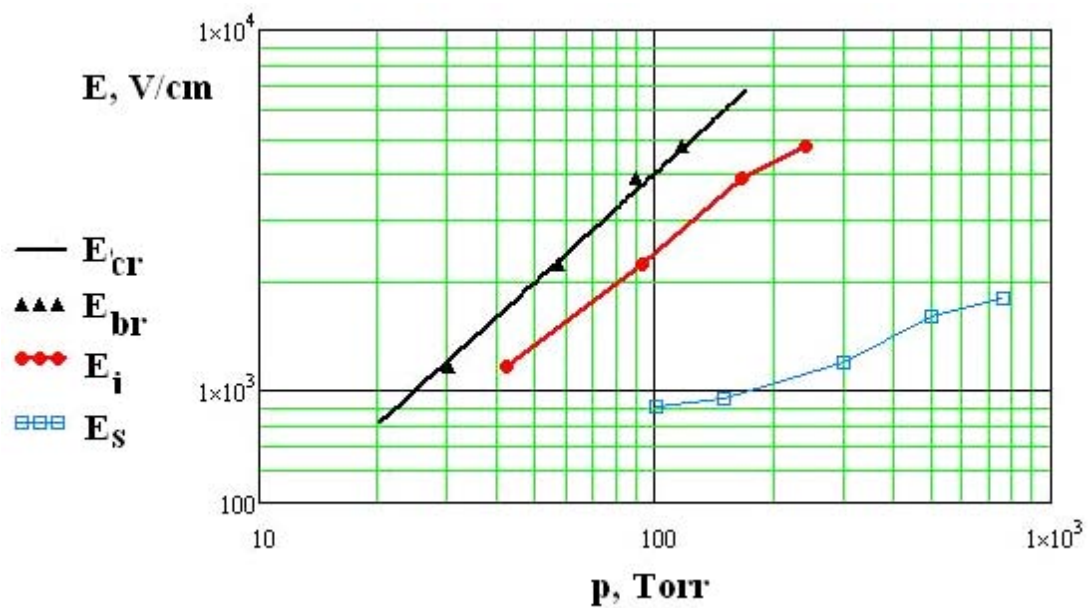


Fig.3.4. A boundary separating the surface and surface- volumetric discharges, – red line, $\lambda=8.9\text{cm}$. The initiator is located on the dielectric film from the side of the mirror

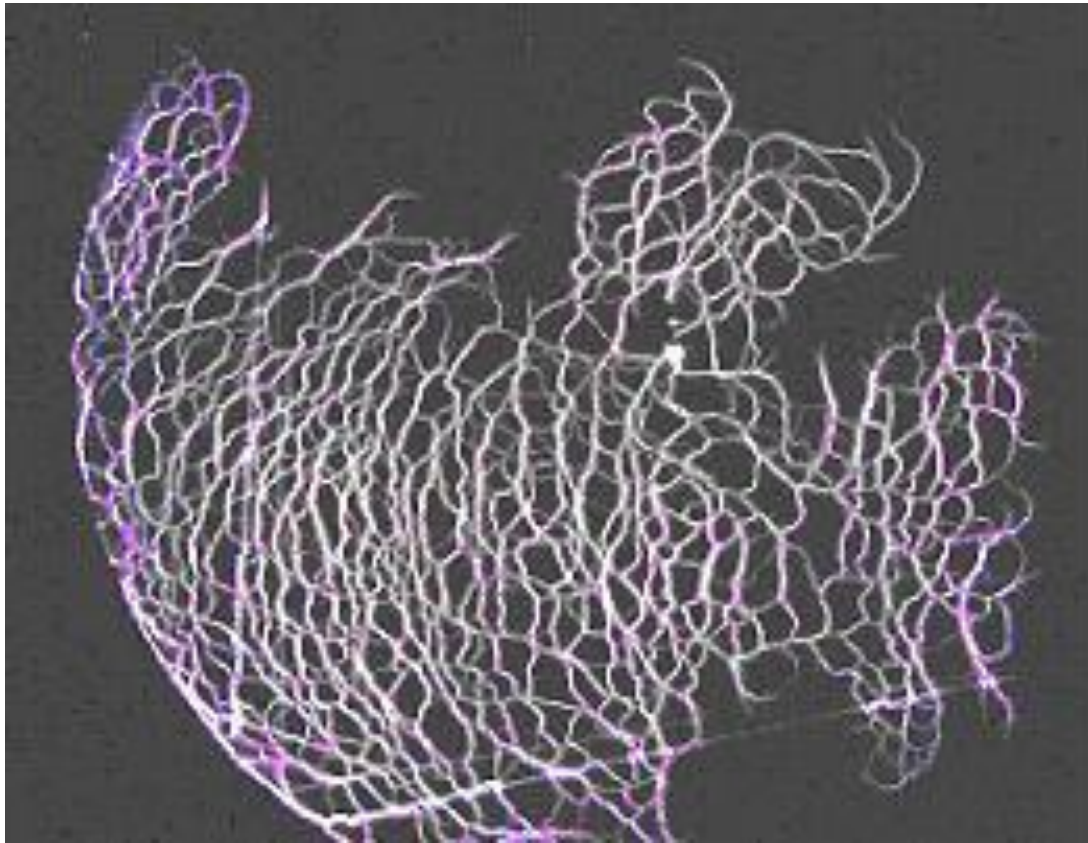


Fig.3.5a. Surface initiated discharge at the longitudinal placing of the dielectric layer (the quartz disc of 1.0cm thickness and 20cm in diameter)). Focusing mirror is located to the left.

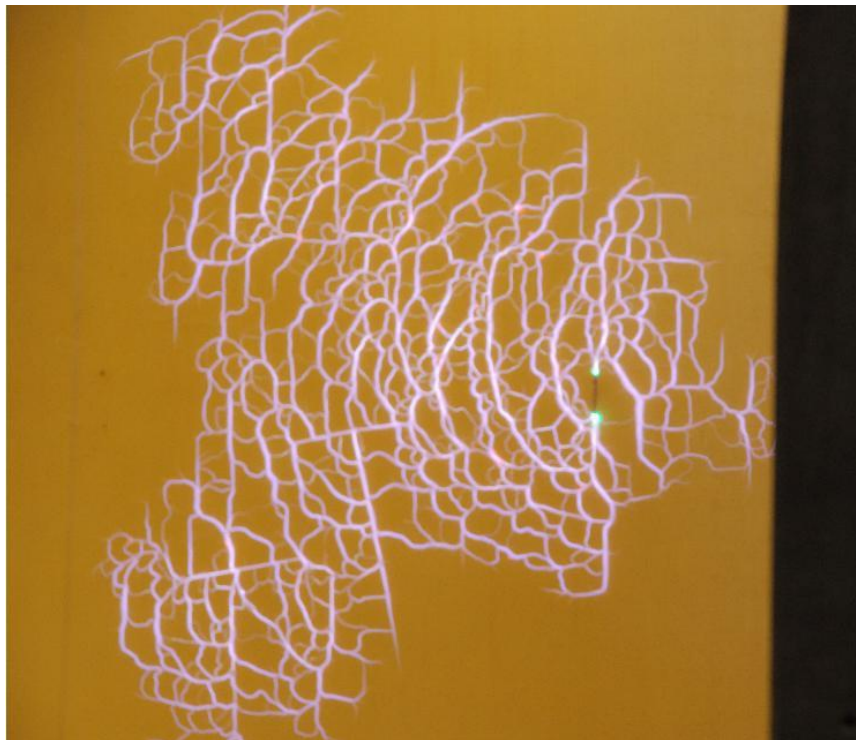


Fig.3.5b. Surface initiated discharge at the longitudinal placing of the dielectric layer (the textolite plate of 0.1cm thickness). Focusing mirror is located to the left

The zone of the surface streamer discharge propagation is substantially wider than the focus area. The discharge propagation is limited by the sizes of the dielectric layer.

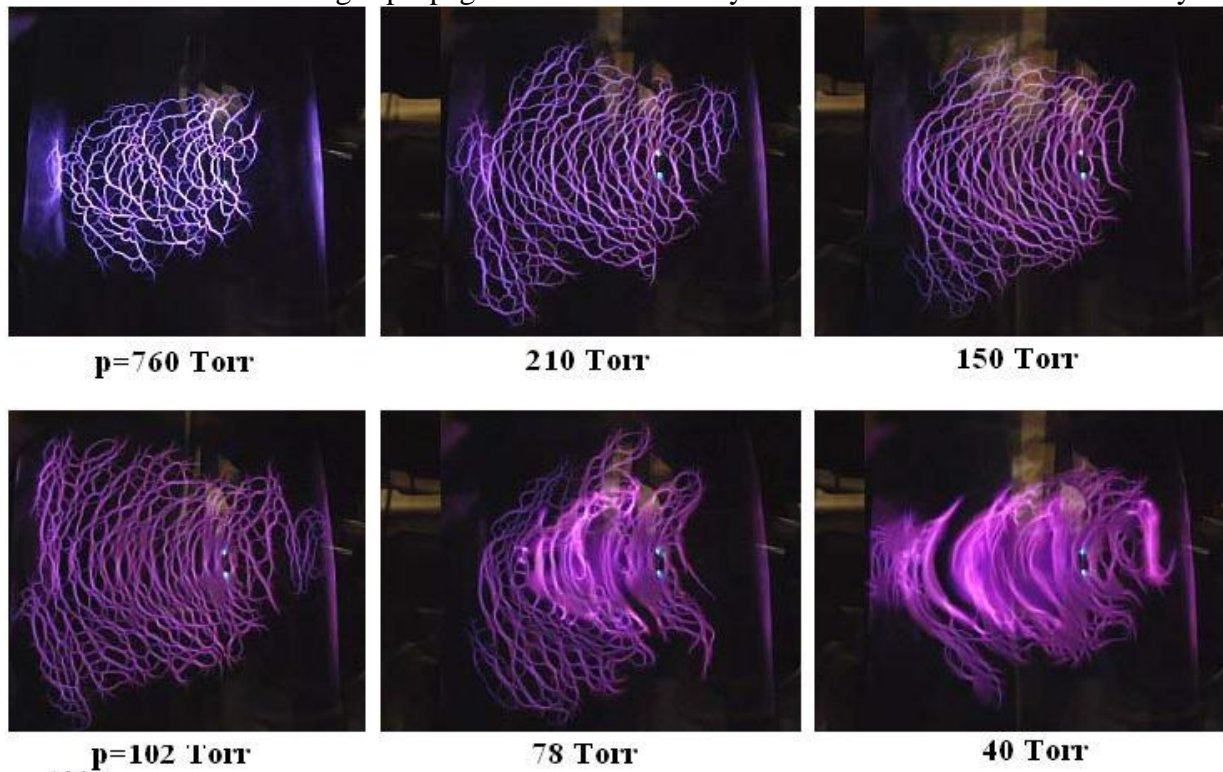


Fig.3.6. Photos of the «longitudinal» surface discharge. $E_0=4\text{kV/cm}$, $\lambda = 8.9 \text{ cm}$

Detailed researches of the initiated "longitudinal" discharge are carried out on a thin polyethylene film of $40 \mu\text{m}$ thickness as the thin film does not disturb a radiation field distribution. Researches have shown, that in all the area of subcritical streamer discharge (the area between lines E_{cr} and E_s in Fig.3.4) the discharge remains purely surface. Only in the area of over critical discharges (above the line E_{cr} in Fig.3.4) the discharge develops in areas in a volume.

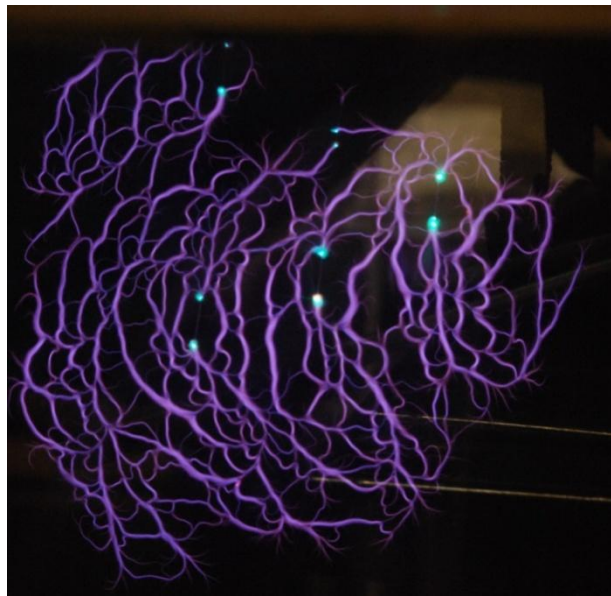


Fig.3.7. Typical appearance of the surface discharge at «longitudinal» placing of the layer (a system of 5 initiators). $\lambda=8.9 \text{ cm}$, $p=150\text{Torr}$

In Fig.3.6 photos of the "longitudinal" surface discharge at the electric field amplitude of 4kV/cm in radiation focus at various values of air pressure in the chamber are represented.

As the initiator the piece of a copper wire of 1.2cm in length 1.2cm and 0.031cm in diameter (in photos bright points on its ends are visible) is used. At the amplitude given value the takes place at pressure below 100Torr. Below this value the discharge from a surface comes into a volume, taking a diffuse character.

Experiments in the installation with a wavelength $\lambda = 8.9\text{cm}$ on initiation of the surface discharge by the system of vibrators have not revealed new properties of the surface discharge in comparison with the initiation by the single vibrator. The typical form of the surface discharge at the "longitudinal" placing of the layer is represented in Fig.3.7 (the system of 5 initiators). Position of initiators can be seen by bright points on their ends.

Researches of evolution of the "longitudinal" surface discharge initiated by the system of 5 vibrators depending on air pressure (see Fig.3.8) have shown that the boundary of the discharge propagation is determined by an existence area of the subcritical surface discharge. The streamer form of the surface discharge is replaced by a diffuse one at air pressure smaller than 45Torr.

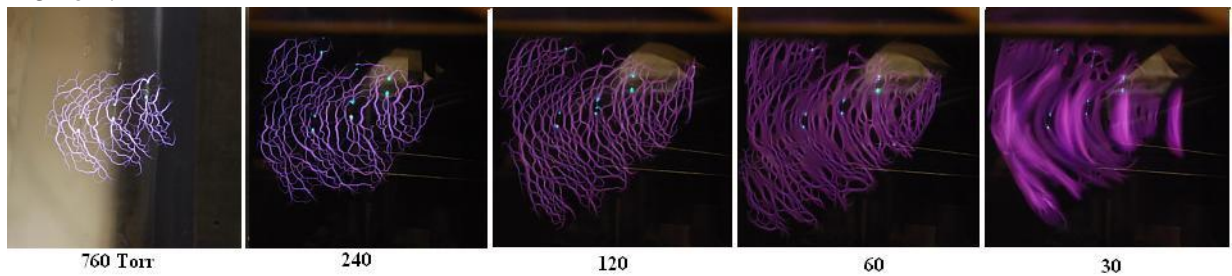


Fig.3.8. The evolution of "longitudinal" surface discharge initiated by the system of 5 vibrators with respect to air pressure. $E=3.7\text{kV/cm}$

At close location of the initiators one has to take into account their electromagnetic connection impacting a distribution of electric currents induced in the vibrators. We have developed a calculation method of a system of strongly interconnected vibrators which can be applied at creation of definite initiating devices.

3.2. Experiments at the wavelength 2.5 cm

As dielectric layers polyethylene films, quartz glasses with thickness of 1 and 2cm (the same, as in the experiments with $\lambda = 8.9\text{cm}$) and a ceramic disk of 12cm in diameter were used at their thickness of 0.4cm. Experiments were carried out at the electric field strength in the focal area of the system $1.7\div 3.2\text{kV/cm}$.

Two variants of the initiator were applied. The first (thick) vibrator represented an aluminum wire 0.965cm in length 0.965cm and 0.15cm in diameter with the sharpened ends, the second (thin) - a copper wire was of 0.95cm in length and 0.02cm in diameter 0.02cm. The initiator was glued to the dielectric in the area of the field maximum. The vibrator axis was parallel to a vector of the field E . The form of the vibrator located on a ceramic disk, is presented in Fig.3.9.

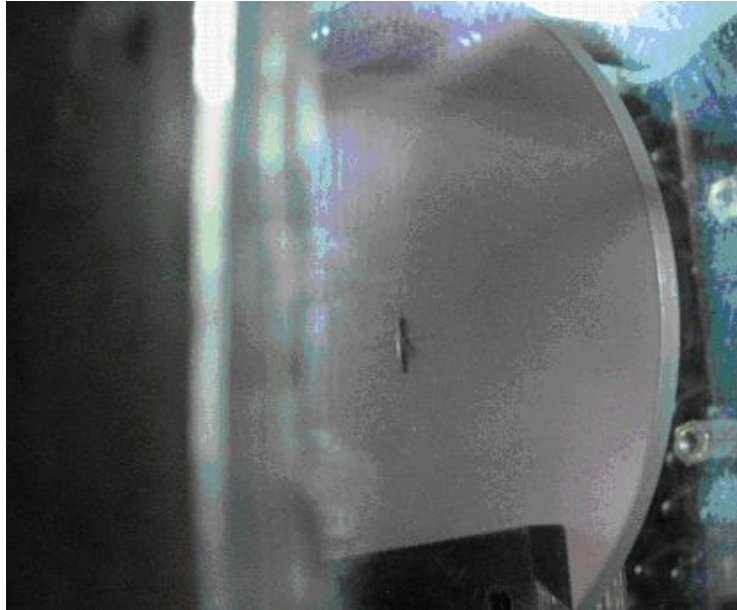


Fig.3.9. An appearance of the vibrator placed on the ceramic disk

In experiments with the "transversal" surface discharge data on boundary value of pressure at which in case of placing of the initiator from a mirror side there is a separation of the streamer discharge from the surface and its development in the volume takes place. Typical photos of purely surface discharge and surface discharge with the developed volume structure are represented in Fig.3.10.

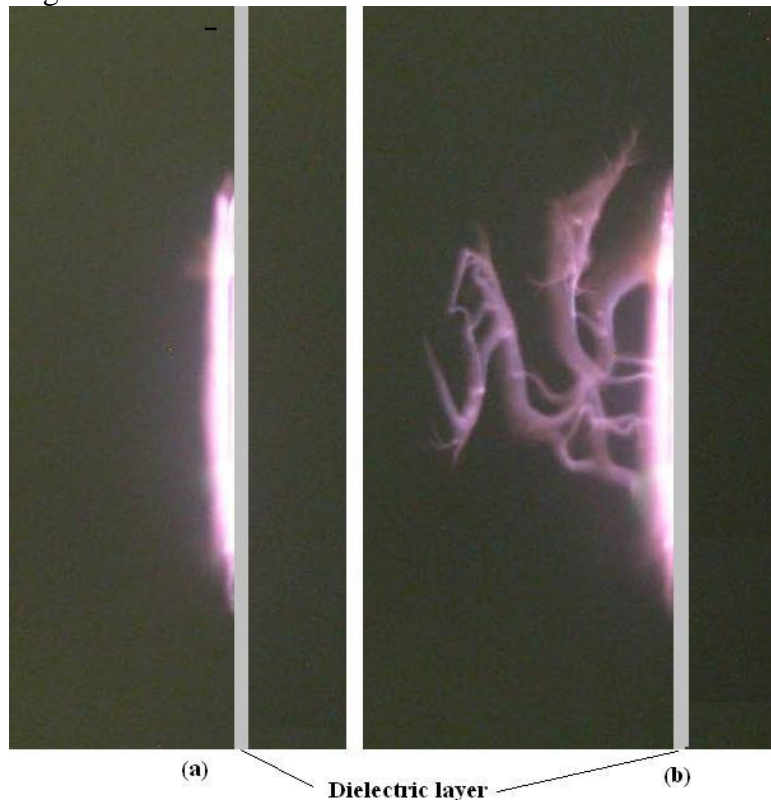


Fig.3.10. The initiated discharge at transversal location of the dielectric layer: (a) – $p=700\text{Torr}$, (b) – $p=480\text{Torr}$

Photographing was made for determination of the boundary of initiated volumetric-surface discharge transition in the purely surface discharge at various values of pressure in the chamber and of electric field strength. Over the photos the required boundary was determined.

The field strength on a surface of a dielectric layer was varied by its moving along the system axis. Known distribution of the field along the system axis was used at that. The polyethylene film with the initiator from a mirror side was placed perpendicularly to the system axes at the corresponding distances from the mirror. The obtained photos are presented in **Fig.3.11** and the result of their processing - in **Fig.3.12**.

In case of the initiator location in the focus of the system from the horn side the streamer discharge does not create a spatial structure. The polyethylene film resists the discharge development towards the radiation, and it remains purely the surface one up to atmospheric pressure.

Similar process occurs also in case of the quartz glass with the initiator in the area of the system focus. At a longitudinal placing of the dielectric layer a separation of streamers into the volume does not occur.

At $E=3.2\text{kV/cm}$ the diffuse discharge also transits into the streamer one at pressure of 30-40Torr. However the transition process of the diffuse discharge into the streamer one does not occur sharply as at $E=1.0\text{kV/cm}$, but smoothly changes in the range of pressure approximately from 70 to 150Torr. Unlike the case with $E=1.0\text{kV/cm}$ the streamer discharge has clearly expressed spatial form. With pressure increase the spatial structure of the streamer becomes simpler, but, nevertheless, it exists at atmospheric pressure also.

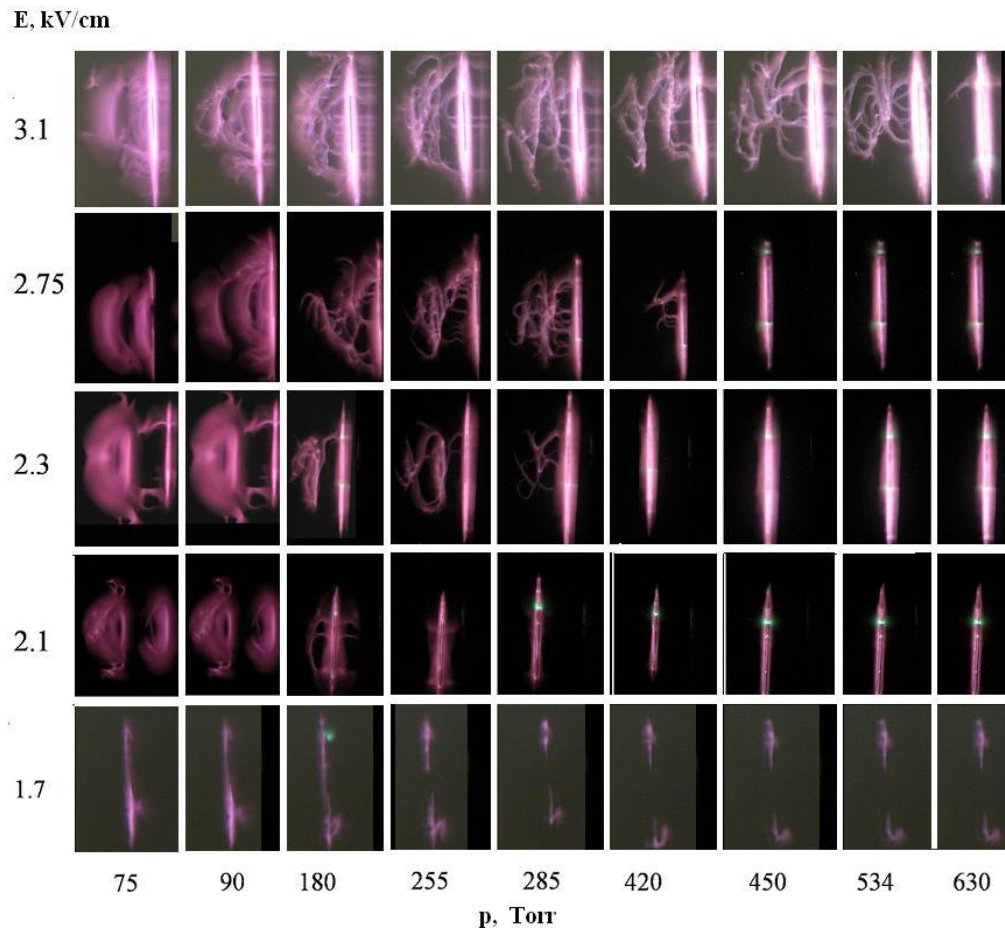


Fig.3.11. «Transversal» initiated discharge at different values of the electric field strength and air pressure, $\lambda=2.5\text{cm}$

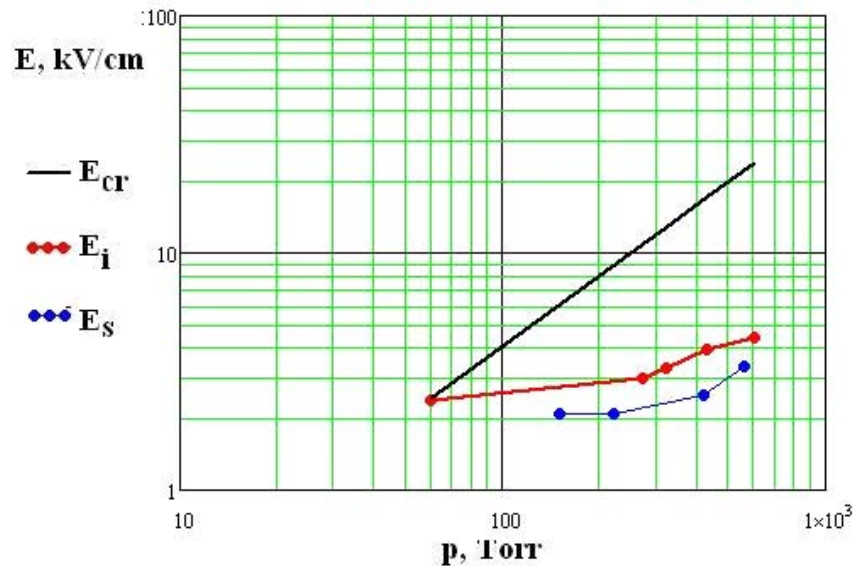


Fig.3.12. A boundary separating the surface and the surface-volumetric discharges, – red line, $\lambda=2.5\text{cm}$. The initiator is located on the dielectric film on the mirror side

Similar process occurs also on the quartz glass with the initiator in the area of the focus. Comparison of photos of the initiated discharge on a dielectric layer with the initiated discharge without it speaks about an absence of the film influence on the volumetric streamer discharge development. The basic distinction consists in that the surface streamer discharge with a complex structure exists on the dielectric surface up to atmospheric pressure. In **Fig.3.13** photos of the "transversal" discharge are shown at the atmospheric pressure, they were made at the removed casing of the vacuum chamber under the angle of 45° to the surface of the polyethylene film (a) and the quartz disk (b).

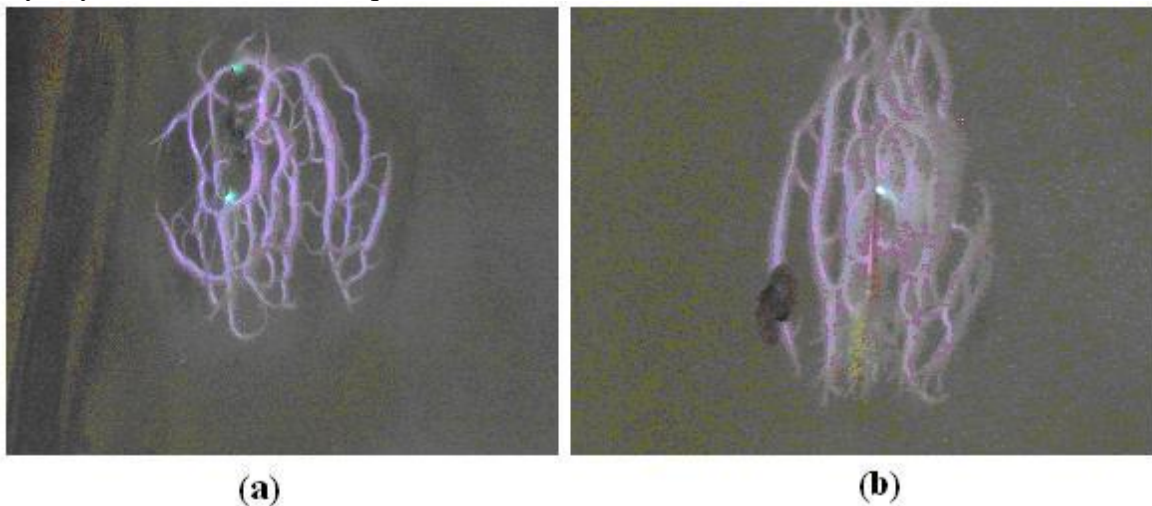


Fig.3.13. Photos of the "transversal" discharge at the atmospheric pressure, made at the removed casing of the vacuum chamber under the angle of 45° to the surface of the polyethylene film (a) and the quartz disk (b)

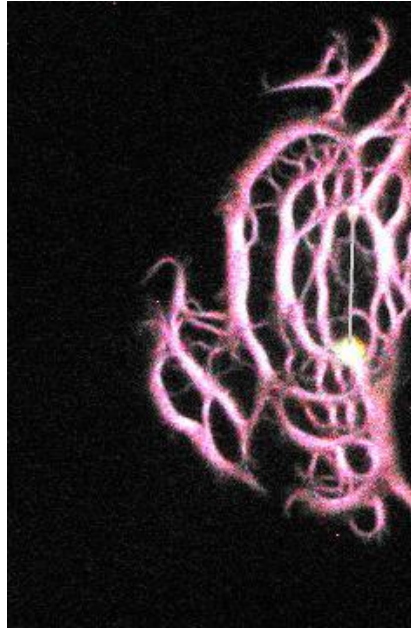


Fig.3.14. *A photo of the “longitudinal” surface initiated discharge. The straight line – the initiator. The mirror is to the right, $p=370\text{Torr}$*

In case of the "longitudinal" placing of the dielectric film (along the system axis in parallel to vectors \mathbf{k} and \mathbf{E} , the initiator is on the dielectric in the system focus) spatial streamer discharge does not appear. The form of the longitudinal surface discharge on the polyethylene film is represented in Fig.3.14. Its structure and dynamics of development is similar to the transversal surface discharge with respect to pressure.

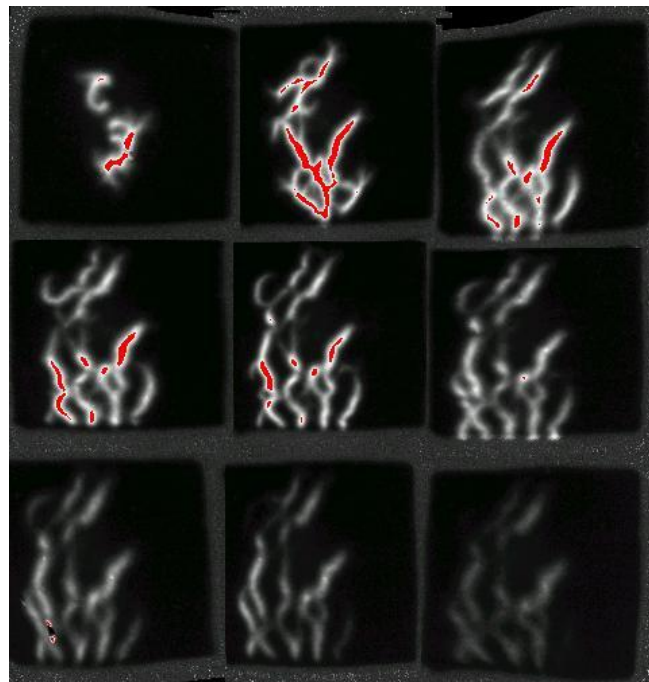


Fig.3.15. *Frame to frame scan of “longitudinal” initiated discharge at the atmospheric pressure and $E_0=3.1\text{kV/cm}$ by the high-speed chamber. Exposure time is – $0.5\mu\text{s}$, pause – $3\mu\text{s}$*

Development of the surface discharge in time was investigated by means of high-speed electron-optical chamber K011 (manufacture of Russia). Time-scan of the "longitudinal" discharge development on a film at atmospheric pressure and the field amplitude of 3.1kV/cm are shown in **Fig.3.15**. The period of change of shots c is $3.5\mu\text{s}$ at the exposition $0.5\mu\text{s}$. Red color singles out the brightest parts of the image. Decrease in the radiation level during the pulse by 40% affects spatial development.

Visual survey of the film after the experiments reveals trace presence from the surface discharge on a surface of the film. It confirms earlier obtained results on change of properties of a surface by the surface MW discharge.³

Chapter 4. Determination of boundary transition pressure of transition of MW discharge diffuse form in air into a streamer one at perpendicular and longitudinal locations of a dielectric plate in EM beam at wavelengths of 8.9cm and 2.5cm (Tasks 9 and 10)

4.1. Experiments at the wavelength of 8.9cm

Experiments on a boundary between the diffuse and the streamer surface discharge determination at the wavelength of 8.9cm were carried out under the uniform program with the **Task 5**.

Change of the discharge type at a variation of pressure and amplitude of the field amplitude in the presence of a dielectric layer was carried out in all accessible range of parameters. In **Fig.4.1** the photos of the discharge made at amplitude of the field 4kV/cm at different values of air pressure are represented at absence of the layer, at the "transversal" and "longitudinal" it's placing.

As a dielectric layer the polyethylene film of 40 μm thickness was used. **Fig.4.1** illustrates the general conclusion that film presence practically does not influence a development of the volumetric discharge diffuse form, but creates conditions for development of the surface streamer discharge. Development limits of the streamer surface discharge in a plane of the layer of much greater dimensions than those of the volumetric discharge. It is especially distinctly revealed in the case of "the longitudinal" discharge. Transition boundaries of the diffuse discharge form into the streamer one practically are not sensitive to presence of the dielectric layer.

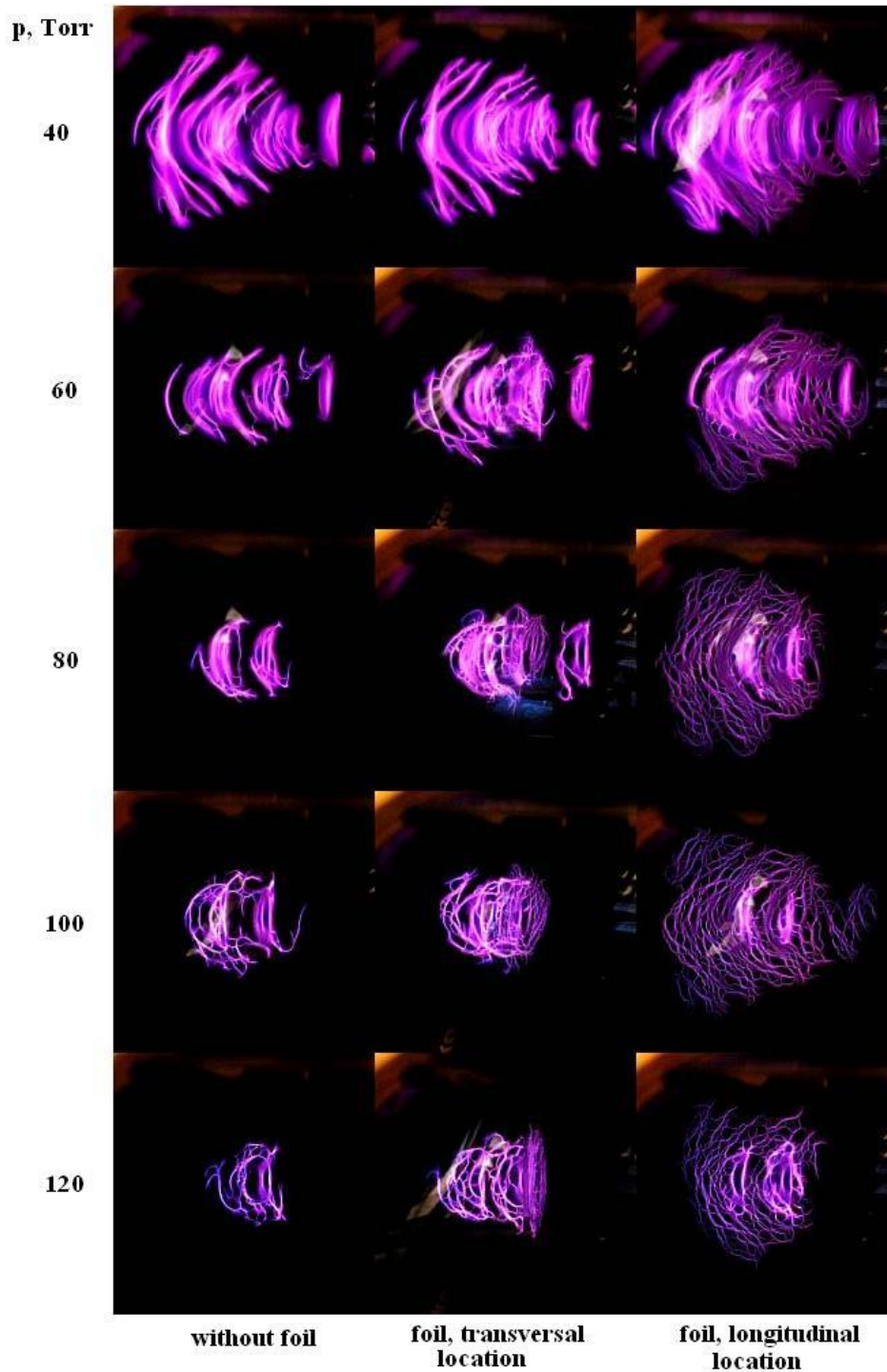


Fig.4.1. Initiated discharge at $E_0=4\text{kV/cm}$ with respect to pressure

4.2. Experiments at the wavelength 2.5cm

By a variant 1 ("transversal" placing) with each of the samples a series of 10 experiments on determination of the maximum pressure at which there is a transition of the diffuse discharge into the streamer one has been carried out.

Both in the presence of a film, and without it, the diffuse discharge transits into the streamer one at $p \geq 75\text{Torr}$ ($E = 3.2\text{kV/cm}$) and $p \geq 30\text{-}40\text{Torr}$ ($E=1.0\text{kV/cm}$). Photos of the diffuse discharge with a film and without it for $E=3.1\text{kV/cm}$ are represented in Fig.4.2.

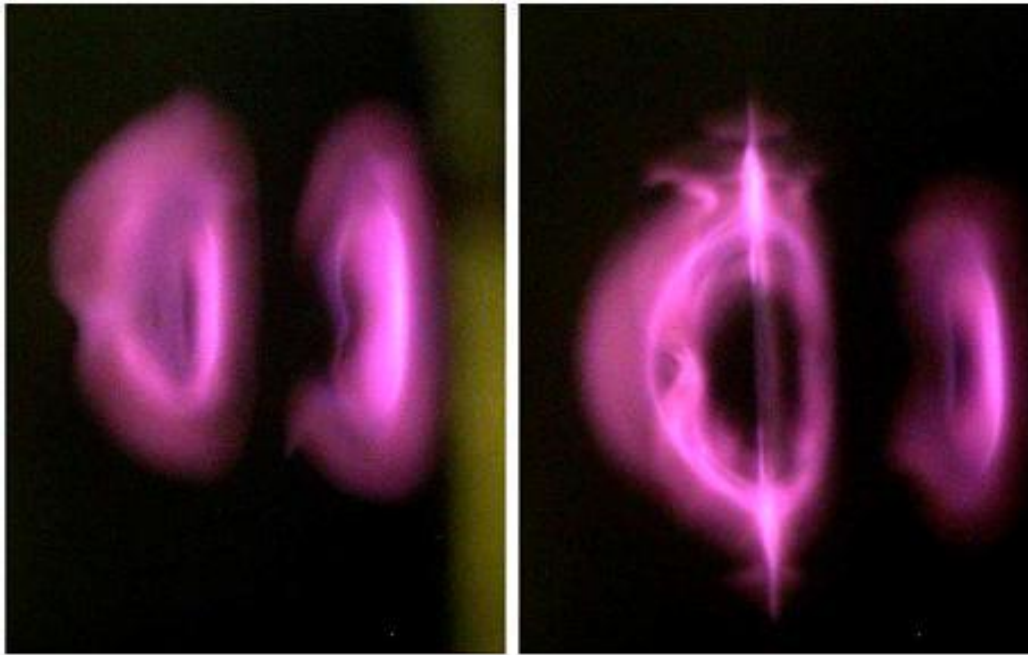


Fig.4.2. Discharge photos without a film (to the left) and with it (to the right) at its transversal placing. $E_0=3.1\text{kV/cm}$, $p=70\text{Torr}$

Comparing the obtained data with photos of the discharge initiated by the vibrator, placed in the focus without a dielectric plate, it is possible to draw a conclusion, that irrespective of a dielectric kind the diffuse discharge at $E=1.0\text{kV/cm}$ transits into the deeply subcritical streamer discharge at $p \geq 30\text{-}40\text{Torr}$.

At $E_0=1.7\text{kV/cm}$ the streamer discharge on a film surface did not arise. The given result quite agrees with the diagram of various kinds of MW-discharges for $\lambda=2.5\text{cm}$, obtained during the previous researches. According to it, the experiment conditions correspond to zones where without only the diffuse over critical discharge is possible without presence of the initiator.

Similar researches were carried out at placing of samples by a variant 2 (longitudinal placing, in parallel to the vector E and a wave vector \mathbf{k}). As samples the same polyethylene films, quartz glasses and a ceramic disk were used. As in the variant 1 the diffuse discharge on a surface of the sample disappears at $p \geq 75\text{Torr}$ for $E=3.2\text{kV/cm}$ and the streamer discharge does not arise.

Chapter 5. Determination of boundary field separating a subcritical surface MW discharge with developed streamer structure from deeply subcritical surface MW discharge with streamer channels attached to an initiator (Tasks 12-15)

5.1. Transversal discharge

a) Transversal discharge in the installation with the wavelength of 8.9cm

By the method described earlier we have carried out studies of the discharge type dependence on the electric field amplitude in the place the location of a film with the initiator location and we determined the boundary dividing existing areas of the developed streamer and the attached discharges. At the given pressure was changed the attenuator position in the waveguide path of antenna system feeding, and the discharge type was detected by means of photographing.

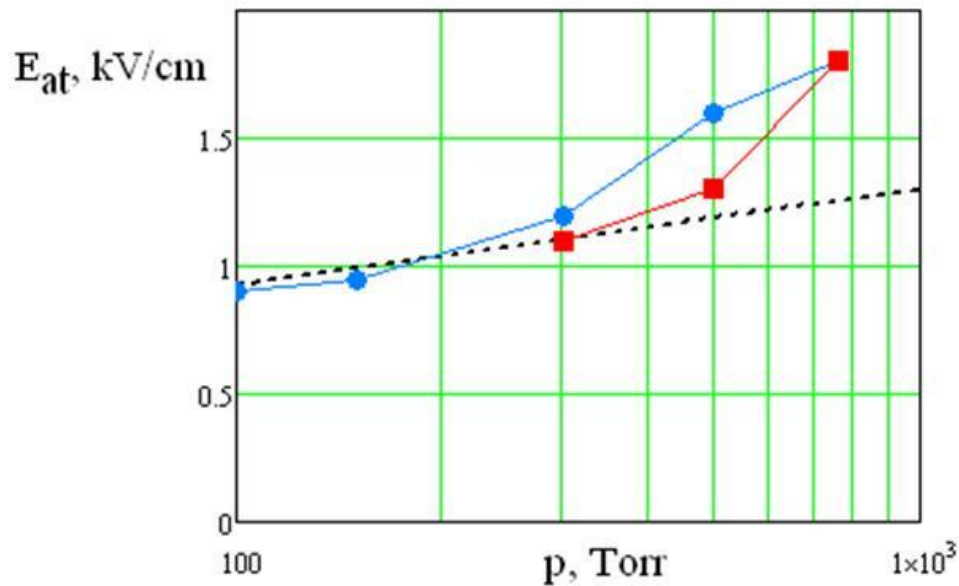


Fig.5.1. Dependence of threshold value of the electric field amplitude with a wavelength of 8.9cm via air pressure separating the attached discharge from the streamer one: with the initiator without a film - blue points (experiment) and a black dashed line (calculation), with the initiator on a film - red points (experiment)

In **Fig.5.1** boundary values of the electric field amplitude for the initiator located on a dielectric film at various air pressure values are compared with the values obtained earlier for the initiator without a film. Differences in the boundary position between these two cases are in limits of accuracy of the discharge type determination.

b) The transversal discharge in the installation with a wavelength of 2.5cm

For determination of the electric field boundary value corresponding to the transition of the attached surface discharge into the streamer one, depending on air pressure at the fixed values of electric field strength E of MW, pressure in the chamber was changed, and the discharge type was visually determined. Values of electric field strength E were varied by choice of position of a dielectric film with the initiator. Dependence of field amplitude on distance z to the bottom of the mirror at invariable power of the MW-generator has been measured earlier (see **Fig.5.2**).

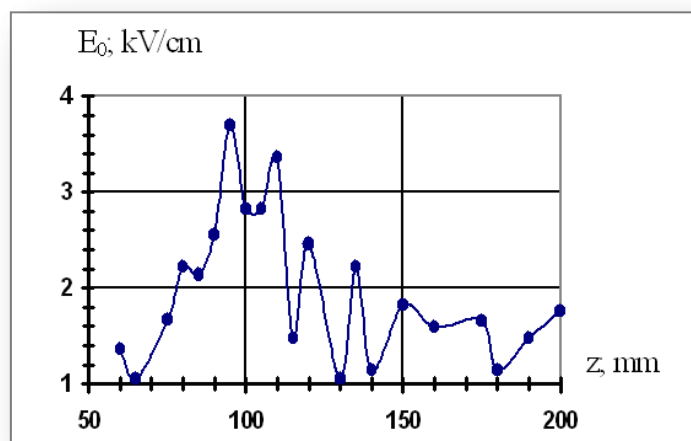


Fig.5.2. Measured earlier electric field amplitude distribution

On the graph of **Fig.5.2** a field in the distribution maximum is equal to $E_{\max} = 3.75 \text{ kV/cm}$. However at carrying out of experiment the generator power was a little below so the maximum field in distribution was $E_{\max} = 3.1 \text{ kV/cm}$. In the assumption of an invariance of the distribution

a real value of a field in the experiment was determined as $E_i^{\text{exp}} = \beta \cdot E_i^{\text{graph}}$, where $\beta = 3.1/3.75 = 0.83$.

The film with the initiator was placed at the distance z , corresponding to required value of amplitude of MW-field E_i amplitude to perpendicularly to the Pointing vector.

The initiator in the form of a copper wire 9.5mm in length and 0.2mm in diameter was glued to the surface in the centre of the film in parallel to the vector of the electric field strength on a side of the MW generator horn.

Discharge photographing was carried out under the scheme represented in Fig.5.3.

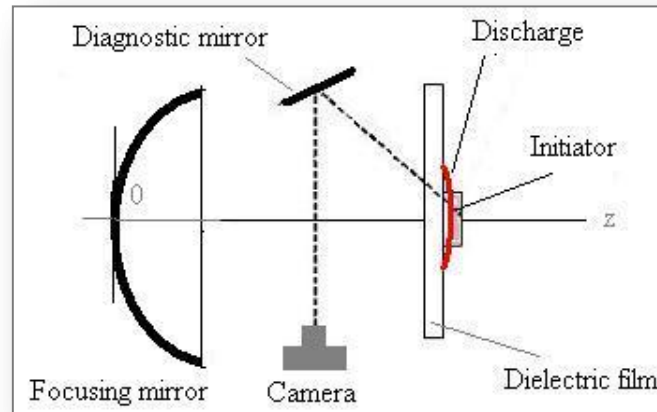


Fig.5.3. Discharge photographing scheme

The discharge photos obtained at various values of a field amplitude and air pressure for processing are collected in the form of a matrix. In the rarefied kind it is represented in a Fig.5.4.

The matrix in Fig.5.4 allows drawing a border between the discharge types. The obtained data are presented in mentioned below Table 5.1 and in the form of red points on the diagram with measured earlier similar border in the absence of the dielectric film, Fig.5.5.

Table 5.1

N	z_i, mm	$E_i^{\text{graph}}, \text{V/cm}$	$E_i^{\text{exp}}, \text{V/cm}$	p_{\min}, Torr	p_{\max}, Torr
1	150	1.8	1.5	----	----
2	160	1.6	1.3	400	450
3	115	1.4	1.2	300	350
4	178	1.3	1.1	150	200
5	140	1.2	1.0	----	----

Here

z_i – is a distance between a film plane and a mirror;

E_i^{graph} – electric field strength on an axis in the point z_i of the film placing;

E_i^{exp} – electric field strength on an axis in the point z_i of the film placing in the experiment;

p_{\min}, p_{\max} – limits of uncertainty of pressure threshold value in the chamber of the discharge separating discharge types.

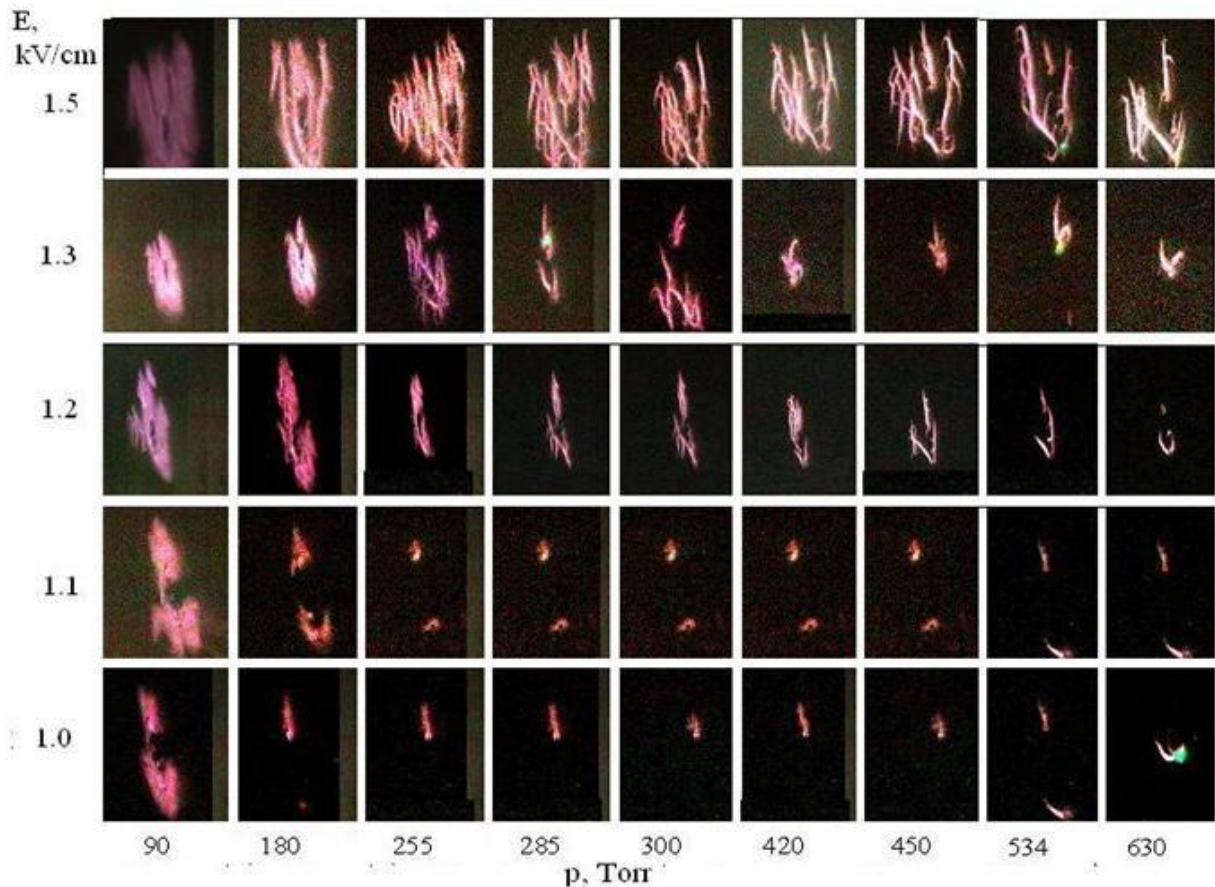


Fig.5.4. Photos of the transversal discharge dependence on air pressure and the electric field amplitude changed by moving of a film along an axis of the system (see Fig.5.2)

The obtained border between the attached and the streamer surface discharges lies a little below the similar border for the volumetric discharge (**Fig. 5.5**).

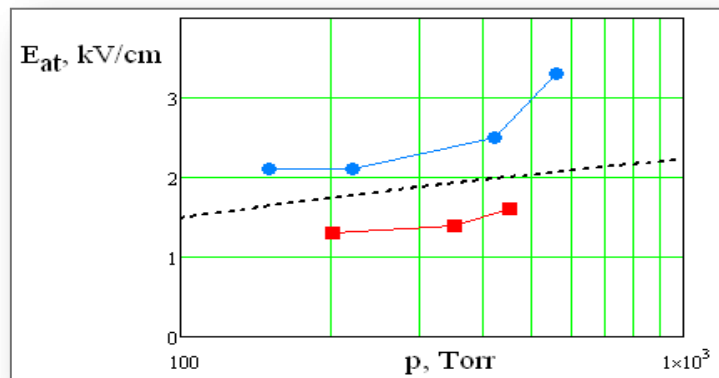


Fig.5.5. Dependence of threshold value of the electric field amplitude with the wavelength of 2.5cm on air pressure separating the attached discharge from the streamer one: in the presence of the initiator - blue points (experiment) and a black dashed line (calculation), in the presence of the initiator on a film - red points (experiment)

It is necessary to mark, that the used method allows estimating only qualitatively the transition border of the subcritical surface streamer discharge into the deeply subcritical one owing to sharp change of electric field strength E on an axis of the system with a distance to a focusing mirror.

For specification of the obtained data other method of carrying out of the experiment based on the film placing precisely in the focal area of the system has been fulfilled and used. Electric field strength in this area changes due to adjustment of the outlet power of the MW generator by change of the glow voltage of the cathode of the outlet cascade of the MW generator. Experiment, as well as earlier, was carried out on the polyethylene film located perpendicularly to the Pointing vector. The initiator in the form of a copper wire of 9.5mm in length and 0.2mm in diameter was placed on the surface in the center of the film in parallel to the vector of MW field electric field strength on the generator side. The field strength was determined by means of the MW sensor located in the waveguide path directly in front of the horn of the MW generator. Discharge photographing was carried out under the scheme represented in Fig.5.3.

The obtained data of the transversal surface subcritical discharge transition into the transversal surface deeply-subcritical discharge are presented in the **Table 5.2** represented below.

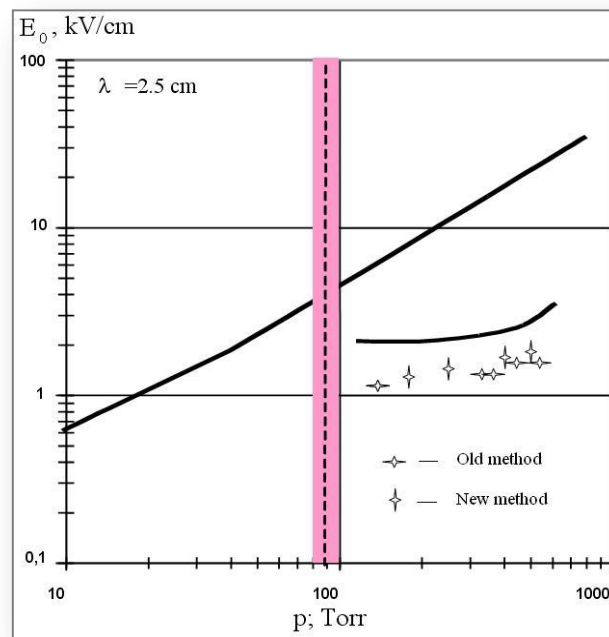


Fig.2.6. The upper boundary of the attached discharge at the film transversal location

Table 5.2

N	p (Torr)	U _{wave} (mV)	E _{i calc} (V/cm)
1	-	620	2.1
2	630	560	1.7
3	420	550	1.6
4	255	520	1.1
5	180	450	1.3

where

E_{i calc} – is calculated electric field strength over the axis Z in the system focus;
p – pressure in the chamber at appearance of developed surface streamer discharge;

U_{wave} - pike value of the pulse amplitude, read on a calibrated MW sensor placed in front of the generator horn.

The curve of the transversal subcritical surface discharge transition dependence into the deeply subcritical surface discharge constructed on the basis of a represented below matrix of photos, is presented in Fig.2.6.

Results of measurement by a new method have confirmed results obtained earlier, that one can see from comparison of data in Fig.5.5 and Fig.5.6. At presence of the dielectric the boundary of the attached discharge passes at smaller values of the electric field amplitude, than in its absence.

5.2. Longitudinal discharge

a) Longitudinal discharge in the installation with the wavelength of 8.9cm

Earlier the border of the attached discharge of transition into the volumetric streamer discharge initiated by the vibrator at absence of a dielectric layer has been determined. For applications and understanding of the surface discharge physics it is important to determine an influence of a dielectric layer on position of the mentioned border. For the solution of this problem the experiment has been carried out which essence consisted in the following. On a surface of the thin dielectric layer oriented along a wave vector and a vector of the electric field was placed an initiator in the focus of MW radiation. The initiator represented a piece of a steel wire of 0.35mm in diameter and of 11mm length oriented along the electric field. As a dielectric layer was used a textolite glass sheet of 1mm thickness. Other materials were used as well. The dielectric sort poorly affects results of measurements. Experiments have shown that the required border is located in the area of small values of MW radiation level, difficultly achievable in the installation with the wavelength of 8.9cm. For an exit in a required range of values of the electric field amplitude in the radiation focus in addition to the main attenuator has been included a special knife attenuator with the fixed coefficient of attenuation into the waveguide path connecting the generator with a radiator. It has allowed revealing the border (though only in one point) at air pressure of 300Torr.

In Fig.5.7a is shown the discharge photo on a surface of the dielectric layer at pressure of 300Torr and electric field of 1kV/cm that corresponds to the border of the attached discharge at absence of the dielectric layer. One can see that the discharge has the developed character. In Fig.5.7b and Fig.5.7c are represented photos of two realizations of the discharge at the same pressure and included additional attenuator. The discharge in these conditions lies on the border of the attached and volumetric types.

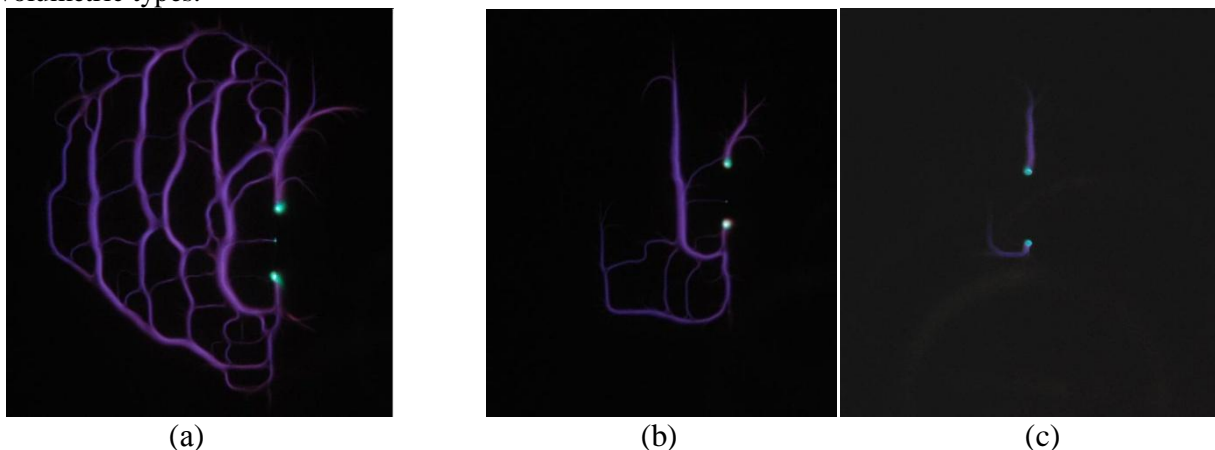


Fig.5.7. Discharge photos on the surface of the dielectric layer at air pressure of 300Torr:
(a) - at the electric field amplitude of 1kV/cm, (b) and (c) - at additional attenuator

For determination of the electric field amplitude value in the radiation focus the method of contactless measurement of the amplitude value developed earlier was used in the set place of space. In the location of the initiator (at absence of a layer with the initiator) on a dielectric

thin thread the lead ball of 0.5cm in diameter was hanged. As is known an electric field on the ball poles is by 3 times greater than its undisturbed value. Measuring the maximum air pressure p at which a breakdown takes place on ball poles, it is possible to determine the required value of the field in a point of placing of the ball using known dependence of a critical field on pressure $E_{cr}(p)$.

$$E_0 = \frac{E_{cr} p}{Q} \quad (5.1)$$

where the coefficient Q in the simplest case of the ball is equal to 3.

Experiments have shown, that the maximal breakdown pressure with a ball instead of the initiator equals to 15Torr. In Fig.5.8 the photo of the discharge initiated by the ball at pressure of 15Torr is shown. At this pressure the discharge has partially diffuse character. Therefore at calculations it is necessary to consider a diffusion influence. The coefficient Q can appear to be not 3, but a little bit smaller.

In Fig.5.9 is shown a theoretical dependence of the coefficient Q on the product of the ball radius on pressure of air, defined by the equation²

$$ap = A \frac{\beta \left(\frac{Q_{\max} E_0}{E_{cr} p} \right)^\beta}{\left(\left(\frac{Q_{\max} E_0}{E_{cr} p} \right)^\beta - 1 \right)^{3/2}}, \quad A = 4.5 \text{cmTorr}, \quad \beta = 5.2, \quad Q_{\max} = 3 \quad (5.2)$$

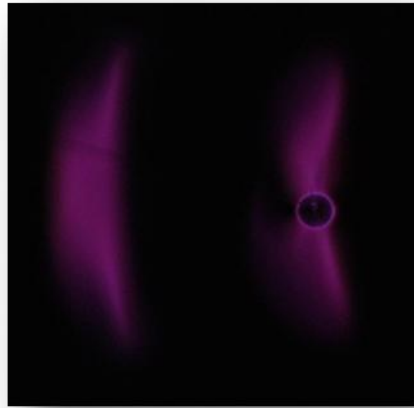


Fig.5.8. Photo of the discharge initiated by a ball at air pressure of 15Torr and additional attenuator included into the scheme

In the conditions of the carried out measurements ($a=0.25$ cm, $p=15$ Torr) $ap \approx 4$, $Q(ap=4) = 1.54$. In Fig.5.10 a dependence of critical field amplitude on pressure for the radiation wavelength of 8.9cm is represented⁴. The critical amplitude of 0.85kV/cm corresponds to pressure of 15Torr. Thus, the field amplitude in the focus at presence of the additional attenuator is equal to $0.65 \cdot 0.85 = 0.55$ kV/cm.

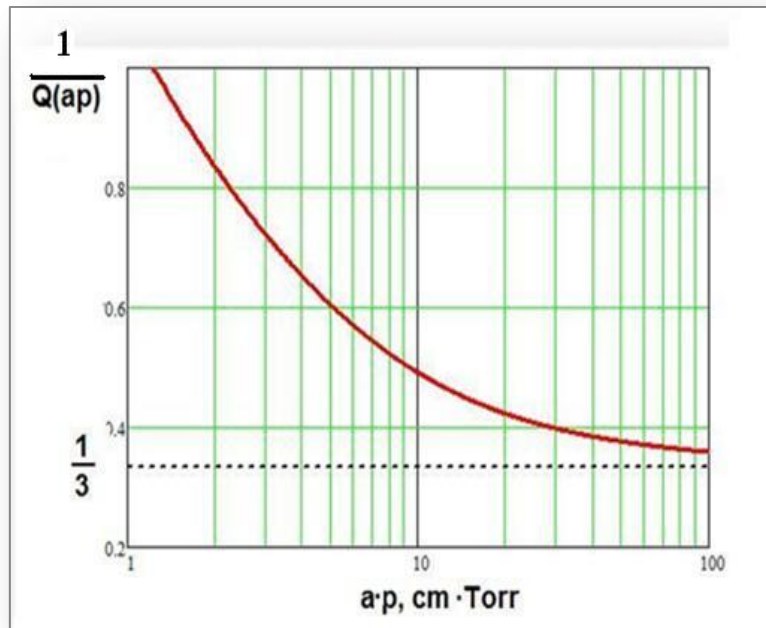


Fig.5.9. Theoretical dependence of the coefficient Q on product of the ball radius on pressure of air

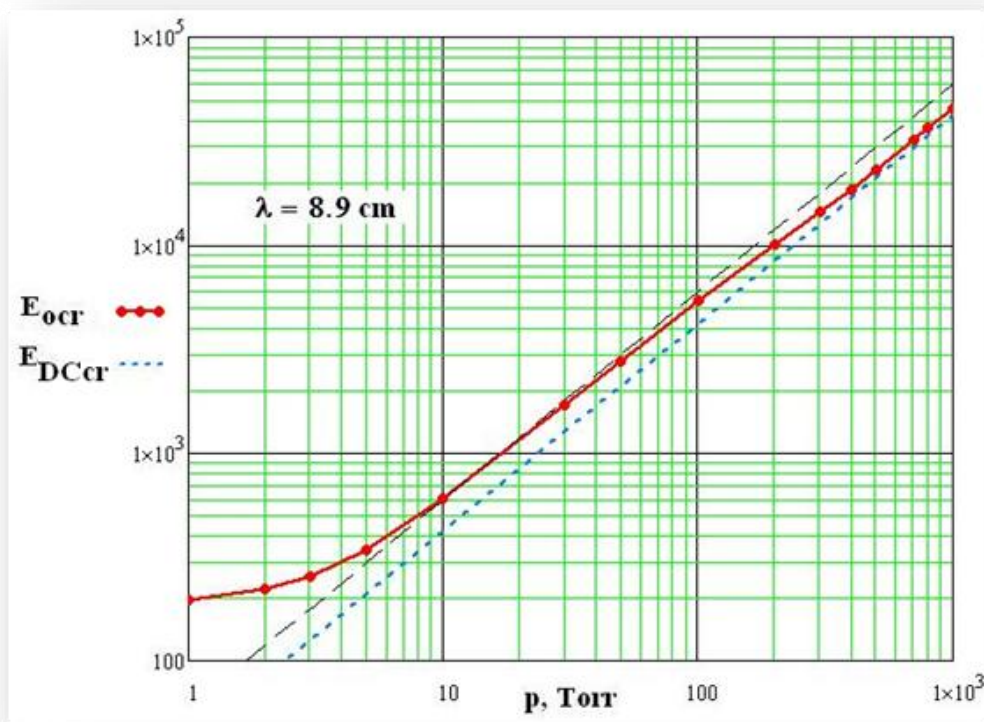


Fig.5.10. Dependence of critical field amplitude on pressure for the radiation wavelength of 8.9cm

The obtained point belonging to the border of the attached discharge transition into the volumetric one, (300Torr, 0.55kV/cm) is shown in Fig.5.11. The separation of the discharge from the initiator in the presence of a subjacent dielectric surface occurs at the electric field

amplitude by 2 times smaller, than in case of the surface absence.

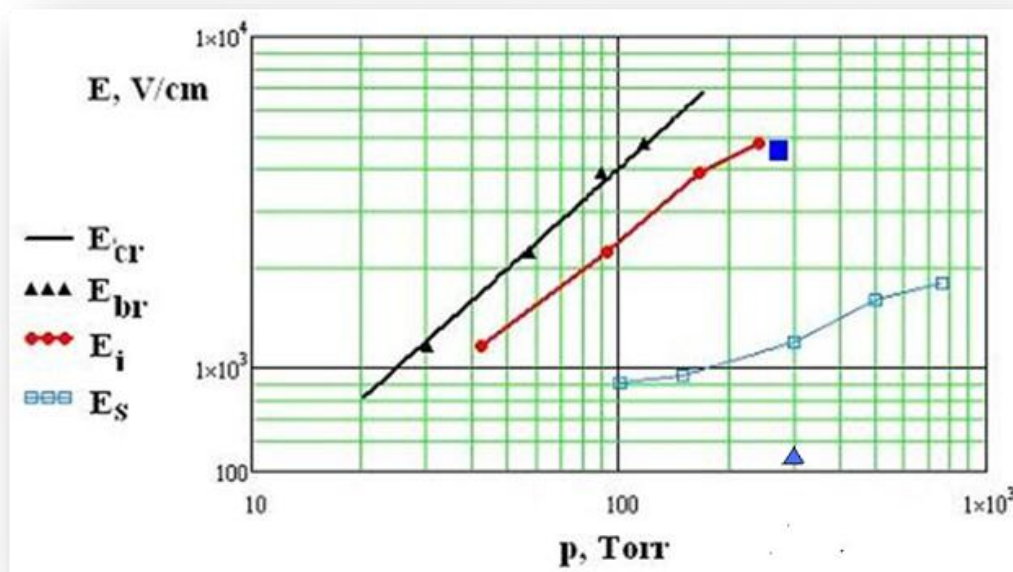


Fig.5.11. The border dividing attached and volumetric discharges: a dark blue line - without a dielectric layer, a dark blue triangle - with a subjacent dielectric surface. $\lambda = 8.9\text{cm}$

b) Longitudinal discharge in the installation with the wavelength of 2.5cm

In EM beam with $\lambda = 2.5\text{cm}$ in air pressure range p experimental determination of the boundary field E_0 separating the subcritical longitudinal MW discharge with developed streamer structure and deeply subcritical longitudinal MW discharge with surface plasma streamer channels attached to the initiator was carried out by the method similar to described above.

Experiment was carried out on the polyethylene film placed on an axis of the vacuum chamber in parallel to the Pointing vector. The initiator in the form of a copper wire of 9.5mm in length and 0.2mm in diameter was glued to the surface in the center of the film in parallel to the vector of the electric field strength of MW field. The strength of the field in this area was changed due to change of the glow voltage of the cathode of outlet cascade of the MW generator.

The obtained data on transition of the longitudinal surface subcritical discharge into the longitudinal deeply subcritical surface discharge are presented in **Table 5.3** below:

Table 5.3

N	p, Torr	U_{wave} , mV	$E_{i \text{ calc}}$, V/cm
1	-	450	1.3
2	495	410	1.1
3	360	400	1.0
4	204	360	0.8
5	156	350	0.7
6	-	230	0.6

where

$E_{i \text{ calc}}$ – calculated electric field strength on the axis Z in the focus of the system;

p – pressure in the chamber at appearance of developed surface streamer discharge;

U_{wave} - pike value of the pulse amplitude read on the calibrated MW sensor placed in front of the generator horn.

Configurations of the streamer surface discharge with respect to the strength of the MW field and pressure in the chamber are represented in the form of a matrix of photos in **Fig.5.12**.

A curve of longitudinal surface subcritical discharge transition dependence into the longitudinal deeply subcritical surface discharge dependence, constructed on the basis of a matrix of photos, it is presented in **Fig.2.13**.

Comparison of **Fig.5.13** and **Fig.5.6** allows concluding, that the border of the attached discharge on a dielectric does not depend on orientation of the dielectric layer along or across a radiation direction.

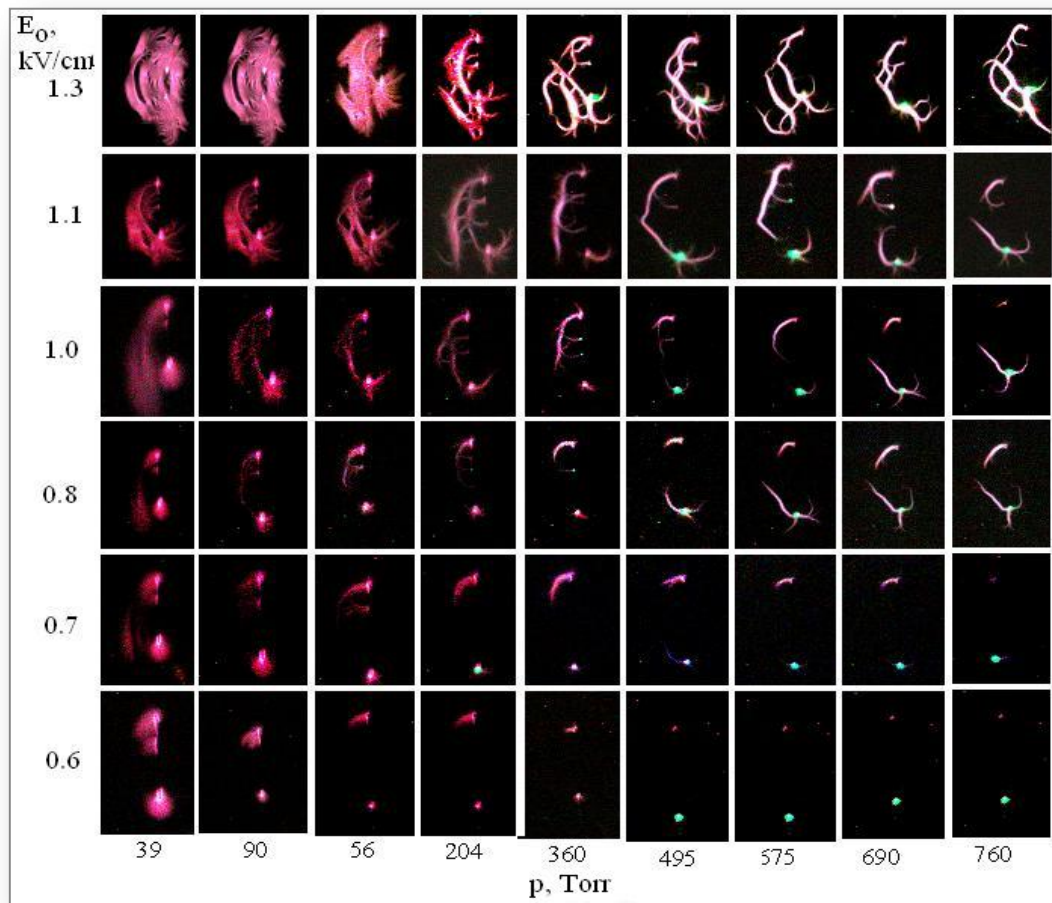


Fig.5.12. Longitudinal discharge photos with respect to air pressure and the field amplitude $E_0, \lambda = 2.5\text{cm}$

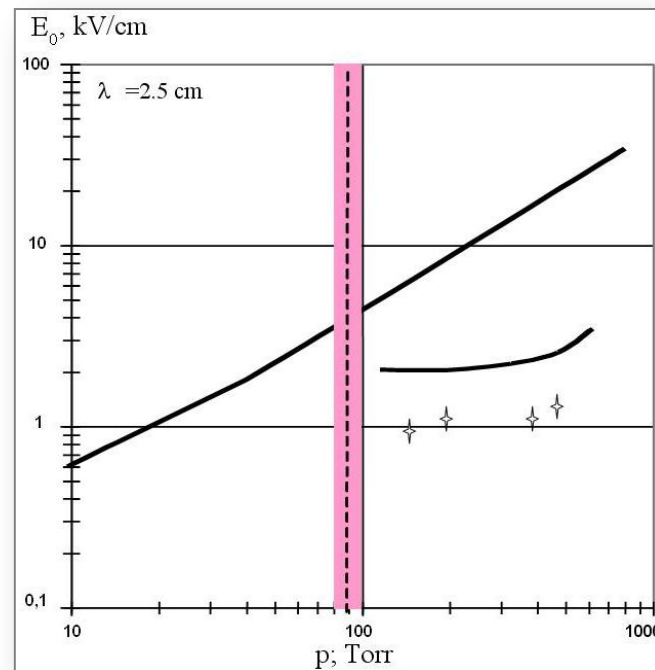


Fig.5.13. Upper border of the attached discharge at longitudinal location of the film, $\lambda = 2.5\text{cm}$

Chapter 6. Ability of the streamer subcritical and deeply subcritical MW discharge to remain a surface one with respect to angular position of a plate concerning Pointing vector of EM field (Task 16).

6.1. Experiments at the radiation wavelength 8.9 cm

For carrying out of measurements in the case of the working chamber the diagnostic window, transparent in an optical range and opaque in MW a range of 20.0cm in diameter has been built in. The window has allowed carrying out discharge photographing from above at various angles of turn of the dielectric plate with the initiator on it round a vertical axis. We remind that MW radiation is vertically polarized. In photos the radiation reflected from the focusing mirror is directed from below upwards, as shown by an arrow.

The experiment has shown, that at a longitudinal placing of the plate (an angle $\beta = 0^\circ$) the discharge remains the surface one in spite of pressure in limits from 10 to 760Torr. In Fig.6.1 series of photos of the longitudinal discharge ($\beta = 0^\circ$) is represented with respect to pressure of air. The plate in photos can be seen under a small angle in order the structure of the surface discharge could be seen. We mark, that the discharge remains the surface one even at pressure smaller than 100Torr at which the MW field is over critical.

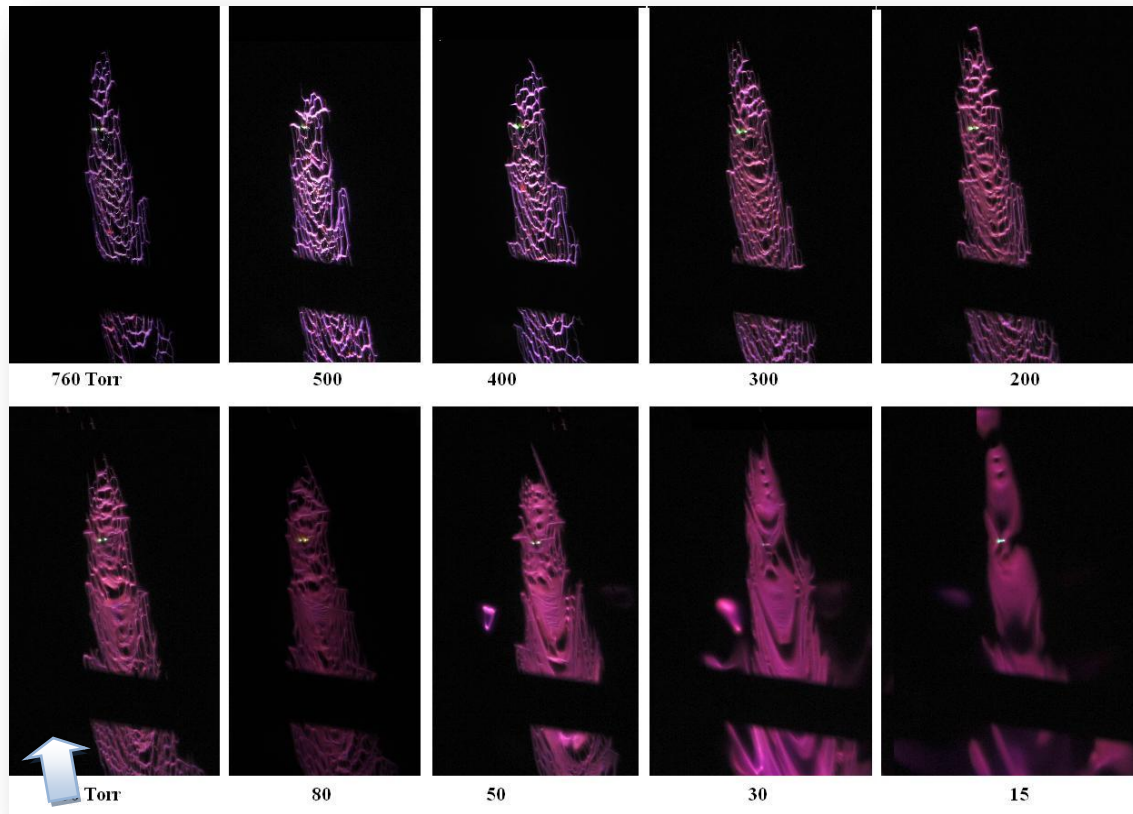


Fig.6.1. Photos of the surface discharge from above, $\beta = 0^\circ$, with respect to air pressure. $E_0 = 4.5\text{kV/cm}$. The MW radiation is directed from below upwards

In Fig.6.2 one can see photos of the discharge at the angle of $\beta = 70^\circ$, i.e. at rather small deviation of a plate from a transversal placing. Thus, as before, the initiator is located on a side of the focusing mirror.

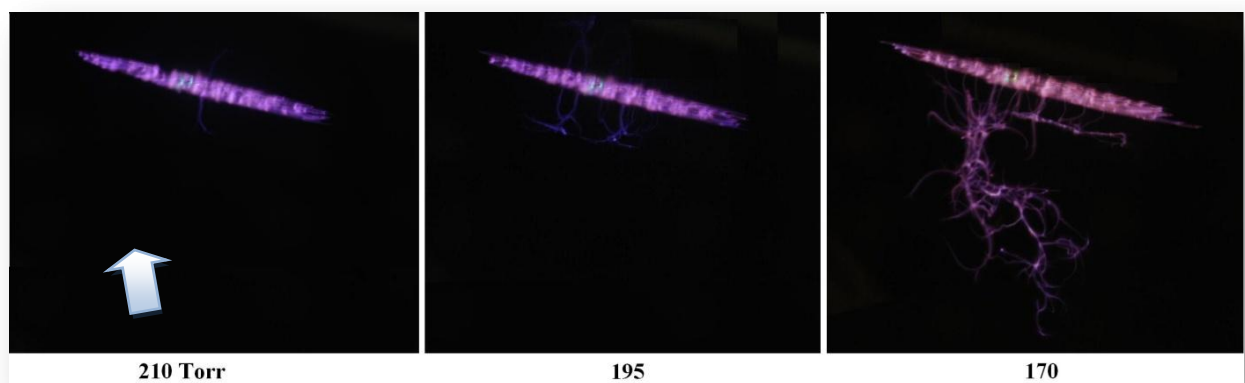


Fig.6.2. Photos of the surface discharge at $\beta = 70^\circ$ with respect to air pressure

At air pressure smaller than 200Torr takes place a separation of the discharge streamers from the surface and an exit of the streamers into the volume.

Dependence of pressure of the discharge separation from a surface on a deviation angle of a plate on a radiation direction (that is, from the axis of a focusing mirror) is shown in Fig.6.3.

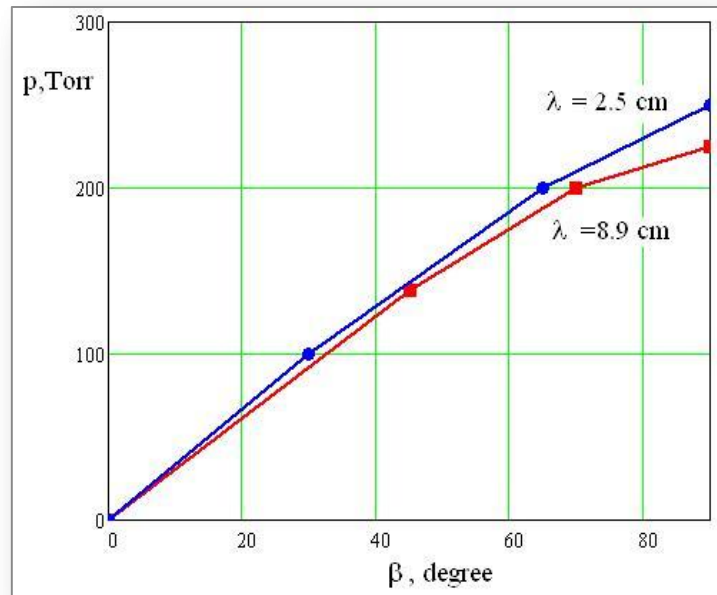
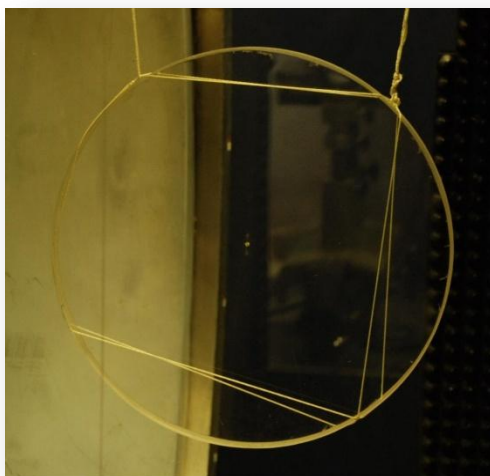


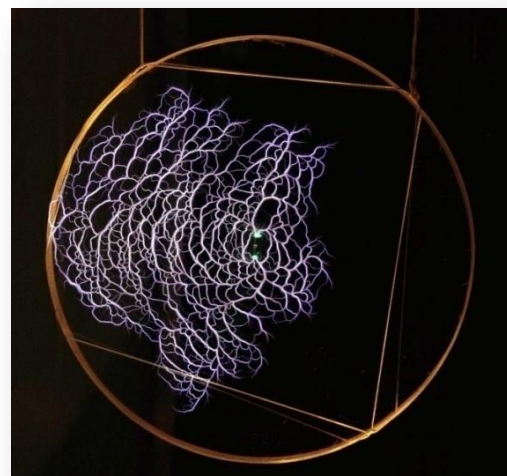
Fig.6.3. A dependence of discharge separation from the surface on a turn angle of the plate β . $E_0 = 4.5\text{kV/cm}$

During discussion of the surface discharge properties there was a question on behavior of the discharge on a border of the longitudinally placed dielectric plate. It has been experimentally revealed, that under certain conditions the streamer surface discharge continues to develop in volume in a direction of a radiation source.

Researches of the longitudinal surface discharge were carried out with use of the quartz disk of 20cm in diameter and of 1.0cm thickness. The disk was fastened by means of nonmetallic threads as it is shown in **Fig.6.4a**. At atmospheric pressure and the maximum amplitude of the electric field strength in the focus $E_0 = 4.5\text{kV/cm}$ and coincidence of the center of the disk and position of the initiator with the position of the radiation focus the front of the surface discharge during the pulse of $43\mu\text{s}$ has time to reach the disk edge and then it stops (see **Fig.6.4.b**).



(a)



(b)

Fig.6.4. (a) The-quartz disk kept by means of nonmetallic threads. (b) the-surface discharge at atmospheric pressure of air, initiated by non resonant vibrator located in the focus

of MW radiation and in the center of the disk. The focusing mirror is located on the left. $E_0 = 4.5\text{kV/cm}$.

Speed of the streamer surface discharge propagation depends on the field amplitude in the place of the discharge front passage. At the central location of the initiator the propagation speed decreases in the process of removal from the radiation focus. However it is possible to create conditions at which the discharge front should extend with accelerating speed. For this purpose the quartz disk has been removed from the mirror at the distance at which its edge turned to a mirror, coincided with position of the radiation focus. In this case the discharge front quickly reached edges of a disk and stopped.

It has been experimentally revealed that at reaching of the discharge front of the dielectric edge in certain conditions takes place a transition of the surface discharge into the volumetric streamer discharge. In Fig.6.5 one can see photos of the discharge on the surface and in the vicinity of the quartz disk obtained at various values of air pressure in the test chamber. It is seen, that at pressure above 270Torr the discharge front remains on the border of the dielectric and the discharge does not move into the volume. However, at pressure below 270Torr at reaching of the dielectric edge the discharge breaks in the usual form of the volumetric streamer discharge, directing in the mirror direction.

The obtained boundary value coincides with the border obtained for the transversal discharge to within identification of the discharge type. In Fig.6.6 the obtained boundary value $p=270\text{Torr}$ at $E_0 = 4.5\text{kV/cm}$ is shown by a dark blue square. It is seen, that the obtained value lies down on the border of the discharge occurrence in the volume measured earlier for the transversal discharge.

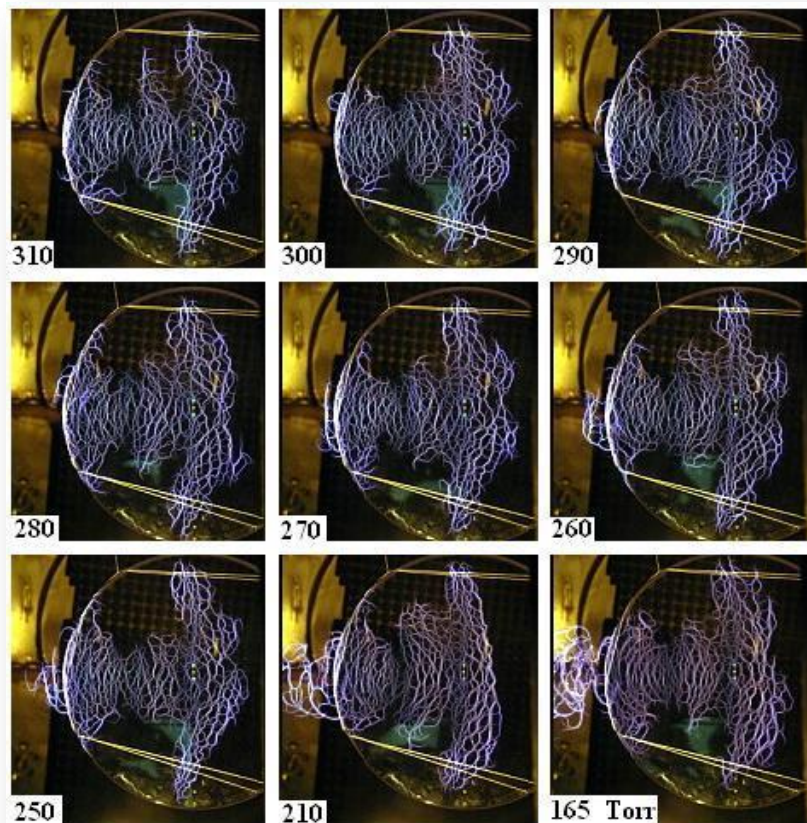


Fig.6.5. The discharge on the disc and in its vicinity at different air pressure in the chamber

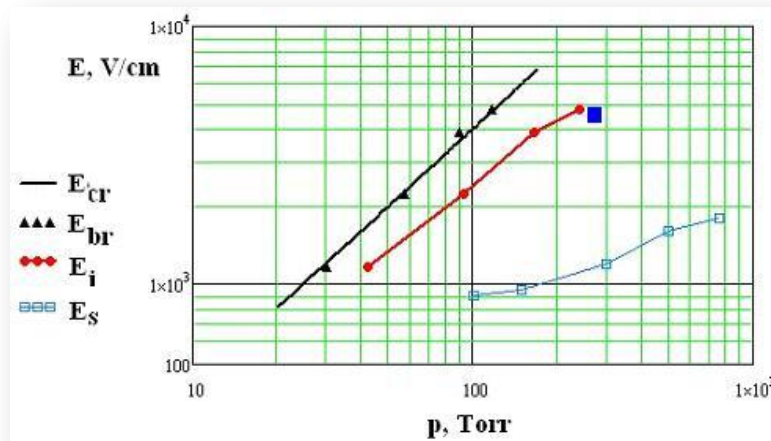


Fig.6.6. The border dividing the surface and the surface-volumetric discharges ; a red line with points - the transversal discharge, a dark blue square - an exit into the volume from the edge of the longitudinally located plate, $\lambda = 8.9\text{cm}$. (The black line - the critical field, the blue line - the border of the attached discharge)

Let's mark, that the discharge exit into the volume at the longitudinal location of the dielectric occurs only from the edge of the dielectric plate and does not occur from the surface.

6.2. Experiments at the wavelength of 2.5 cm

On the wavelength of 2.5cm was investigated an ability of the streamer subcritical MW discharge to remain the surface one with respect to angular position of the dielectric plate concerning the Pointing vector Π . A position of the dielectric plate concerning the vector of the electric field strength remains invariable - parallel to it.

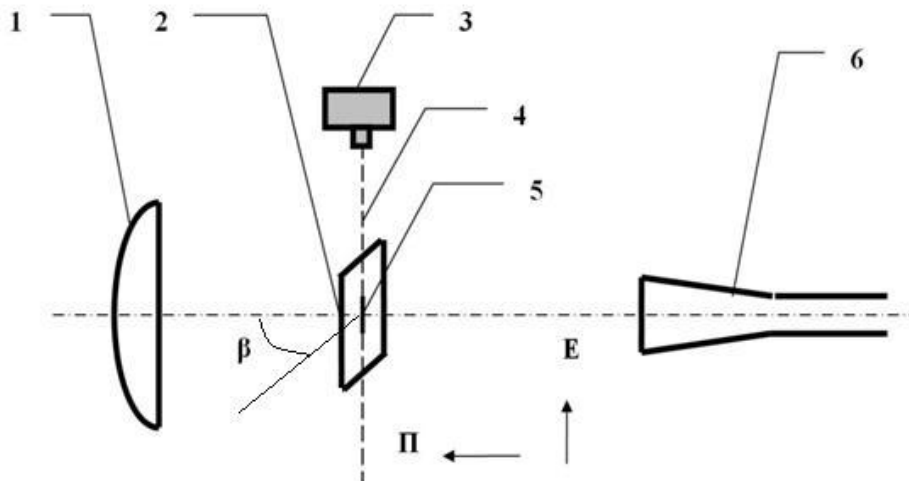


Fig.6.7. A scheme of the experiment (1- a focusing mirror, 2- a dielectric plate, 3- a photo camera , 4- a focal plane, 5- an initiator, 6- MW radiator)

Experimental researches were carried out under the scheme presented in **Fig.6.7**, with use of the plate of plexiglas of 3mm thickness. On the plate surface in the center the initiator in the form of a copper conductor piece of 0.2mm in diameter and of 9.5mm in length has been located. The plate was located in the focal plane so that the initiator has been directed in parallel to the vector of electric field strength. During researches an intensity of the electric field remained constant and sufficient for initiation of the streamer subcritical MW discharge.

The spatial location of the plate was varied concerning the focal plane in the range of angles β from -90° to 90° . At $\beta = +90^\circ$ the plate is orthogonal to the Pointing vector Π and the initiator is located from a side of the mirror. Experiments are carried out in pressure range p from 60 to 760 Torr.

Detection of MW discharges was made by a photo registration method. Ability of the streamer subcritical MW discharge to remain the surface one depending on angular position of the dielectric plate concerning the focal plane (and consequently, concerning the Pointing vector Π) at various pressure is characterized by a matrix of photos in Fig.3.8.

It is revealed that in the range of angles β from -90° to 0° , when the initiator is located in a shade of the dielectric plate concerning the flux of the MW radiation reflected from the mirror, up to the longitudinal orientation of the plate, the streamer subcritical MW discharge remains the surface one. In a range of angles β from 0° to 90° in the process of the angle increase β the MW discharge loses the ability to remain the surface one.

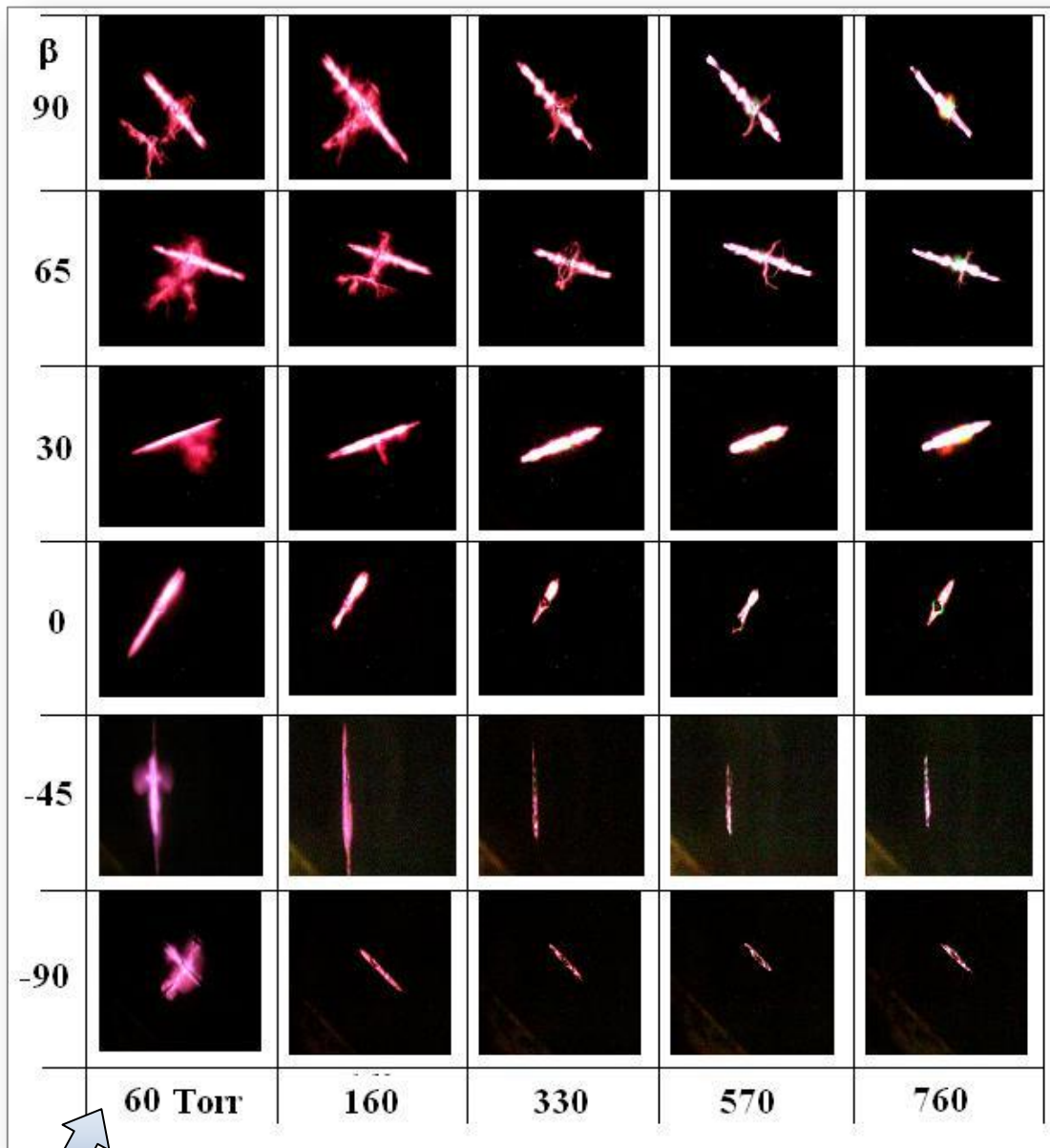


Fig.6.8. Matrix of discharge photos. By the blue arrow is indicated the radiation direction, $\lambda = 2.5 \text{ cm}$

Chapter 7. Determination of streamer channels growth rate when they form a developed structure of subcritical surface MW discharge, and speed of discharge front propagation over a surface of a dielectric in EM wave (Tasks 17 - 20)

The most actual discharge parameter, a speed of its front, was determined as the ration of the traversed way to time of MW radiation pulse. Data on a distribution distance as have allowed to obtain the developed schemes of photographing allowed to obtain data on a propagation distance at longitudinal, and a transversal location of the dielectric plate (see **Fig.5.3**). Speed of the streamer development was measured by means of the high-speed frame to frame camera. Experiments have shown that the propagation speeds in both variants of the dielectric layer placing have close values. Therefore the most detailed investigation was carried out with the longitudinal discharge.

7.1. Experiments with the wavelength of 8.9cm

Typical photo of the MW discharge at a longitudinal arrangement is represented in **Fig.7.1**. It corresponds to $p = 760\text{Torr}$ and $E_0 = 6.5\text{kV/cm}$, i.e. to the field under criticality of $\xi \approx 5$. In this photo two bright points correspond to the ends of the initiator with the linear size $2L = 12\text{mm}$ (a diameter of a disk - 20cm). From the photo follows that the discharge looks like a set of plasma channels. Channels are pressed to the plate surface to which the initiator is fixed.

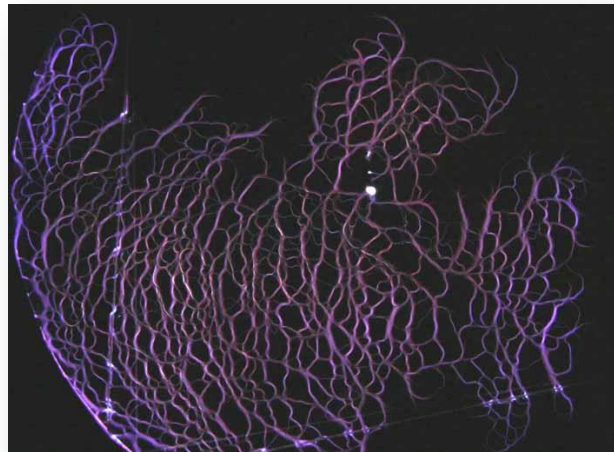


Fig.7.1. Longitudinal surface subcritical MW discharge initiated by the EM vibrator ($\lambda=8.9\text{cm}$; $\tau_{pul} = 40\mu\text{s}$)

In **Fig.7.2** examples of the longitudinal surface discharge propagation are represented at various under criticality degree: (a) - $E_0/E_{cr}=0.2$, (b) - $E_0/E_{cr}=0.03$. In the first case the discharge front speed is $\sim 3\text{ km/s}$, and in the second case - $\sim 1\text{ km/s}$. The streamer propagation speed is approximately by 1.5-2 times greater the speed of the discharge network front.

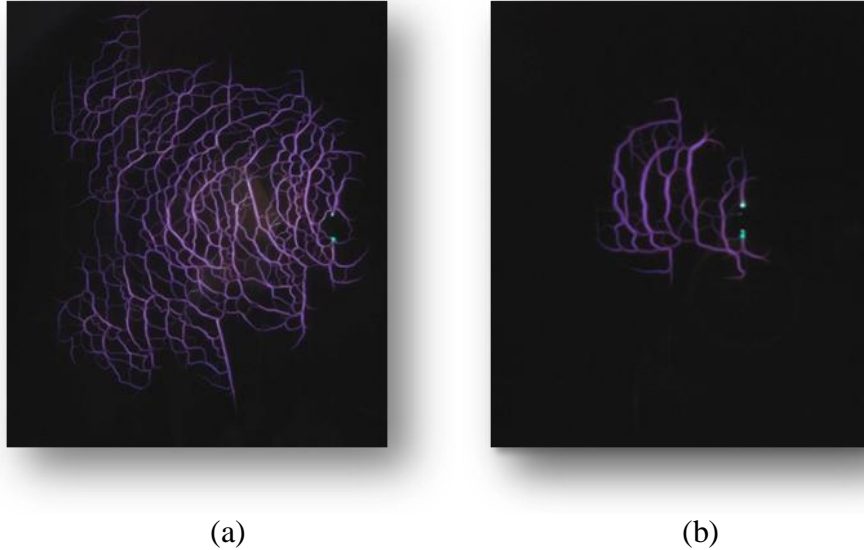


Fig.7.2. Examples of the discharge propagation at different level of under criticality

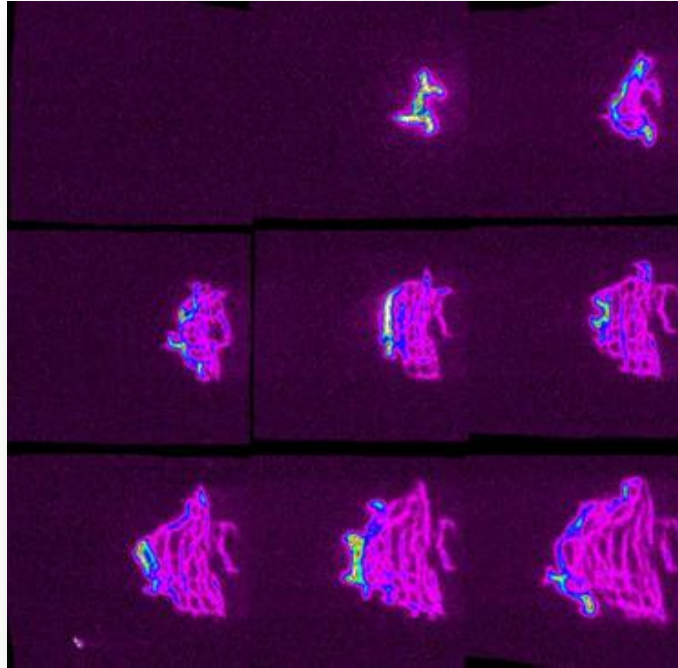


Fig.7.3. Frame to frame scan of the longitudinal subcritical MW discharge initiated by EM vibrator ($\tau_{exp}=0.1 \mu s$; $\tau_p=2 \mu s$, $\lambda = 8.9cm$).

In **Fig.7.3** frame to frame photo scan of the discharge represented in Fig.7.1 is placed. On it an exposure time each frame is $\tau_{exp}=0.1 \mu s$, and the pause time between frames is $\tau_p=2 \mu s$. Nine shots have time sequence from left to right in each line and from top to down on rows. From photos follows, that discharge channels, starting from poles of the initiator, fill a surface of the dielectric propagating mainly towards the radiation exciting the MW discharge. In them it is possible to estimate an average speed of the discharge front propagation $v_{fr} \approx 5 km/s$.

In photos it is seen, that at the discharge front there are brighter extended mainly along E_0 sections of plasma channels. Behind the discharge front up to the initiator brightness of a luminescence of the discharge channels is approximately the same.

In Fig.7.4 one can see the similar to Fig.7.3 photo scan of the initial stage of development of this discharge development with the same time $\tau_{exp}=0.1\mu s$, but with $\tau_p=0.2\mu s$.

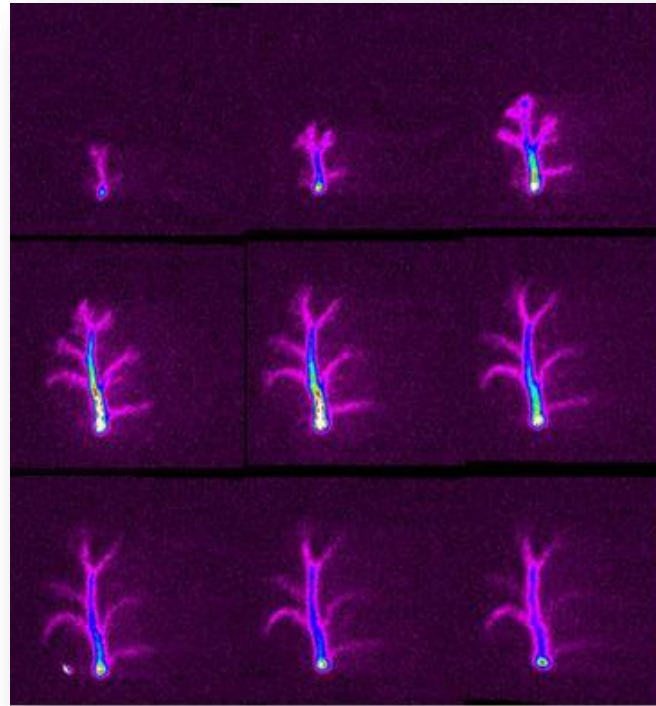


Fig.7.4. Initial stage frame to frame scan of the longitudinal subcritical MW discharge initiated by EM vibrator ($\tau_{exp}=0.1\mu s$; $\tau_p=0.2\mu s$, $\lambda = 8.9cm$)

In frames below brightly shining plasma "point" specifies a position of the top end of the initiator. Its diameter $2a = 0.15mm$ allows to estimate a scale of discharge plasma channels spreading over a surface of the dielectric. A propagation speed of the streamer channels at the initial stage is ~ 5 km/s

Data of measurements of discharge front propagation speed obtained by two methods are represented in **Table 7-1** and **Table 7-2**.

Table 7-1

Pressure.Torr	10	30	45	60	90	200	300	500	760
speed, km/s	7.0	4.2	3.5	3.0	3.5	2.8	2.8	2.9	2.6

Table 7-2

Pressure,Torr	210	270	300	330	380	760
speed, km/s	4.0	4.0	3.25	2.5	2.25	2.5

7.2. Experiments with the wavelength of 2.5cm

Experimental determination of the streamer channels growth velocity v_{str} , forming the developed structure of subcritical transversal surface MW discharge and speed of the transversal discharge front propagation over a surface of the dielectric v_{fr} in EM wave with $\lambda = 2.5cm$.

Experiment was carried out on the polyethylene film located in a focal plane of the vacuum chamber to perpendicularly to the Pointing vector. The initiator in the form of a copper

wire of 9.5mm in length and 0.2mm in diameter was placed on the surface in the center of the film in parallel to the vector of MW field strength on a side of the generator.

For determination of the transversal discharge propagation front over a surface of the dielectric a duration of the MW pulse was varied from 3 to 30μs, and in the range from 3 to 10μs with a step of 1μs. Pressure in the chamber was changed in a range from 90 to 760Torr. The characteristic form of the transversal discharge is shown in **Fig.7.5**.

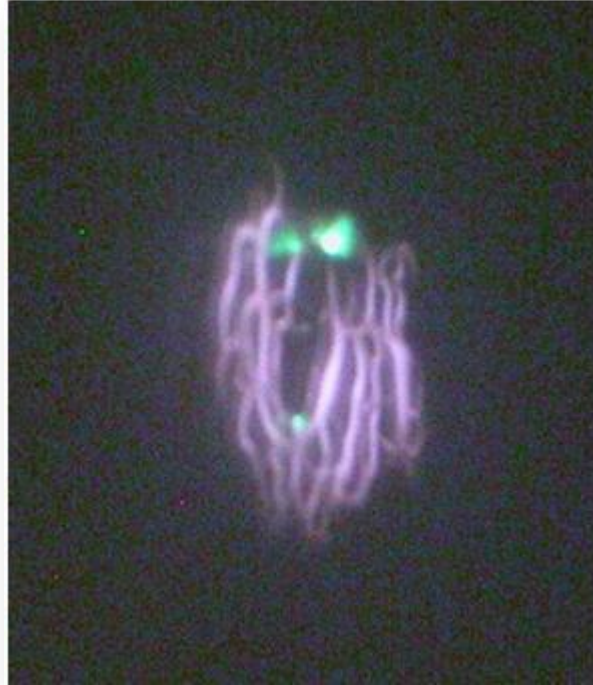


Fig.7.5. Typical form of the transversal discharge. $\lambda = 2.5\text{cm}$

Transversal discharge spot is more or less symmetrical concerning the initiator, therefore during the experiments a diameter of the spot was measured, and dependence of the diameter size of the spot of the transversal discharge on duration of the MW pulse and pressure in the chamber was determined.

The front speed of front of the transversal discharge was determined under the formula

$$V_{fr} = \frac{D_{av}}{2 \cdot \tau} \quad (7.1)$$

where

τ – MW pulse duration;

D_{av} – average diameter of the spot in photos (for a scale we used sizes of the initiator).

The propagation speed of the transversal discharge poorly depends on pressure in the investigated range, it somewhat decreases with pressure growth. The graph of the transversal discharge front change in time is represented in **Fig.7.6**. At the initial stage of the discharge development (units of micro seconds) the transversal discharge front speed V_{fr} reaches 1km/s, and then its speed sharply falls (for 30 μs almost for an order of magnitude) and the size of the transversal discharge spot practically does not vary.

Falling of the propagation speed with increase in duration of the pulse is determined by a radius of a focal spot in the given installation out of which the propagation is impossible. As the characteristic of the discharge process it is necessary to accept a speed value during the initial moment - 1.3 km/s.

Experiments with the longitudinal discharge were carried out on the polyethylene film located in a vertical plane along the axis of the chamber in the area of the focus. The initiator in

the form of a copper wire of 9.5mm in length 9.5mm and 0.2mm in diameter was placed on the surface in the center of a film in parallel to the vector of MW field strength.

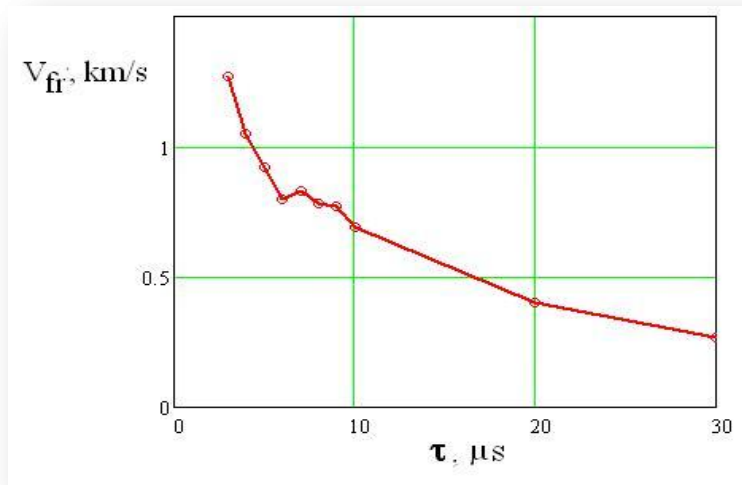


Fig.7.6. Discharge front propagation velocity dependence with respect to MW pulse duration.
 $\lambda = 2.5\text{cm}$

For determination of the longitudinal discharge front propagation speed over a surface the dielectric a duration of MW pulse was varied from 3 to 30 μs , at that in the range from 3 to 10 μs with a step of 1 μs . Pressure in the chamber was changed in a range from 90 to 760 Torr. During the experiments a dependence of the longitudinal discharge spot diameter size on duration of the MW pulse and pressure in the chamber was determined. The characteristic form of such a discharge is shown in **Fig.7.7**.

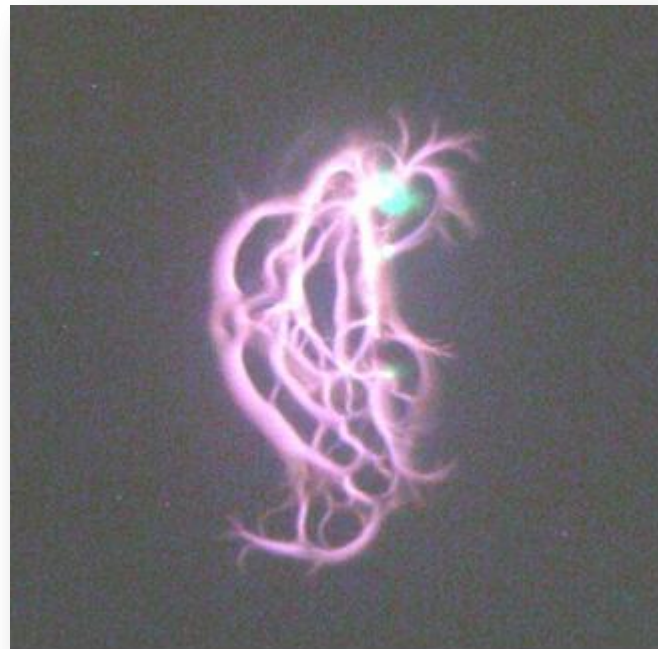


Fig.7.7. A typical appearance of the longitudinal discharge on the dielectric film $\lambda=2.5\text{cm}$

For the longitudinal discharge it makes sense to determine both the speed of the front towards the mirror v_{fr1} , and towards the horn of the MW generator v_{fr2} .

Graphs of the longitudinal discharge front speed change towards the mirror (a dark blue continuous line) and towards the horn (a dark blue dashed line) are represented in **Fig.7.8**.

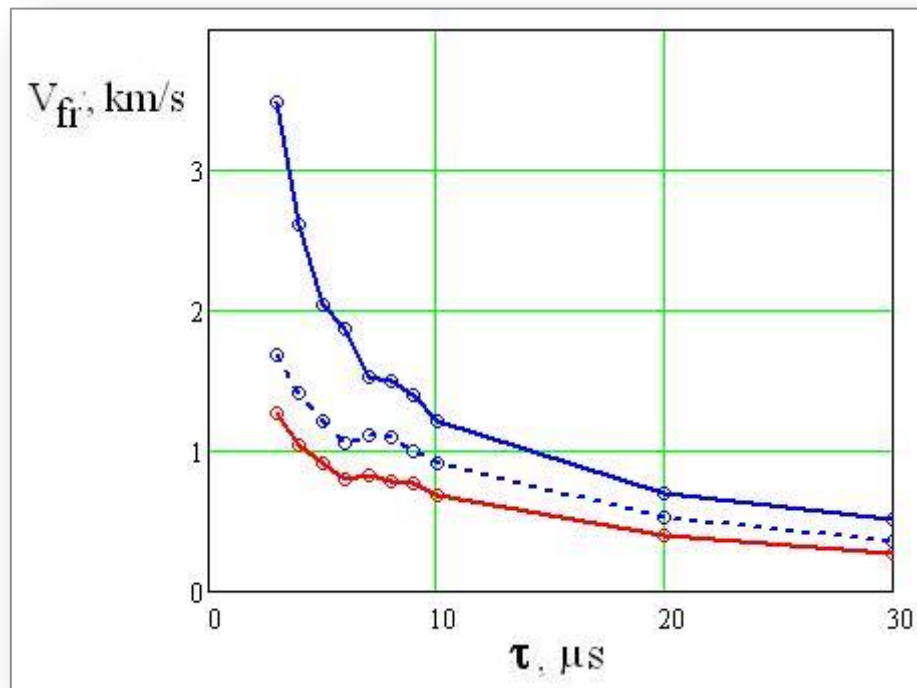


Fig.7.8. Longitudinal discharge front speed towards the mirror (solid blue line) and in the horn side V_{fr2} (blue dashed line) in comparison with the front of the transversal discharge (red solid line). $\lambda = 2.5\text{cm}$

As it is seen from the graphs, initial speeds of the longitudinal discharge front towards the mirror and towards the horn at the initial stage differ approximately by two times, but get the same value through 20-30 μs after beginning of the MW pulse. It is caused by the same reason - limitation of the focal area in the longitudinal direction. Speeds of the longitudinal discharge front are higher than those of the transversal discharge and they are 3.5 and 1.8 km/s for V_{fr1} and V_{fr2} respectively.

Chapter 8. Influence of the form of a dielectric surface on propagation characteristics of surface subcritical SW discharge with developed streamer structure (Tasks 21 и 22)

As a surface of the complex form the most typical case of a curvilinear surface - dielectric tubes of various diameters with placing of the initiator on an external and internal surfaces has been chosen. Two variants of an arrangement of tubes were investigated: vertically across the axis of the system and horizontally along the system axis. In both cases the initiator has been oriented along the electric field (or in parallel to the envelope, or over an azimuth).

8.1. Experiments at the wavelength 8.9cm

In the installation with the wavelength of MW radiation 8.5cm the experiment on initiation of the streamer discharge on a cylindrical dielectric surface with curvature radius of 36.5mm is made. The discharge was excited on internally surface of a quartz tube of 73mm in diameter at a 2mm thickness of a wall. The initiator in the form of the EM vibrator was placed along the cylinder envelope on its internal surface, distant concerning the mirror. The cylinder

axis is focused along the electric field vector (vertically). In **Fig.8.1** one can see the photo of the discharge made along the axis of the tube at atmospheric pressure and at the electric field amplitude in the initiator location of $E_0 = 2.5\text{kV/cm}$.

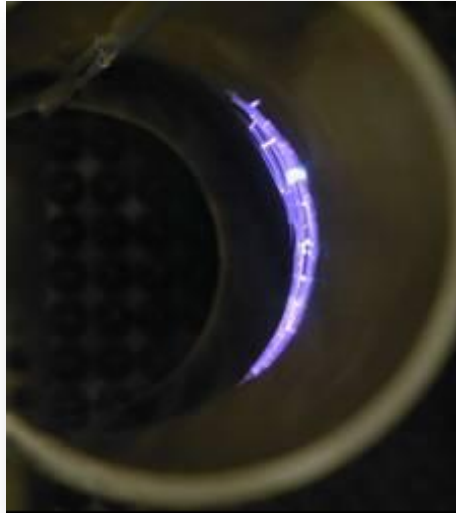


Fig.8.1. Discharge photo at the initiator location on the internal surface of the quartz tube

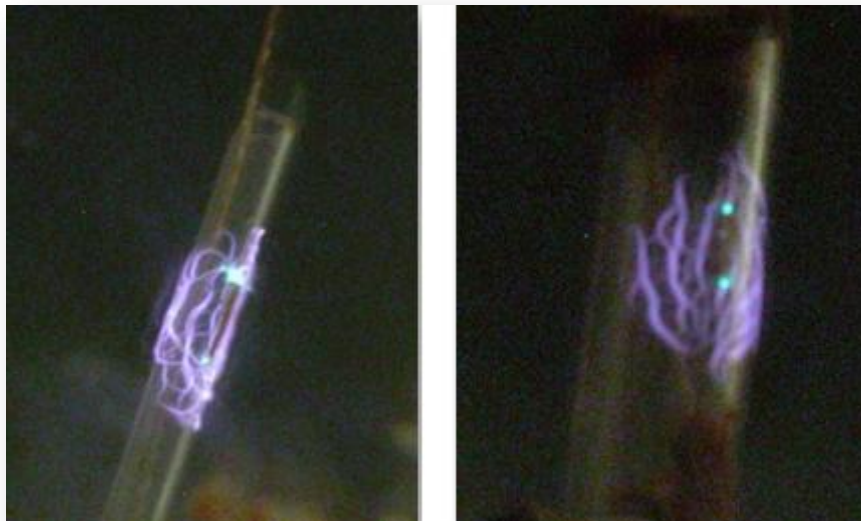
The discharge, keeping its streamer character, develops along a surface, reaching limits of radiation caustics out of which the electric field is small.

Experiment with the horizontal orientation of the tube axis and an arrangement of the initiator over the azimuth has given similar results.

8.2. Experiments at the wavelength of 2.5cm

a) Experiment with “transversal” placing of a tube

Experiment with “transversal” placing of a tube (the tube axis is directed vertically) was carried out with glass tubes of 5 and 15mm in diameter under the scheme similar to experiments with a polyethylene film.



Ø 5mm

Ø 15mm

Fig.8.2. Typical appearance of the “transversal” subcritical MW discharge with developed streamer structure on the glass tubes. $\lambda = 2.5\text{cm}$

Typical appearance of the “transversal” subcritical MW discharge with developed streamer structure on the glass tubes is presented in **Fig.8.2**.

Obtained data are represented in **Table 8.1**.

Table 8.1

№	$\tau, \mu\text{s}$	R, mm	$v_{fr}, \text{km/s}$	D_{tube}, mm
1	3	3	1,0	15
2	5	3,5	0,70	
3	7	5	0,71	
4	10	6,5	0,65	
5	20	8	0,40	
6	30	8	0,27	
7	3	5	1.6	5
8	5	5	1.0	
9	7	5.5	0.8	
10	10	5	0.5	
11	20	6	0.3	
12	30	5.5	0.2	

R - discharge spot maximal radius during time τ .

It is seen from **Table 8.1** that on a tube of 5mm in diameter the area of the transversal discharge reaches the maximum size in time smaller than $3\mu\text{s}$. Dynamics of the transversal discharge speed change on a glass tube in diameter of 15mm in diameter is close to corresponding dynamics on a surface of a polyethylene film.

b) Experiment with the longitudinal placing of a tube

Experiments with a "longitudinal" arrangement of the tube (the tube axis is located horizontally and the initiator is located over the azimuth) also were carried out with glass tubes of 5 and 15mm in diameter under the similar scheme. The characteristic form of the "longitudinal" subcritical MW discharge with developed streamer structure on glass tubes for $\tau = 3\mu\text{s}$ is represented in **Fig.8.3**.

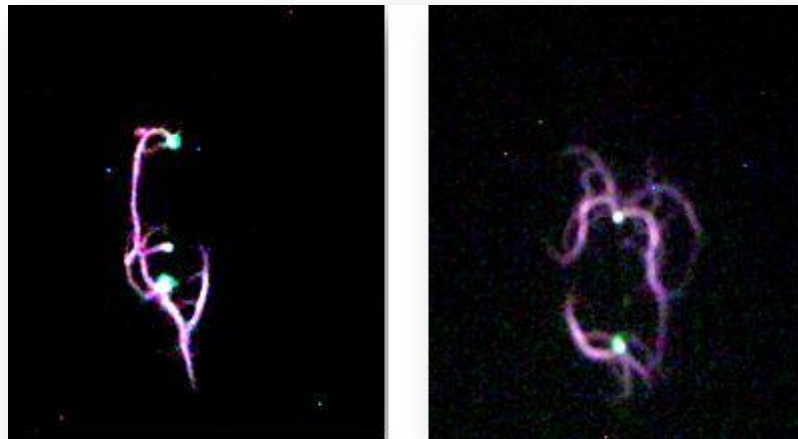
On a tube of 5mm in diameter 5mm the sizes of plasma formation practically do not vary at MW pulse duration starting from $3\mu\text{s}$ and above.

Data on dynamics of change of the sizes of a plasma spot for a tube of 15mm in diameter are represented in **Table 8.2**.

Table 8.2

$\tau, \mu\text{s}$	p, Torr												$v_{fr2}, \text{km/s}$
	90	150	240	330	360	450	480	540	600	660	707	760	
3	7,4	6,9	7,9	6,6	6,1	7,1	7,4	5,3	9,8	8,7	6,9	10,3	2,51
5	13,2	7,7	6,6	5,8	9,0	7,1	10,3	7,1	7,4	8,2	8,5	9,0	1,67
7	15,1	10,8	8,5	7,1	6,6	6,6	8,2	8,5	10,8	9,5	9,8	8,7	1,31
10	17,5	14,8	6,9	7,1	10,3	9,5	8,5	7,4	9,0	14,3	10,8	12,4	1,07
20	14,8	10,6	9,0	11,4	9,6	8,7	7,7	9,5	12,4	9,3	11,4	9,3	0,54

30	16,9	11,9	9,3	11,9	11,1	7,7	13,0	6,9	13,0	15,1	10,6	10,6	0,38
----	------	------	-----	------	------	-----	------	-----	------	------	------	------	------



Ø 5mm

Ø 15mm

Fig.8.3. Typical appearance of “longitudinal” subcritical MW discharge with the developed streamer structure on glass tubes (a view from a face of the tube), $\tau = 3 \mu s$

Thus, in all cases the surface discharge propagates with the speed exceeding 1km/s and weakly depending on pressure at $p > 60 \text{ Torr}$.

Chapter 9. Experimental investigation of the surface streamer MW discharge features in different conditions (Tasks 24 - 30)

9.1. Experimental estimation of air temperature T in streamer plasma channels of transversal and longitudinal subcritical and deeply subcritical surface MW discharge in EM beam with $\lambda = 8.9 \text{ cm}$ by means of discharge ignition in a flammable propane-air mixture.

One of ways of estimation from below gas temperatures in the streamer channel of the surface MW discharge is demonstration of its ability to initiate gas mixture burning. As a gas mixture we used a stoichiometric mixture of air with propane. The mixture was injected into discharge area through a quartz tube with internal diameter of 2.5cm as it is shown in **Fig.9.1**.

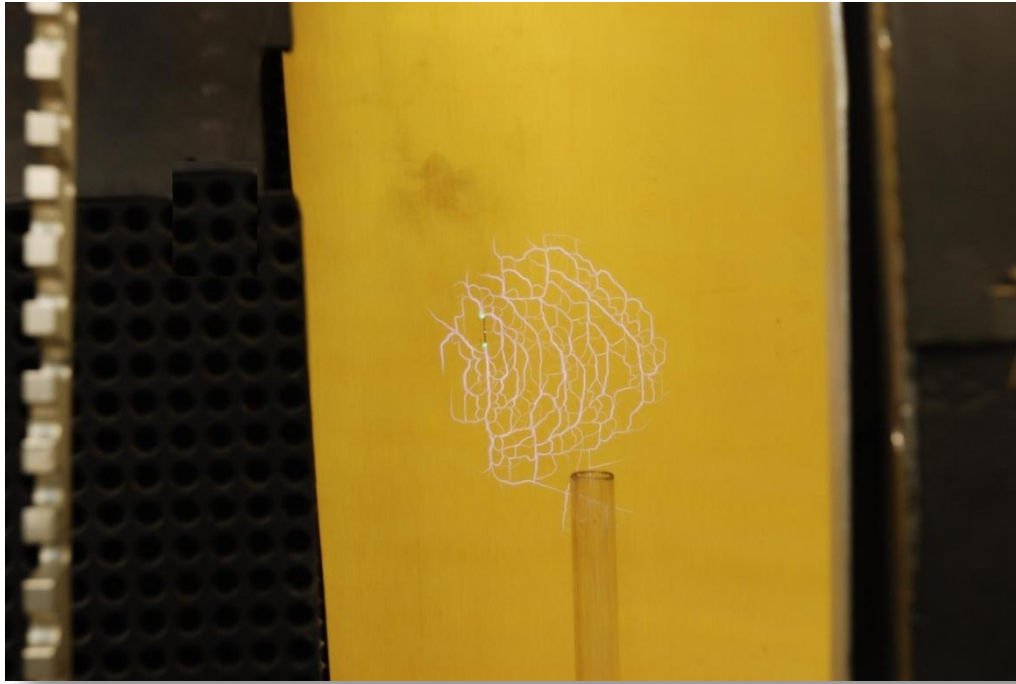


Fig.9.1. Experiment formulation: initiated surface MW discharge on the textolite plate and the quartz tube for propane-air mixture injection

The initiator was located on a surface of the plate in the field of the radiation focus. Experiments were carried out at atmospheric pressure with discharges of various type, such as subcritical (see **Fig.9.2**), and deeply subcritical (see **Fig.9.3**). The discharge type was determined by the electric field value in the focus varied in limits from 5kV/cm to 1kV/cm with a help of the attenuator in the waveguide path connecting the generator with the antenna system.

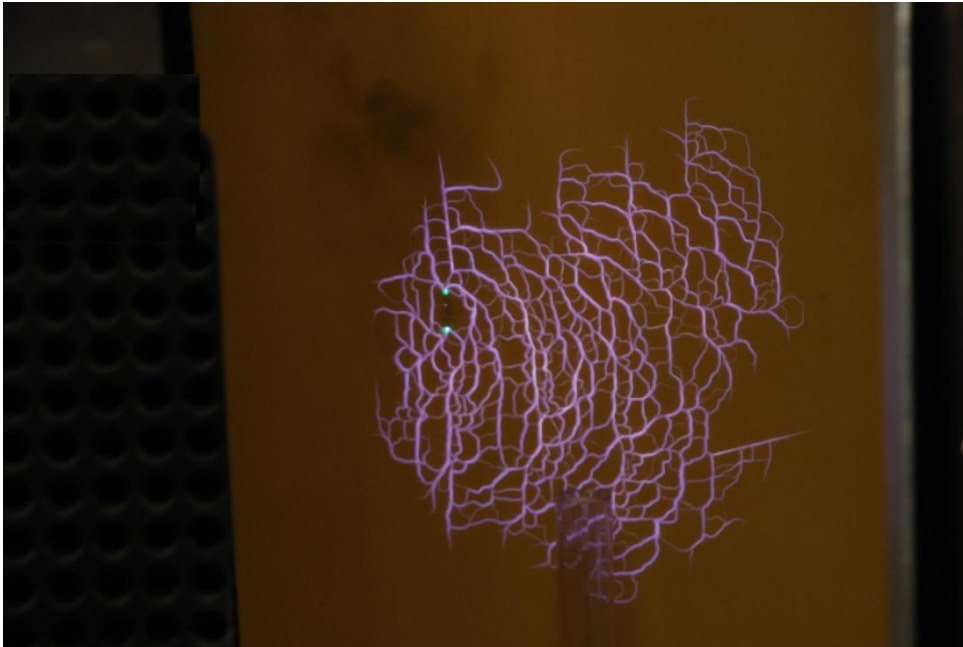


Fig.9.2. Initiated subcritical surface MW discharge without injection of propane-air mixture. $E_0=5\text{kV/cm}$

The angle of a wave falling on a plate was varied in limits from 0 to 90° that corresponds to a longitudinal and transversal location of the plate. The duration of MW radiation pulse – 40μs.



Fig.9.3. Initiated deeply subcritical surface MW discharge without injection of propane-air mixture. $E_0=1.5\text{kV/cm}$

Experiments have shown that at any positions of the dielectric plate and any type of the surface discharge an ignition of the gas mixture takes place by one pulse. In **Fig.9.4** photos of discharge zones at flammable mixture injection are shown: (a) - at pulse injection of small quantity of the gas mixture, (b) - at quasi-stationary injection. The fact of ignition of the gas mixture testifies that gas temperature in the streamer channels of the surface discharge (the same as and in the volumetric) is substantially higher the ignition temperature of the mixture which is ~ 2000K for the stoichiometric propane-air mixture.

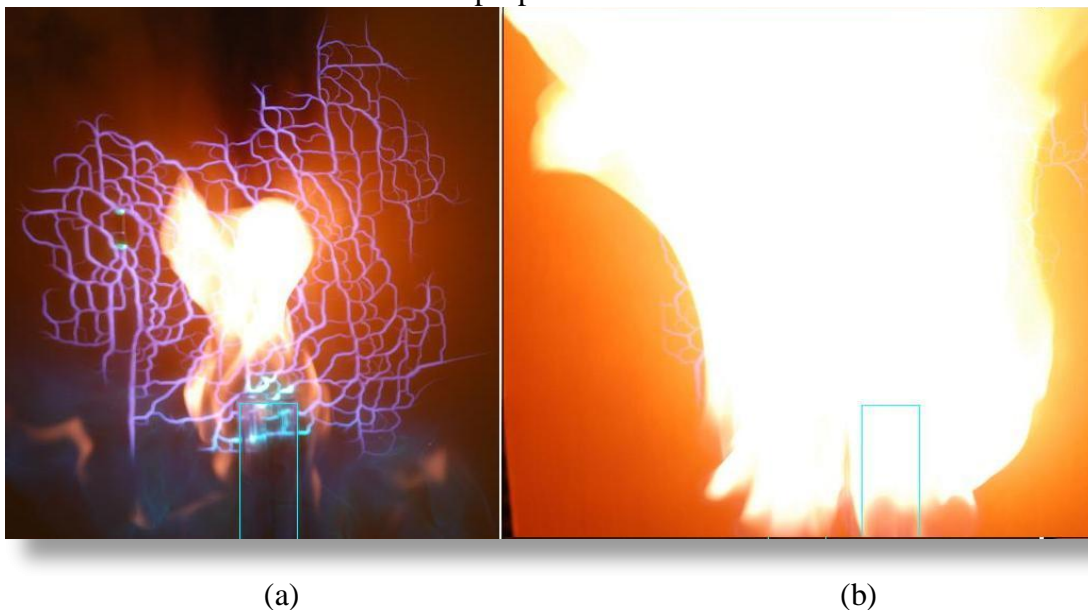
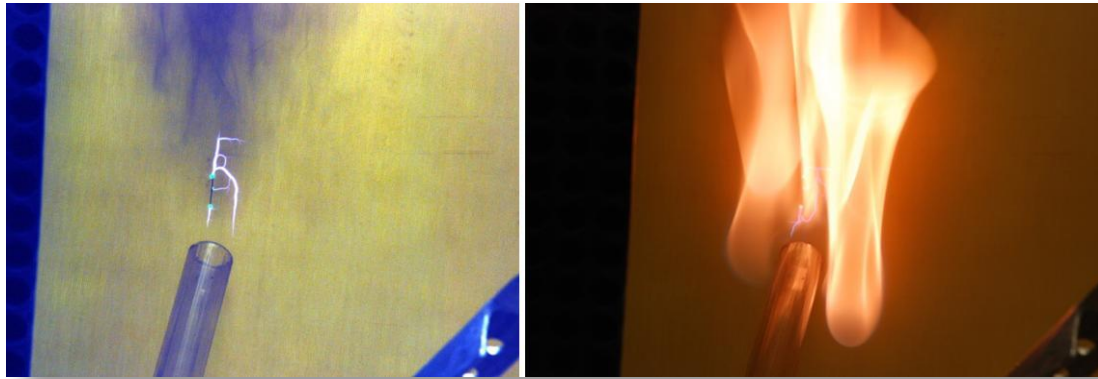


Fig.9.4. The ignition of the injected flammable mixture initiated by the surface MW discharge, (a) - at pulse injection of small quantity of the gas mixture, (b) - at the quasi-stationary injection

The **Fig.9.5** shows the photo of air-prone mix combustion initiated by deeply subcritical surface discharge.



(a)

(b)

Fig.9.5. *The ignition of the injected flammable mixture initiated by the surface deeply subcritical MW discharge, (a) - the discharge in air (one can see the initiator and a tube of the mixture injection), (b) - the discharge at the stoichiometric mixture injection to the discharge area.*

9.2. Studying of the transversal and longitudinal surface discharge properties in EM beam with $\lambda = 8.9\text{cm}$ at discharge ignition in humid air

In experiments the humidity change in the working chamber method described in the Final report under the Project ISTC №2820p was applied. The experimental scheme on the humidity influence on the surface initiated MW discharge is represented in **Fig.9.6**. In the test chamber the open vessel with water was placed. The adjustable electric heater was placed in water, it was - the ohmic resistance fed by an external source. After chamber pumping out to small values of pressure the chamber was filled with atmospheric air through a dehumidifier to required pressure. Then the heater was switched on and over the humidity sensor the required value of humidity in the test chamber was set. For the humidity control the sensor IH-3602L (HYCAL Sensing Products Inc.) was used. Values of humidity were varied from 30% to 100% (to a dew-point). The gas temperature in the chamber in all experiments was equaled to the room one, that was supervised by the thermometer placed in the test chamber.

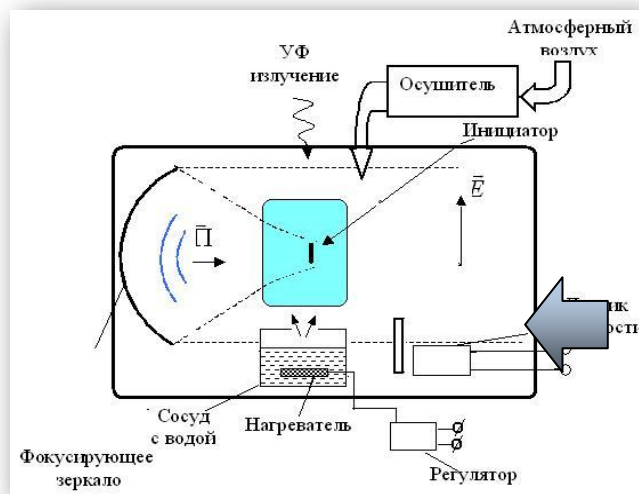
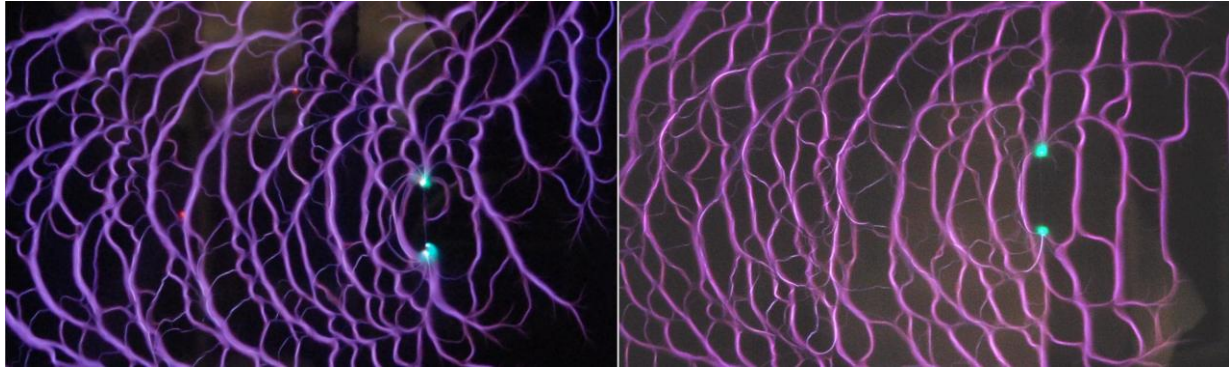


Fig.9.6. *Experimental scheme with varying humidity in the test chamber*

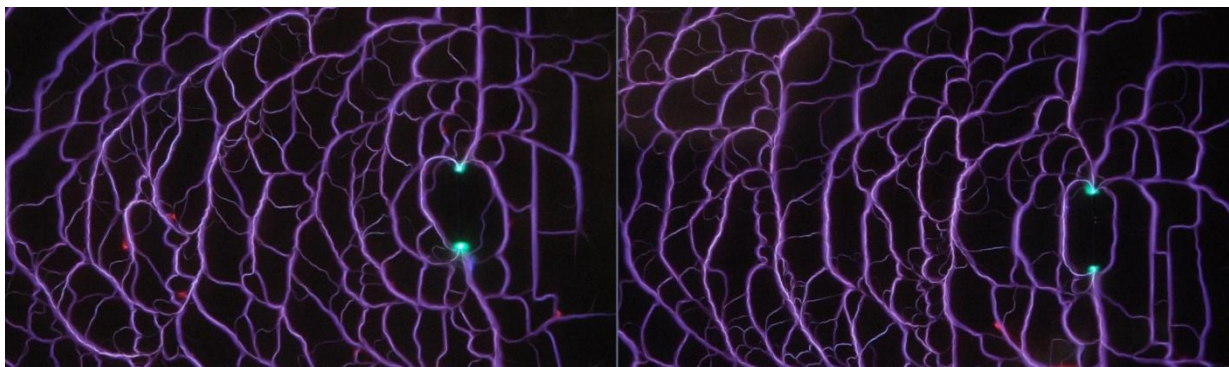
In Fig.9.7 and Fig.9.8 are presented photos of MW subcritical discharges in humid air on a surface of a textolite plate at pressures 300 and 760Torr respectively at a humidity of 30% (a) and 95% (b).



(a)

(b)

Fig.9.7. Surface initiated MW discharge in humid air: (a) - at humidity of 30% and (b) - at humidity of 95%. Pressure in the chamber is 300Torr, temperature 23C



(a)

(b)

Fig.9.8. Initiated surface MW discharge in humid air, (a) - at humidity of 30% and (b) - at humidity of 95%. Pressure in the chamber is 760Torr, Temperature - 23C.

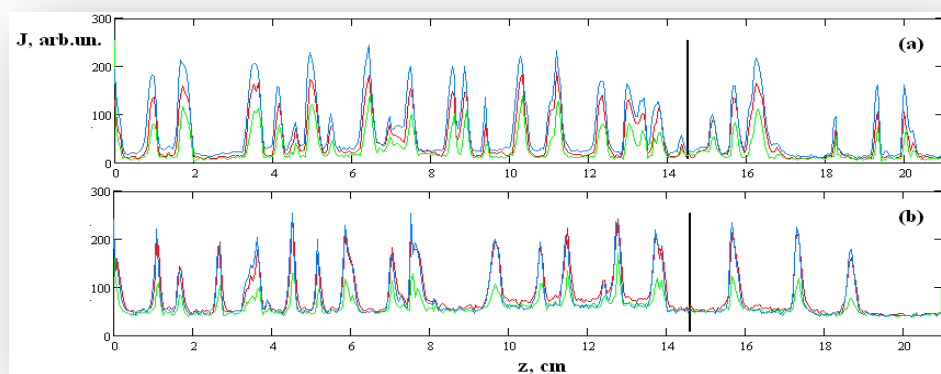


Fig.9.9. Result of photos of a Fig.9.7 densitometry over the line passing along the axis of the system. Color of lines corresponds to intensity of radiation in red, green and dark blue parts of a spectrum. (a)-at humidity of 30% and (b) at humidity of 95%. Pressure in the chamber is 300Torr, temperature 23C

Comparison of photos (a) and (b) leads to a conclusion, that humidity practically does not affect geometrical parameters of the streamer channels network. The longitudinal and transversal sizes of cells of the network do not depend on humidity and pressure, having values $\sim \lambda/8$ and $\sim \lambda/4$. It is necessary to clarify a reason for these values.

Densitometry of color photos of **Fig.9.7** in red, green and dark blue parts of a spectrum has specified in prevalence of a dark blue component in the radiation spectrum of the surface streamer discharge that testifies in favor of high gas temperature in channels (**Fig.9.9**). The characteristic diameter of the developed channel determined by half-height of intensity curves for each channel, at pressure 300Torr is irrespectively of humidity value 0.1-0.3cm, that quite agrees with the estimations carried out earlier for volumetric discharges.

Experiments have shown that humidity of air, even at it 100%, does not influence essentially parameters the surface streamer discharge. Geometrical parameters of the streamer channels network (the sizes and the form of cells, radius of channels), temperature of channels, initiation conditions are not sensitive to the air humidity value.

9.3. Studying of transversal and longitudinal surface discharge properties in EM beam with $\lambda = 8.9\text{cm}$ at discharge ignition in air containing water aerosol

A formulation of experiments on discharges initiation on a dielectric surface in air with aerosol is illustrated in **Fig.9.10**.

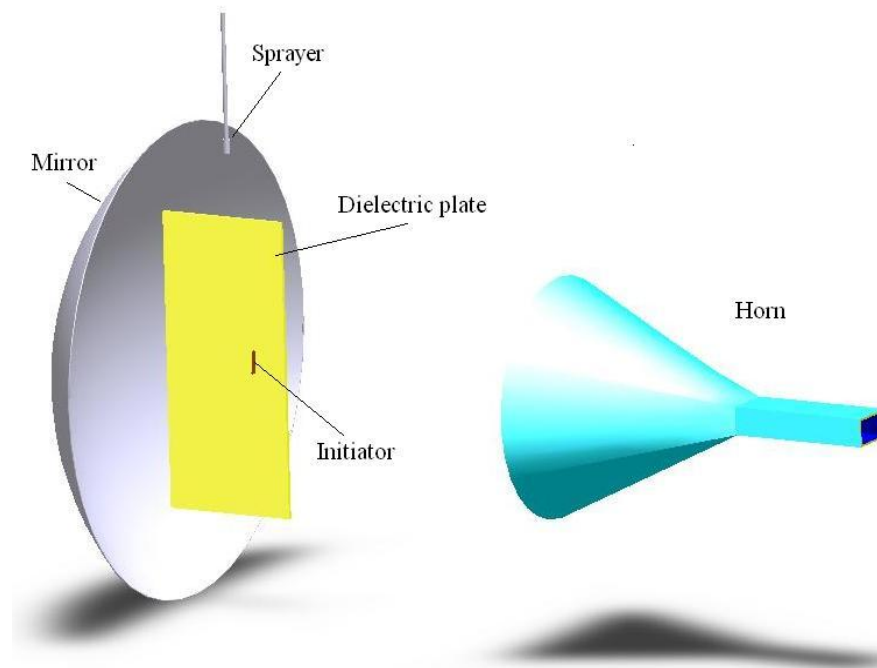


Fig.9.10. Experimental scheme of the surface discharge in air with aerosol

Into the area of the focus along the axis of the system and in parallel to the electric field of MW is located a dielectric plate of textolite with a thickness of 2mm with the initiator on its surface, it is in the form of the electromagnetic half-wave vibrator. Along the plate surface by means of a standard atomizer the stream of water aerosol was injected. The characteristic diameter of the aerosol - $50\mu\text{m}$. Water arrives in the atomizer under pressure of 4 atm. Experiments were made at atmospheric pressure in motionless air. Amplitude of the electric field in the focus is 4.5kV/cm . The pulse duration is $43\mu\text{s}$. For the control of a surface condition the plate was illuminated by a lamp.

A photo of the illuminating lamp and the atomizer in operation is represented in Fig.9.11. Water mass flow rate in the atomizer was $\sim 1\text{g/s}$, aerosol concentration in the discharge area is $n_{\text{aer}} \approx 200\text{cm}^{-3}$ at their diameter $d_{\text{aer}} = 50 \div 80\mu\text{m}$ [6].



Fig.9.11. A photo of the sprayer (to the right) and the illuminating lamp (to the left)

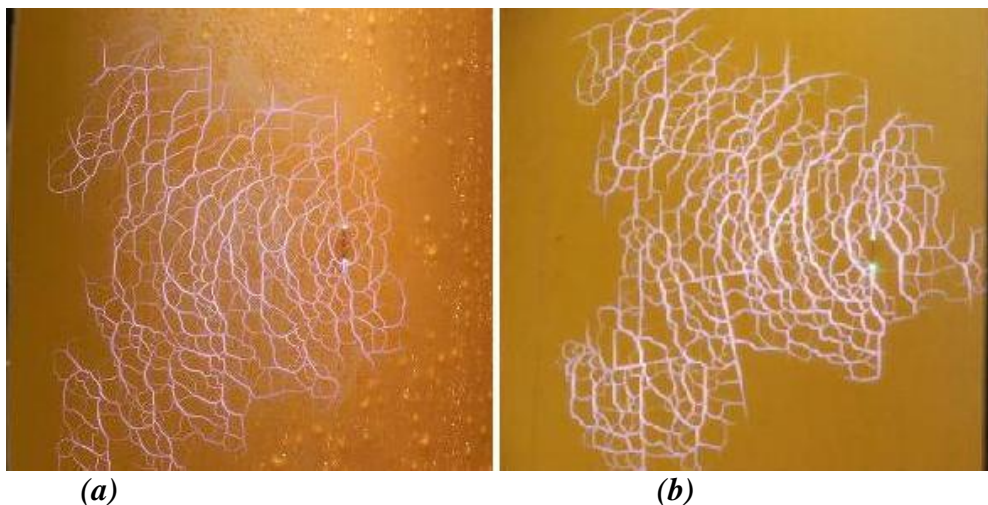


Fig.9.12. Surface discharge on a longitudinally placed textolite plate: (a) in air with aerosol flow, (b) – in air without aerosol flow. Air pressure - 1 atm, $E_0=4.5\text{kV/cm}$

Experiments have shown that the surface discharge on the textolite plate irrigated by a stream of aerosols, directed along it, develops with other things being equal in the same borders, as on a dry plate in air without aerosols.

In Fig.9.12 a discharge photo on the surface of the textolite plate in the stream of aerosols (a) is compared with the photo of the discharge obtained earlier⁵ without a stream of aerosols (b). Presence of aerosols in air practically does not influence on initiation and development of the surface discharge.

The surface washed by a stream of aerosols, is moistened non-uniformly. In a zone covered by the surface discharge, drops are not formed. In it the surface is covered by a thin sheet of water. Out of this zone large drops hang. It is well seen in Fig.9.13, where the plate

photos in a continuous stream of aerosols with the pulse surface discharge **(a)** and without the discharge **(b)** are represented.

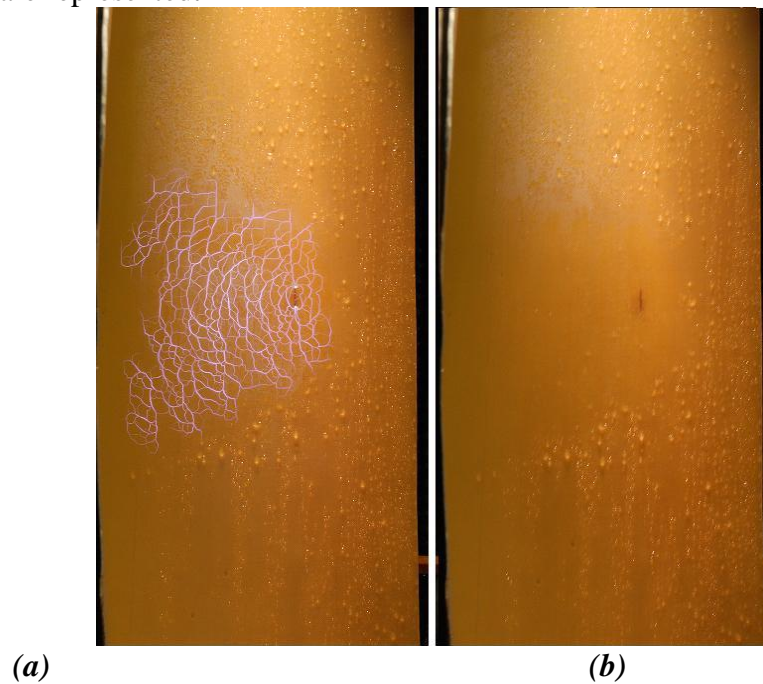


Fig.9.13. Photo of the plate surface in the aerosol stream at its longitudinal arrangement:
(a) - with the discharge, (b) - without the discharge. Air pressure 1 atm, $E_0=4.5\text{kV/cm}$

The increase in wettability of the textolite surface under the influence of the surface streamer discharge investigated earlier on polyethylene film, specifies that this influence can be revealed also on other dielectric materials with a smooth surface.

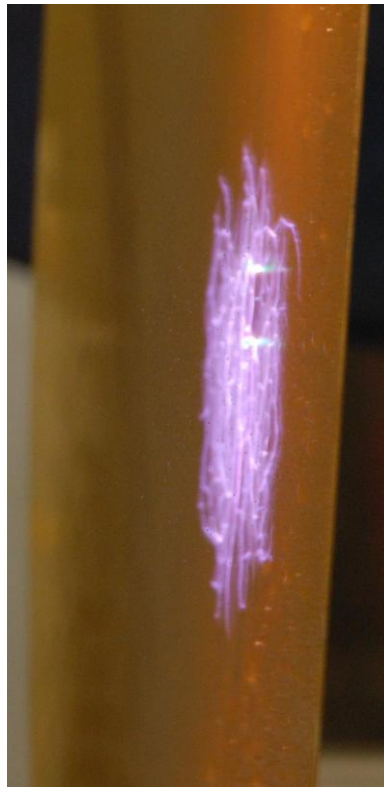


Fig.9.14. Surface discharge in air with aerosol, air pressure 1 atm, $E_0=4.5\text{kV/cm}$

The features of the surface discharge studied in the variant of the longitudinal placing of the dielectric plate in the stream of aerosols, were revealed in the same measure and at its

transversal placing. In **Fig.9.14** the photo of the transversal discharge made under the angle of $\sim 20^\circ$ to the surface of the dielectric plate is shown. The discharge develops in the caustics limits of the focal spot. Its structure and parameters of channels also are not sensitive to aerosols presence in air and a water film on the plate surface.

The streamer discharge raises a wettability of the dielectric surface, and presence of water aerosol in the air stream complicates the discharge initiation at placing of the initiator on it reducing a threshold value of air pressure to 430Torr at which the breakdown takes place.

9.4. Studying of subcritical and deeply subcritical surface discharge properties in EM beam with $\lambda = 2.5\text{cm}$ at discharge ignition in a high-speed air flow containing water aerosol

The scheme of experimental installation with EM beam with $\lambda = 2.5\text{cm}$ and the pulse duration of $30\text{ }\mu\text{s}$ is represented in **Fig.9.15**.

The formation system of air high-speed stream in the form of the submerged stream consists of the input device, the operated valve forming a stream of a nozzle, perceiving a stream of a confuser and a receiver. The chamber with the receiver connected to it is preliminary pumped out to $p = 90\text{Torr}$. At giving on the valve of an operating signal to the valve it opens, and a leak in of air from the atmosphere to the chamber begins.

The stream is formed by the axisymmetric Laval nozzle. At initial pressure of air in the working chamber of the installation $p = 114\text{Torr}$ the nozzle forms the submerged air stream with the following parameters: a transversal diameter - 23mm; Mach number of the flow $M = 2$ at static temperature of air in the stream $T = 150\text{K}$ and a stream speed of $v = 500\text{m/s}$; a vector direction vector \mathbf{v} of the stream is collinear to the vector \mathbf{E}_0 . At increase of initial pressure in the chamber and a receiver to 700Torr the speed in the stream decreases, as it is shown in **Fig.9.16**. Dependences are calculated by the method similar to the described in the Final Report under the Project ISTC №2429p (2003), with reference to the design of the experimental stand with the wavelength 2.5cm of the MW radiation.

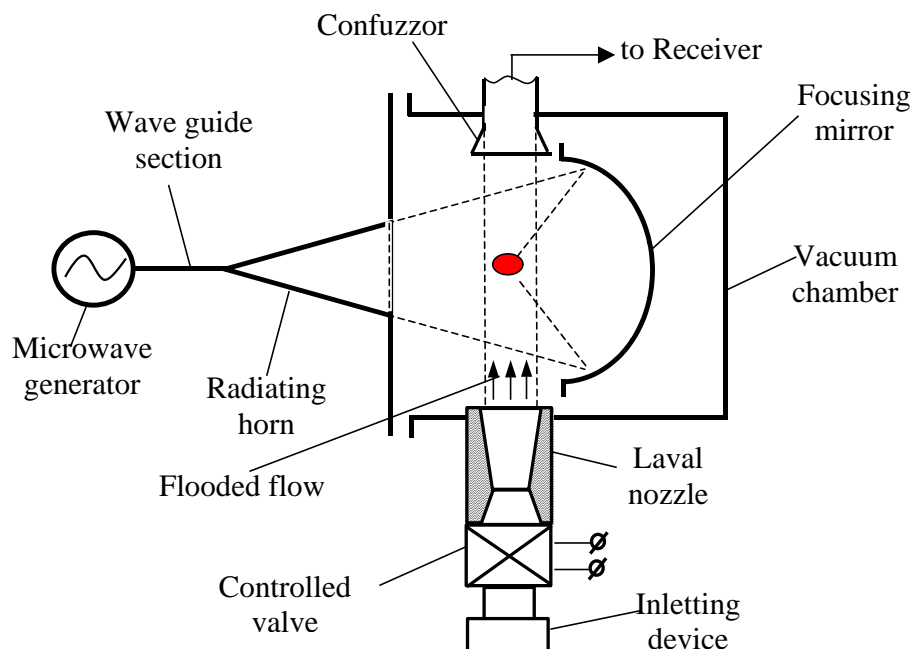


Fig.9.15. The scheme of the installation with $\lambda = 2.5\text{cm}$ completed by devices for creation of the supersonic submerged stream containing water aerosol

The initiator in the form of a copper wire of 9.5mm in length and 0.2mm in diameter was settled down on a surface in the centre of the plate of glass textolite of 0.5mm in the thickness in parallel to the MW field strength on a side of the generator.

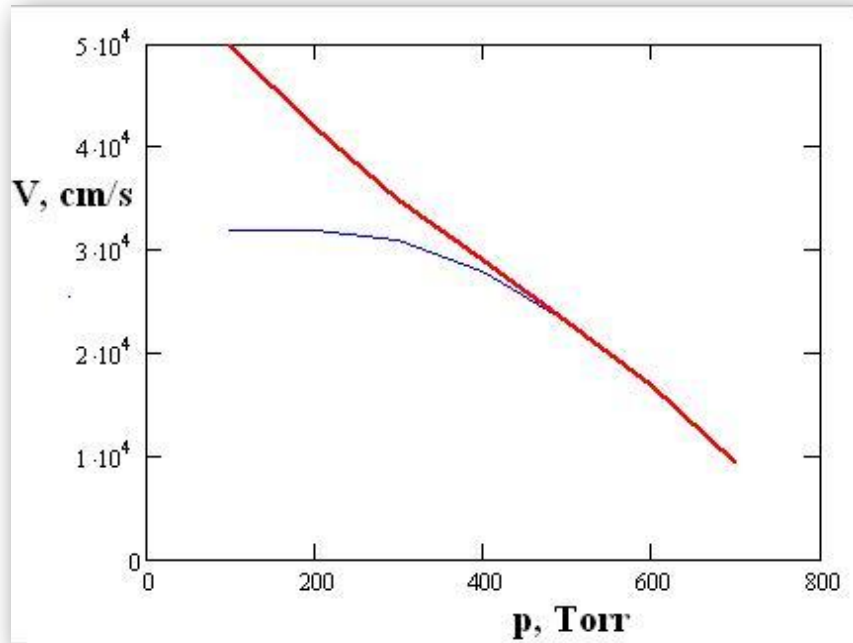


Fig.9.16. A speed of an air stream with the aerosol, a dark blue curve - a speed of the stream in a critical section of the nozzle, a red curve - a speed of the stream at a nozzle exit

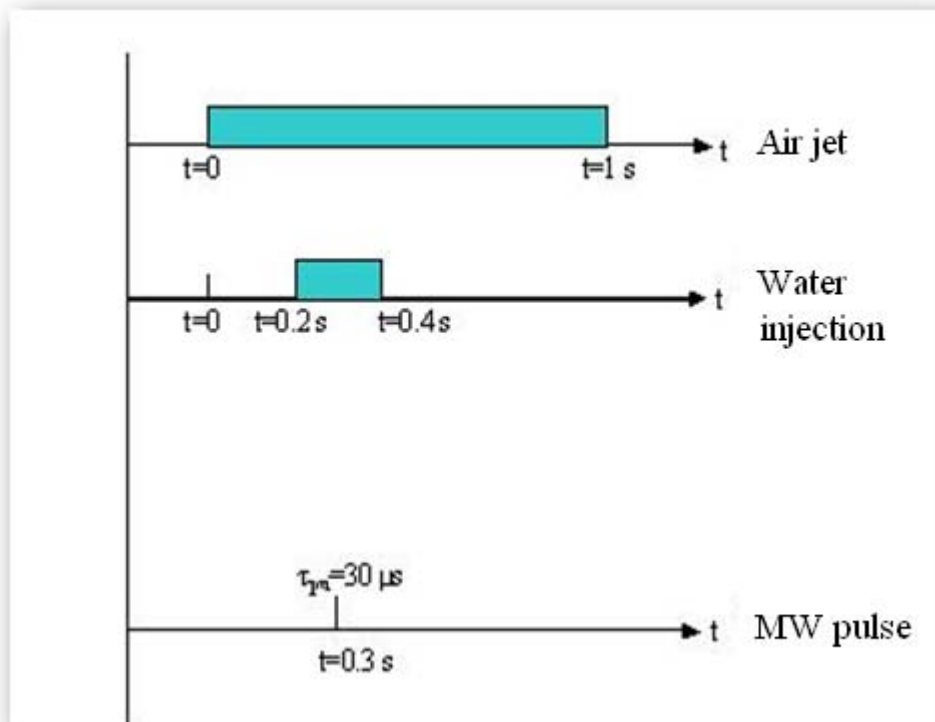


Fig.9.17. Temporary sequence of the installation equipment switching on

In the input device takes place water injection to the air stream. For this purpose over the input device pipe diameter of the input device the tube with holes in its lateral surface is

located. The inner diameter of the tube is equal to 10mm. Number of holes in it is 21. A diameter of each of them is 1.5mm. Water is brought to a tube by a flexible hose of 10mm in diameter from the buffer capacity of $V = 770\text{cm}^3$ volume. The electromechanical valve is included to a bringing path with a through passage of 10mm in diameter 10mm. In more details the system of injection of an aerosol in a high-speed stream of air is described in the Final technical report under the project ISTC № 2820p (2006).

The time sequence of the equipment work is represented in **Fig.9.17**. The high-speed stream of air existed during $\tau_{fl} = 1\text{s}$. Into this stream water was injected during $\tau_{wat} = 0.2\text{s}$ with some delay concerning switching of the air valve in the path of the stream formation, and a duration of the microwave pulse was $\tau_{MW} = 30\mu\text{s}$.

A scheme of creation of the air stream with the aerosol similar to those described in the Final report under the Project №2820p⁶, is represented in **Fig.9.18**.

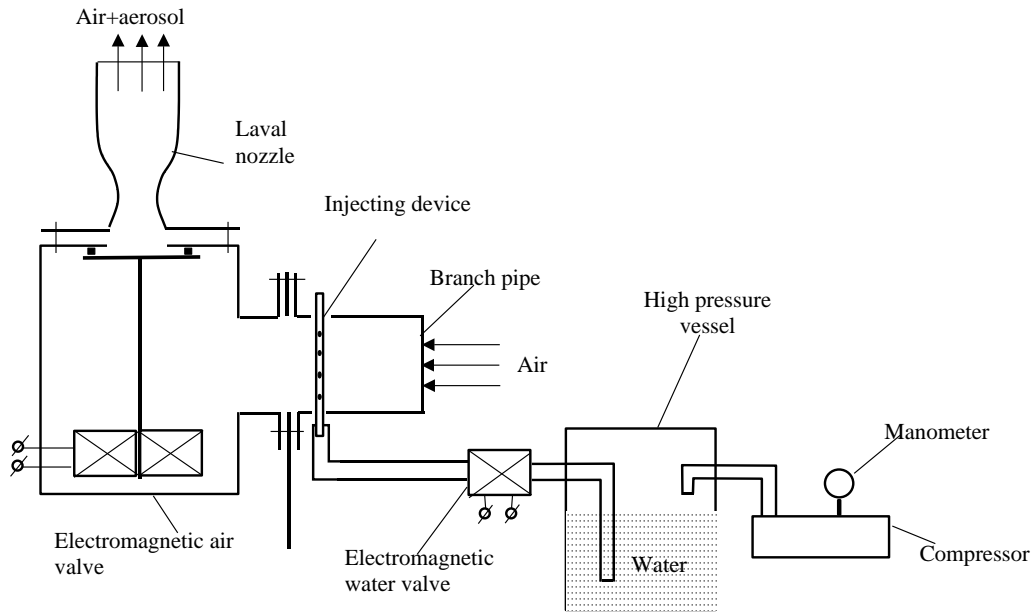


Fig.9.18. A scheme of water aerosol injection to the high-speed air stream

Air mass flow rate F and the flow velocity in the critical cross section of the Laval nozzle V_{cr} are estimated by formulas (9.1) and (9.2)

$$F_{p_1, p_2} = C_{s1} \cdot \rho_1 \cdot \pi \cdot a_{cr}^2 \cdot \sqrt{1 - \left(\frac{p_2}{p_1}\right)^{\frac{\gamma-1}{\gamma}}} \cdot \frac{2}{\gamma-1} \cdot \left(\frac{p_2}{p_1}\right)^{\frac{1}{\gamma}} \quad (9.1)$$

$$V_{cr_{p_1, p_2}} = C_{s1} \cdot \begin{cases} \sqrt{\frac{2}{\gamma+1}}, & \text{if } \frac{p_2}{p_1} < \left(\frac{2}{\gamma+1}\right)^{\frac{\gamma}{\gamma-1}} \\ \sqrt{1 - \left(\frac{p_2}{p_1}\right)^{\frac{\gamma-1}{\gamma}}} \cdot \frac{2}{\gamma-1}, & \text{if } \left(\frac{2}{\gamma+1}\right)^{\frac{\gamma}{\gamma-1}} \leq \frac{p_2}{p_1} \leq 1 \end{cases} \quad (9.2)$$

where

p_1 – atmospheric pressure,

p_2 – pressure in the working chamber,

C_{s1} – sound velocity in the atmosphere,

ρ_{s1} – air density in the atmosphere,

a_{cr} – radius of the nozzle critical cross section;

γ – adiabatic exponent.

Air mass flow rate and the velocity in the critical cross section of the Laval nozzle in experimental conditions (without water injection) estimated by formulas (9.1) and (9.2) are shown in **Fig.9.19** and **Fig.9.20**.

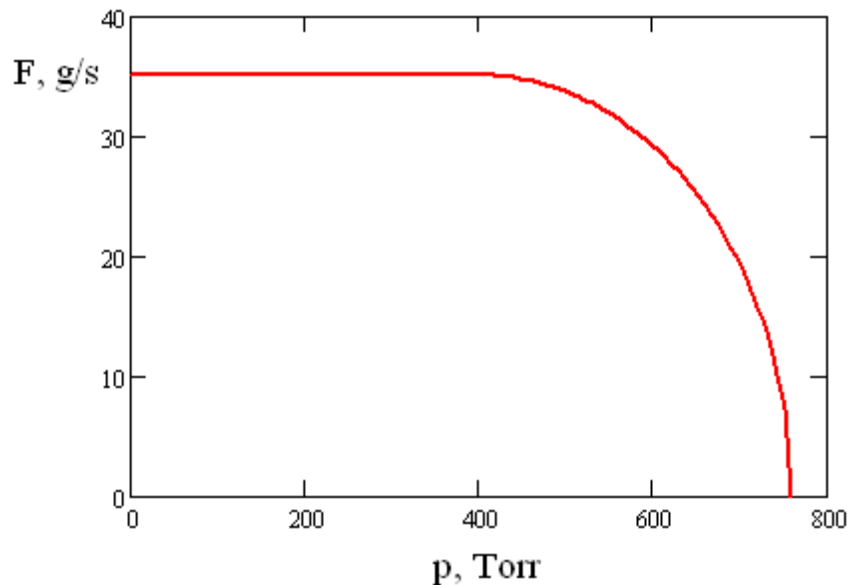


Fig.9.19. Air mass flow rate through the nozzle with respect to pressure in the working chamber

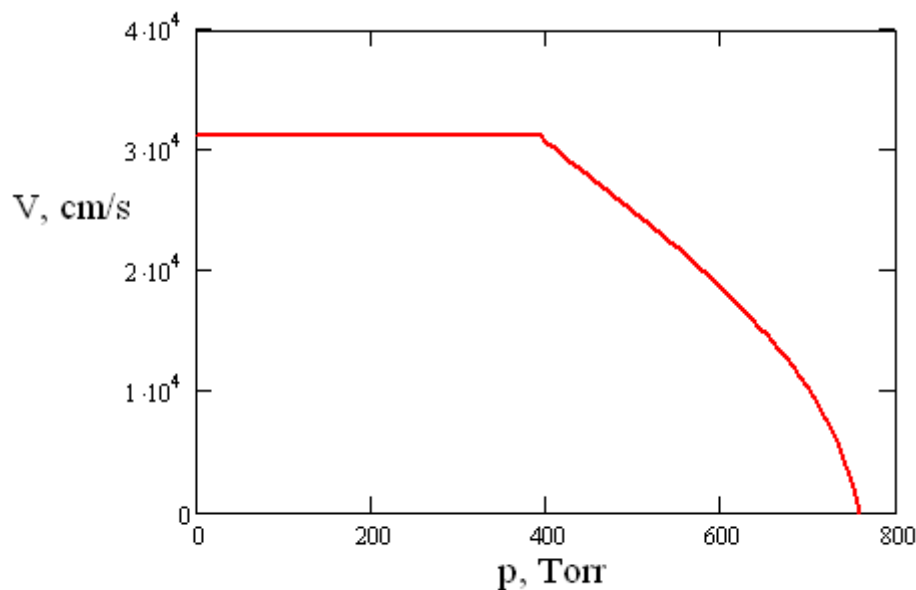


Fig.9.20. Air flow velocity in the critical cross section of the nozzle

a) Transversal discharge

It was above marked that surface discharges in motionless air at radiation with the wavelength of 8.9cm are insensitive to presence of aerosols even at atmospheric pressure. However, at the wavelength of 2.5cm an influence of aerosol components in the high-speed air stream has appeared to be essential. Therefore research of aerosols influence on the discharge has been carried out in a range of air pressure values in the working chamber and various conditions of injection at the fixed value of the electric field amplitude in the focus $E_0=3.5\text{kV/cm}$.

The influence of aerosol components in the high-speed stream of air was revealed first of all in the discharge initiation threshold change. The matrix of photos of the surface discharge on a plate at its transversal placing, corresponding to various values of air pressure in the working chamber and to various conditions of injection is represented in **Fig.9.21**. Presence of aerosols at the water expense in the injector of 40g/s and greater lowers the threshold value of discharge initiation pressure to 260Torr. At the specified expense of water and threshold value of pressure the water aerosol component presents approximately 0.1% over the volume that is close to parameters of a tropical downpour. Really, at tropical downpour precipitations reach a value of 0.01cm/s. The speed of drops can be estimated by a relation (9.3)

$$V_{drop} = \sqrt{\frac{8 \cdot g \cdot a}{3 \cdot C_x} \cdot \frac{\rho_w}{\rho_{air}}} \quad (9.3)$$

where

g – is an acceleration of the gravitation force;

C_x – aerodynamic coefficient;

ρ_w – water density;

ρ_{air} – air density.

At typical radius of drops $a \approx 0.1$ cm their speed is of the order of 5m/s. Considering the ratio of the precipitations intensity at a downpour ~ 0.01 g/(s·cm²) and speed of falling drops and the ratio of density of water and air, we obtain the value of the order $\sim 0.1\%$.

Поток с водной аэрозолью, расход воды 80г.сек									
Поток с водной аэрозолью, расход воды 40г.сек									
Поток без аэрозоля									
Без потока и аэрозоля									
р, Torr	90	180	255	285	300	420	450	534	630

Fig.9.21. A matrix of the surface discharge photos at the transversal placing of the plate corresponding to various values of air pressure in the working chamber and to various conditions of injection

One can see in the represented matrix of photos that with increase in quantity of an aerosol in air stream conditions of subcritical discharge occurrence sharply worsen and the area of the discharge existence moves to the zone of lower pressure.

The aerosol a component does not influence other characteristics of the discharge.

Worsening of the discharge initiation seemingly speaks about presence of a water layer on a surface blown by the stream with the aerosol which thickness is greater than a diameter of the initiator.






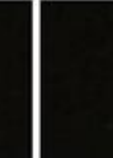








Aerosole content 146g/m ³							
Aerosole content 76g/m ³							
"shot" #	1	2	3	4	5	6	7

Fig.9.22. Typical dynamics of MW subcritical surface discharge degradation in the pulse consequence

Besides, even at the same parameters of the air stream and the same pressure after several "shots" the discharge disappears in this zone and is restored only after drying of the surface of the textolite glass plate. Typical dynamics of the subcritical discharge "degradation" is represented in Fig.9.22. It is possible to assume, that the aerosol stream covers with time the surface and the initiator on it with a sheet of water so the discharge initiation stops.

b) Longitudinal discharge

At longitudinal placing of the plate a threshold initiation pressure of the surface discharge decreases to 430Torr at the water expense of 76 g/s and to 290Torr at 14 6g/s, that follows from the matrix of photos in Fig.9.23.





































Airflow with aerosole flux 80g/s									
Airflow with aerosole flux 40g/s									
Poare airflow									
Poare still air									
p, Torr	90	180	255	285	300	420	450	534	630

Fig.9.23. A matrix of photos of the surface discharge at longitudinal placing of the plate, corresponding to various values of air pressure in the working chamber and to various conditions of injection

Near to the initiation border the discharge gets deeply subcritical character. The various behavior of the surface discharge at longitudinal and transversal placing of the dielectric plate is connected with infringement of the azimuthal symmetry of the injected submerged stream of air with the aerosol component.

9.5. Studying of subcritical and deeply subcritical surface discharge properties in EM beam with $\lambda = 2.5\text{cm}$ flow of propane-air flammable mixture at their different percentage

A scheme of the experimental installation with EM beam with $\lambda = 2.5\text{cm}$ and the pulse duration of $30\text{ }\mu\text{s}$ is presented in Fig.9.24.

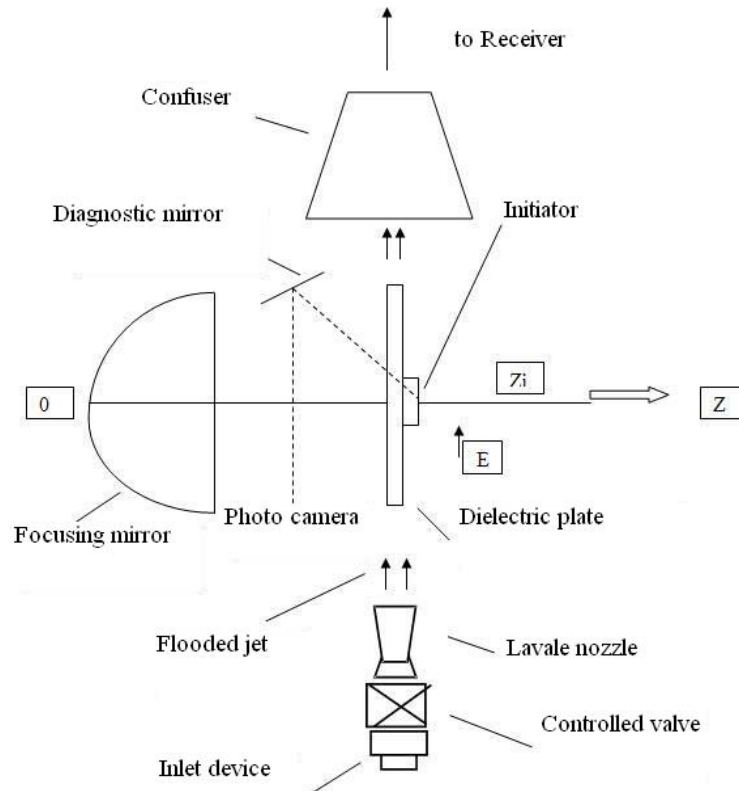


Fig.9.24. The scheme of the installation with $\lambda = 2.5\text{cm}$ completed with devices for creation of the supersonic submerged stream containing a mixture of air with propane

The system of formation of air high-speed stream in the form of the submerged stream consists of the input device, the operated valve forming a stream, of a nozzle and a receiver, perceiving this stream. The chamber with the receiver connected to it is preliminary pumped out to $p = 100\text{Torr}$. At giving on the valve of an operating signal it opens, and air leak in from the atmosphere begins in the chamber. The leak in time of air is equal to 1 s.

The stream is formed by the axisymmetrical Laval nozzle. At initial pressure of air in the working chamber of the installation $p = 114\text{Torr}$ the nozzle forms the submerged stream of air with following parameters: the transversal diameter - 28mm; Mach number of the stream $M = 2$ at static temperature of air in the stream $T = 150\text{K}$ and the stream speed $v = 500\text{m/s}$; a direction vector \mathbf{v} of the stream is collinear to the vector \mathbf{E}_0 . The textolite glass plate with the thickness of 0.5mm with the initiator is placed in the focal area of the mirror. The initiator in the form of a copper wire of 9.5mm in length 9.5mm and of 0.2mm in diameter is settled down on the surface in the center of the plate in parallel the vector of MW field strength on a side of the generator.

In the input device shown in Fig.9.24 the unit of propane injection into the air stream is built in. This scheme allows setting the certain maintenance of propane quantity in a high-speed stream of air delivered to the experimental chamber. The device of propane injection is presented in Fig.9.25.

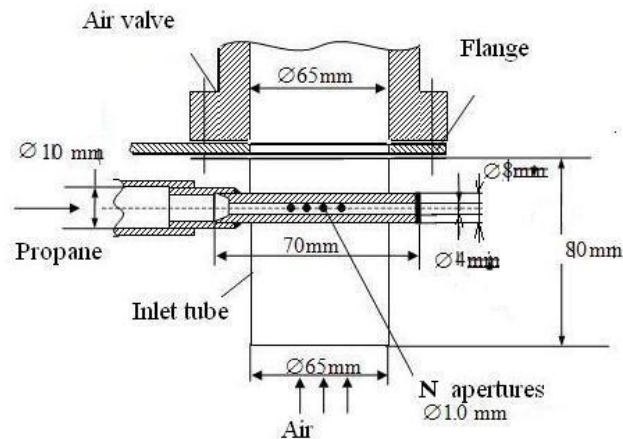


Fig.9.24. The device of propane injection into the high-speed air flow. $N \leq 15$

Time of propane injection is equal to 0.2s. The selection of photos of MW discharge gas discharge area for a single pulse with $\tau_{MW} = 30\mu s$, lighted in the high-speed stream of propane-air mixture, is presented in Fig.9.26. The discharge propagates within limits of the focal spot.

Pressure in camera 100Torr							
Equivalence ratio	1.11	1.04	1.01	0.85	0.69	0.65	0.58

Fig.9.26. Transversal discharge in propane-air mixture of different composition

The weight expense of propane F_p through the injector holes was varied in a range from 8.2 to 5g/s. Its dependence on excess pressure in a balloon with propane is shown in Fig.9.27.

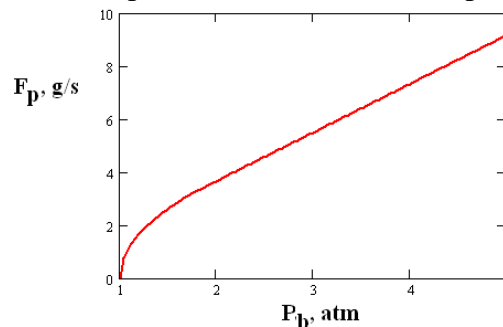


Fig.9.27. The weight expense of propane F_p through the injector holes with respect to pressure in the balloon with propane

Air expense through the nozzle with respect to pressure in the working chamber shown in Fig.9.28 and at pressure in the chamber of 100Torr is equal 106g/s.

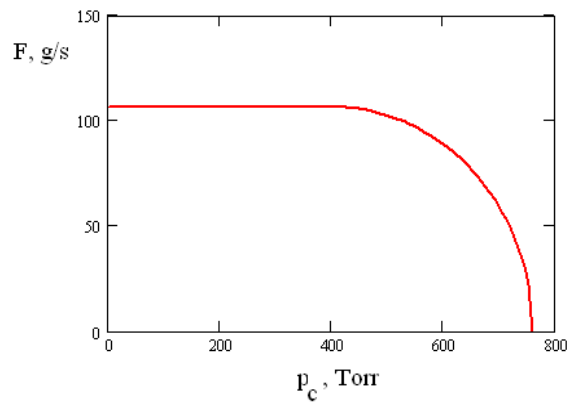


Fig.9.28. Air expense through a nozzle with respect to pressure in the working chamber

Experiments have shown, that the surface MW discharge both the transversal and longitudinal are capable to ignite air-propane mixture in all range of values of fuel excess coefficient $0.6 \div 1.2$ used in the experiment. At the of fuel excess coefficient exceeding the value 1, in the discharge spectrum essential increase of level of lines in a band 385-388 nm (see Fig.9.29) is observed.

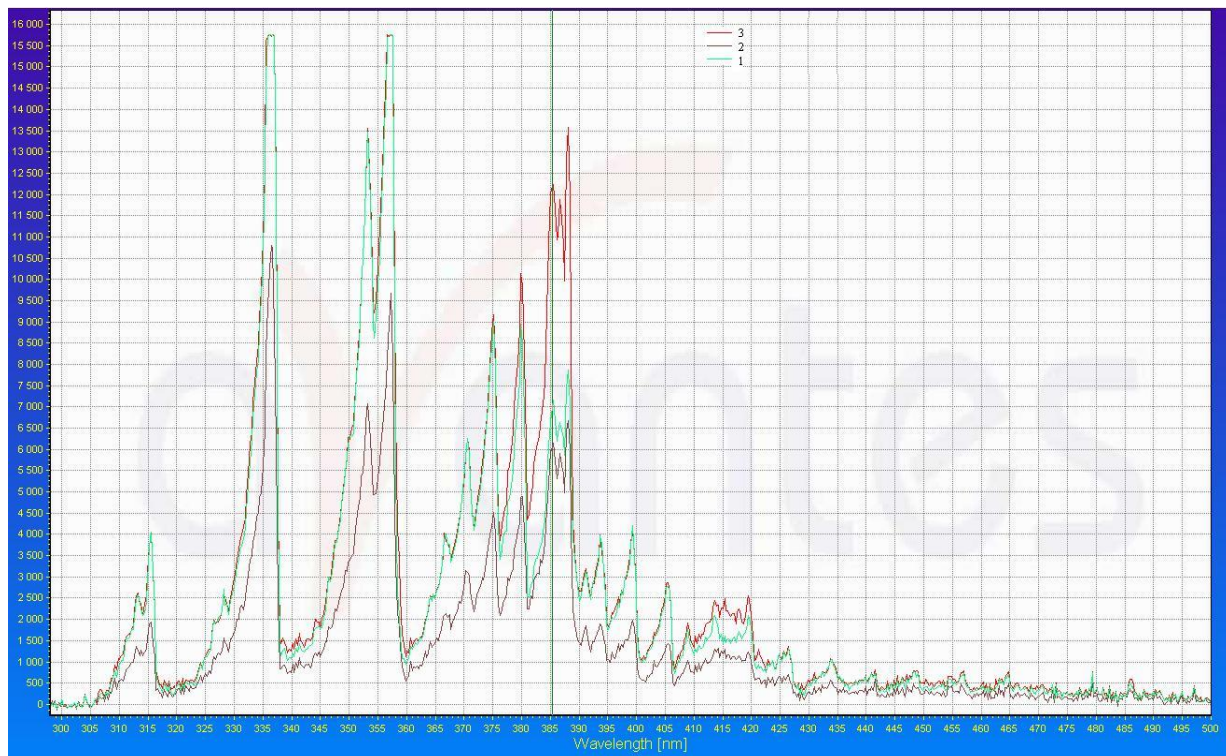


Fig.9.29. Radiation spectra of the surface discharge in motionless air - the black line 2, in the high-speed stream of air - the green line 1, in the high-speed stream air-propane mixes - a red line 3

Burning of propane at the fuel excess coefficient greater than unity is accompanied by soot formation on the dielectric surface.

9.6. Influence of dielectric material and thickness properties on surface streamer discharge.

During project performance have been obtained and investigated initiated subcritical streamer MW discharges of middle and high gas pressure developing exclusively on the dielectric surface. The surface discharges initiated by means of passive electromagnetic

vibrators, located on the dielectric surfaces are similar to the streamer network of usual volumetric discharges, but pressed to the dielectric surface.

As the reasons causing primary discharge propagation over the dielectric surface electrostatic effects and physical and chemical surface processes in the presence of the discharge were considered. For revealing of the defining factor the experiments with surface discharges on the dielectric plates of a different thickness executed from various materials have been carried out.

Experiments with dielectric plates from textolite, textolite glass, usual and quartz glass, ceramics and polyethylene have revealed independence of the discharge properties on a sort of a dielectric material (see **Fig.9.30**). Experiments have been carried out in installations with the wavelengths of 8.9cm and 2.5cm of MW of radiation.

Experiments have shown that properties of the streamer discharge (a network form of the channels, their radius, and the characteristic sizes of the network cells, speed and limits of propagation, border of transitions of one discharge kind into another) do not depend on a material sort of the dielectric. It testifies that physical and chemical surface processes are not the key factor dictating primary propagation of streamers over a surface.

Special interest represents experiments with thin dielectric films. At the thickness of films even 100 microns the surface discharge possesses the same properties as discharges on a surface of unlimited thick plates.



(a)

(b)

(c)

Fig.9.30. The structure of the streamers discharge network does not depend on a material of a dielectric layer: (a) - a polyethylene film 0.02cm in the thickness, (b) - textolite glass of 0.2cm thickness, (c) - quartz glass of 1.0cm thickness

In this connection theoretical research of features of an electromagnetic field distribution round a streamer located over a layer of the dielectric of various thickness (see section 11.5) has been undertaken.

Chapter 10. Experimental estimation of absorbing ability of the transversal and longitudinal subcritical and deeply subcritical surface discharges in MW radiation beam (Task 31)

10.1. Absorbed energy measuring method

Earlier it has been shown, that the subcritical streamer discharge developing in a volume, possesses high absorbing ability in relation to the microwave radiation creating this discharge^{7,8,9}. There is a question, in what measure possesses absorbing ability the surface streamer discharge initiated on a surface of a dielectric body. For determination of the energy absorbed by the discharge, a special experiment has been put. The thin plate of the dielectric

(textolite glass) with the sizes exceeding an area of possible propagation of the surface discharge, was located in the area of the focus of the microwave radiation formed by means of a spherical mirror. The plate was hanged by means of thin dielectric threads, forming a gravitational pendulum. As a result of energy release in the superficial discharge during a pulse of radiation the mechanical impulse was given to the plate, and the pendulum started to make vibrations. By the measured amplitude of vibrations of the pendulum with known parameters (the weight of a body and length of the suspension) was determined a value of a mechanical impulse. Leaning against elements of the theory of a point explosion, with the account back pressure and filamentary structure of the surface discharge, the energy enclosed in the discharge during the radiation pulse was determined. The obtained value was compared with energy of radiation during the pulse for determination of the radiation effectiveness of absorption coefficient of the surface discharge.

The experiment scheme is represented in Fig.10.1.

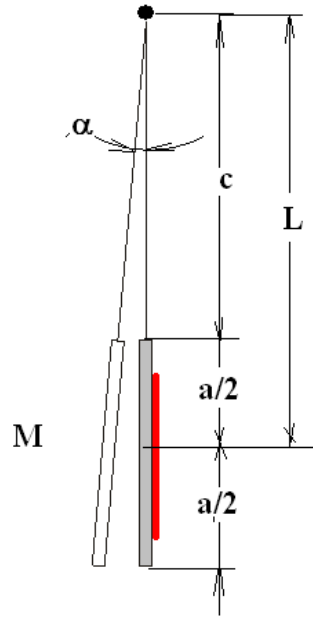


Fig.10.1. A scheme of the ballistic experiment

The experiment was carried out in the installation with the wavelength $\lambda = 8.9\text{cm}$ at duration of the pulse $43\mu\text{s}$ and the electric field amplitude in the radiation focus 5kV/cm . The electric field value was determined by the breakdown pressure of air in the presence of a metal ball with a small radius in comparison with the wavelength. Breakdown pressure defined the amplitude of the electric field by the known dependence¹⁰

$$E_{MW_{cr}} = E_{DC_{cr}} \sqrt{\frac{1.2 + 2 \omega \tau_{rel}^2}{1 + \omega \tau_{rel}^2} 1 + \omega \tau_{tr}^2} \quad (10.1)$$

where $\omega = 2\pi/\lambda$ is a circular frequency of the microwave radiation,

$$\tau_{tr} \approx \frac{1.6 \cdot 10^{-10}}{P_{Torr}}, s \quad (10.2)$$

- time of electron transport collisions at the electron temperature of 2 eV,

$$\tau_{rel} \approx \frac{\tau_{tr}}{\delta} \quad (10.3)$$

- time of electron energy relaxation

$$\delta \approx 0.03 \quad (10.4)$$

$$E_{DCcr} = 33 \cdot p_{Torr}, \text{ V / cm} \quad (10.5)$$

- critical breakdown field in the constant field for air (the right branch of the Paschen curve).
At determination of the electric field value by the breakdown pressure in the presence of a ball an influence of diffuse losses of electrons to the ball was considered under the formula
Ошибка! Закладка не определена.

$$\frac{l_a p}{a} = \frac{\left(\left(\Phi \frac{E}{E_{cr} p} \right)^\beta - 1 \right)^{3/2}}{7.2 \beta \left(\Phi \frac{E}{E_{cr} p} \right)^\beta} \quad (10.6)$$

where l_a – is a diffuse length of electron attachment in air, a – is a radius of the ball, $\beta=5.34$, $\Phi=3$.

Obtained experimental breakdown value of pressure in the presence of the metal ball in the focus of a radiation beam at the wavelength of 8.9cm is 300Torr, that corresponds to the field value $E_m=5\text{kV/cm}$ in the focus. Distribution of a field amplitude in transversal cross-section section of the focus with good accuracy is approximated by the expression

$$E(x, y, 0) = E_m \exp\left(-\frac{x^2}{a_f^2} - \frac{y^2}{b_f^2}\right) \quad (10.7)$$

where $a_f=2.5\text{cm}$, $b_f=5.2\text{cm}$.

The energy flux in the radiation beam is

$$P_{MW} = \frac{c}{8\pi} \int_{-\infty}^{\infty} \int_{-\infty}^{\infty} E(x, y, 0)^2 dx dy \quad (10.8)$$

Integration of (10.8) gives the value $P_{MW}=0.82\text{MW}$. At the radiation pulse duration of $40\mu\text{s}$, the energy of radiation is $E_{MW}=32.8\text{J}$.

10.2. Results of observations and their processing

In Fig.10.2 one can see photos of the plate in profile and three quarters. Over the photo in Fig.10.2b one determines a deviation angle of the pendulum plate

$$\alpha = \arcsin\left(\frac{\Delta}{L}\right) = 0.009 \quad (10.9)$$

Pendulum shoulder (distance from a point of the suspension to the plate center of mass) $L=27.5\text{cm}$. The sizes of the plate: $a=10\text{ cm}$, $b=7\text{ cm}$, $d=0.05\text{ cm}$, relative density of the textolite glass $\rho=1.8\text{g/cm}^3$. The mass of the pendulum M

$$M = abd\rho = 6.3\text{g} \quad (10.10)$$

where the acceleration of the gravitation force is $g=981\text{cm/s}^2$.

Own frequency of the pendulum

$$f_M = \frac{1}{2\pi} \sqrt{\frac{g}{L}} = 0.95\text{s}^{-1} \quad (10.11)$$

The impulse obtained by the pendulum is connected with the maximal deviation angle by a relation

$$J = F \cdot t = M \cdot V = M \alpha \frac{f_M}{2\pi} L = M \cdot \alpha \sqrt{gL}, \quad \alpha \ll 1 \quad (10.12)$$

For determination of the energy released in the pulse discharge on the surface of the plate, we will use the theory developed in the work [11].

Let's assume that energy of one pulse Q of small duration is put into the streamer surface discharge. In this statement pertinently to use analytical theory of Sedov for the thread explosion.

According to Sedov, pressure in the explosion place is described by a relation

$$p_t = \eta \frac{2\delta^2 \rho_1}{\gamma + 1} \left(\frac{q}{\xi \cdot \rho_1} \right)^\delta \cdot t^{-\delta \nu} \quad (10.13)$$

Where $\nu = 1, 2, 3$ -dimension of a problem, ρ_1 - initial density of a gas, $\gamma = 1.4$ - an adiabatic exponent, q [erg/cm^{3- ν}] - specific energy put, η - the ratio of pressure in an explosion place and pressure behind the shock wave front

$$\eta = \left(\frac{\gamma + 1}{2\gamma} \right)^{\delta \nu} \left(\frac{2}{\gamma - 1} \left(\frac{\gamma + 1}{2} - \frac{\gamma + 1}{2\gamma} \right) \right)^{-\frac{\gamma}{2 - \gamma}} \times \quad (10.14)$$

$$\times \left(\frac{2 \nu \gamma - 1 + 2}{3\nu - 2 + \gamma} \cdot \left(\frac{\gamma + 1}{\delta \nu \gamma - 1 + 2} - \frac{\gamma + 1}{2\gamma} \right) \right)^{\beta_4 + 2\beta_1}$$

$$\delta = \frac{2}{2 + \nu} \quad (10.15)$$

$$\beta_2 = \frac{\gamma - 1}{2 \gamma - 1 + \nu} \quad (10.16)$$

$$\beta_1 = \beta_2 + \frac{\gamma + 1}{\nu \gamma - 1 + 2} - \delta \quad (10.17)$$

$$\beta_4 = \frac{2\beta_1}{\delta \ 2 - \gamma} \quad (10.18)$$

$$\xi = 0.36 \cdot \gamma - 1^{-1.253 - 0.184 \cdot \log \gamma - 1} = 1.003 \quad (10.19)$$

The correction coefficient ξ , determined by comparison with the numerical calculation, usually little differs from unity, $\xi - 1 \ll 1$.

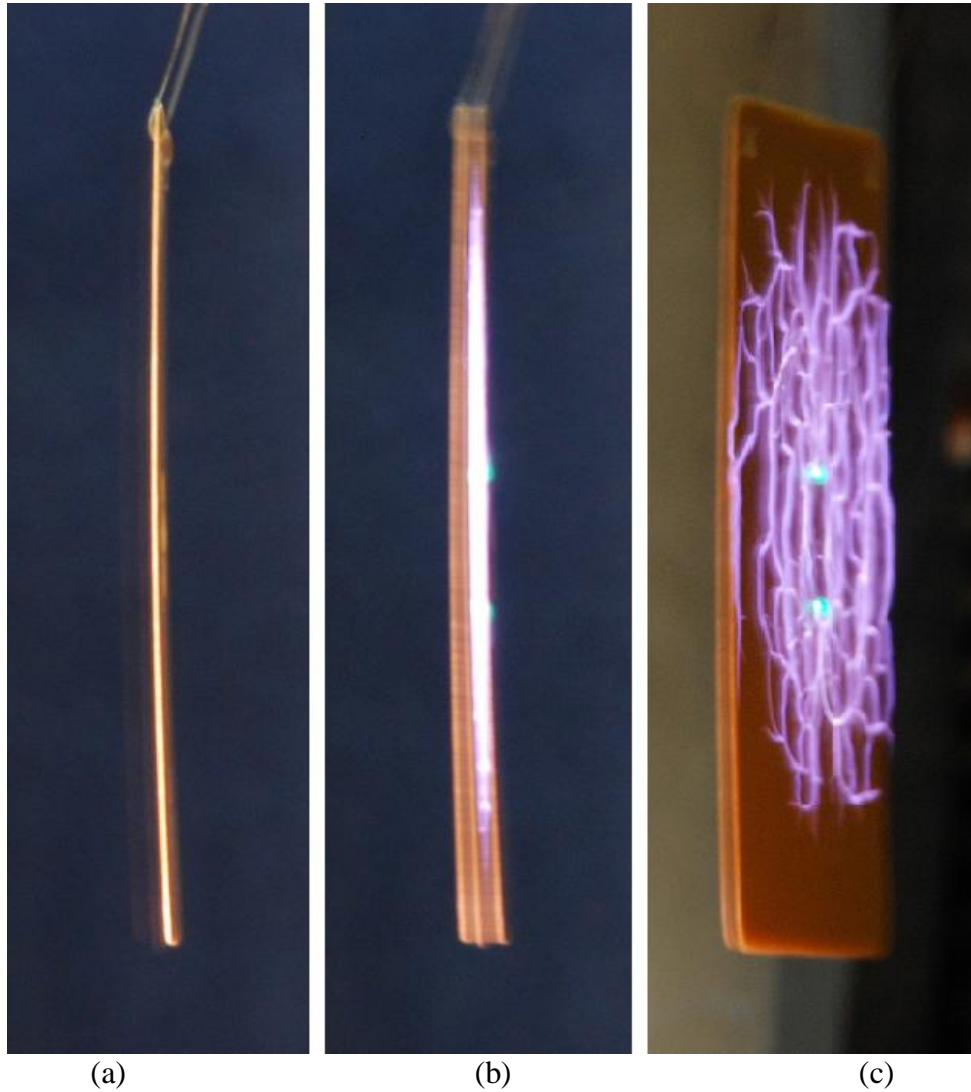


Fig. 10.2. Photos of the dielectric plate: (a) - before a discharge in a profile, (b) - a shaking plate under the influence of the discharge in a profile, (c) - the same in 3/4. The mirror on the right. Dark blue bright points - the ends of the initiator

The distance from a place of the explosion to the shock wave front r_2 grows with time under the law

$$r_2 = \left(\frac{q}{\xi \cdot \rho_1} \right)^{\frac{\delta}{2}} \cdot t^{\delta} \quad (10.20)$$

At the linear explosion, i.e. at the streamer channel explosion,

$$\nu = 2 \quad (10.21)$$

and according to (10.14)

$$\eta = 0.537 \quad (10.22)$$

The formula (10.13) is obtained in the assumption of the negligibly small pressure of initial gas. This formula stops to be correct by the time moment t_s when pressure behind the front becomes equal to pressure of undisturbed gas p_I :

$$t_s = \left(\eta \frac{2\delta^2 \rho_1}{\gamma + 1 p_1} \right)^{\frac{1}{\delta \nu}} \cdot \left(\frac{q}{\xi \cdot \rho_1} \right)^{\frac{1}{\nu}} \quad (10.23)$$

During this time the surface under the streamer of the length L_s will get the impulse

$$J = L_s \cdot \int_0^{t_s} p(t) - p_1 \cdot 2r_2(t) dt \quad (10.24)$$

After insertion of (10.13), (10.20) and (10.23) in (10.24) with accounting for (10.21) and integration we get :

$$J = G \frac{E_o}{C_s}, \quad (10.25)$$

where

$$G = \frac{2\sqrt{\gamma}}{\xi} \left(\frac{2\delta}{1-\delta^2} \right) \left(\eta \frac{2\delta^2}{\gamma+1} \right)^{\frac{3}{2}} = 0.118 \quad (10.26)$$

$$C_s = \sqrt{\frac{\gamma p_1}{\rho_1}} \quad (10.27)$$

- sound velocity in the undisturbed gas

$$E_o = qL_s \quad (10.28)$$

- full energy of the explosion.

Inserting measured value of the angle α in (10.12), we get the measured value of the impulse:

$$J_{\text{exp}} = 9.31, \text{ dyne} \cdot s \quad (10.29)$$

and using (10.25), we get a value of the released energy

$$E_{0\text{exp}} = \frac{C_s}{G} J_{\text{exp}} \quad (10.30)$$

In the SI system we get the value $E_{0\text{exp}} = 0.26 \text{ J}$, that presents ~1% from the energy in the radiation pulse of 40 μs duration at power of 0.8 MW.

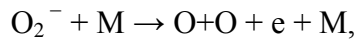
Chapter 11. Theoretical support of experiments and creation of theoretical models of surface MW discharge in quasi-optical EM beam in various conditions (Tasks 11, 23, 32)

11.1. Theoretical support of experiments

Computation-theoretical support of experiments consisted in calculations of electromagnetic field distributions for definite conditions of experiments. (Examples of calculations are presented in Fig.1.3, Fig.2.3a, Fig.2.3b) and processing of observation results (in particular, Fig.2.5, Fig.3.4, Fig.3.12, Fig.5.1, Fig.5.9, Fig.5.10, Fig.5.11, Fig.6.3, Fig.7.8, Fig.9.8, Fig.9.15, Fig.9.18, Fig.9.19, Fig.9.26, Fig.9.27, Chapter 10).

11.2. Construction of theoretical model of a breakdown in the presence of a dielectric layer

Experiments have convincingly shown, that presence of the dielectric influences on a breakdown value of the electric field amplitude only because of distribution of radiation intensity distribution change brought by the dielectric. Diffusion losses of ionization electrons to the dielectric surface are essential only in the case if the distance from the center of an elementary avalanche to the surface is smaller than the radius of the avalanche. The avalanche center is defined by a place of occurrence of the primary free electron appearing either in the result of detachment ,



or because of direct ionization under the influence of the ionizing radiation or other factors. The diffusion losses on a flat surface do not break an avalanche development, but increase time of its development and shift a maximum of the concentration of the growing distribution aside from a surface.

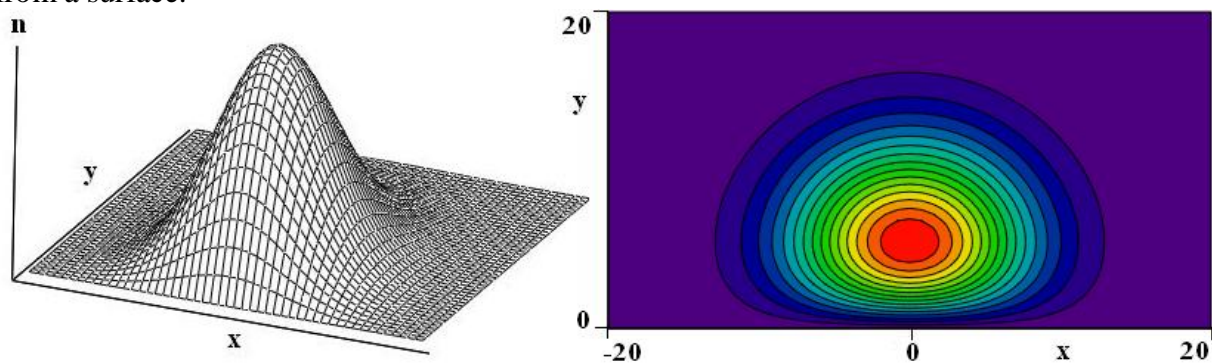


Fig.11.1. Distributions of the ionization avalanche electrons in the presence of a surface at the moment of time $15 / \nu_i$. The distance of a place of free electrons occurrence to the surface - $0.1 (D_e / \nu_i)^{0.5}$

In **Fig.11.1** is represented the calculation example of avalanche ionization electron distribution in surface presence of a surface. The distribution is shown at the moment of time $15 / \nu_i$ (ν_i - total frequency of the ionization) for a distance of a place of free electron occurrence free электрона to the surface, equal to $0.1 (D_e / \nu_i)^{0.5}$. By this moment the maximum of the avalanche distribution departs from the surface by some units of $(D_e / \nu_i)^{0.5}$ and the avalanche starts to develop in a streamer at sufficient density of the gas. This calculation has shown, that the diffusion on a layer surface cannot affect a breakdown threshold.

In **Fig.11.2**, where the dependence of the concentration in the avalanche at the distance $1(D_e / \nu_i)^{0.5}$ from a surface on time is represented , one can see, that closeness of the initial electron to the surface delays a little the avalanche development, but does not reduce an increment of its development.

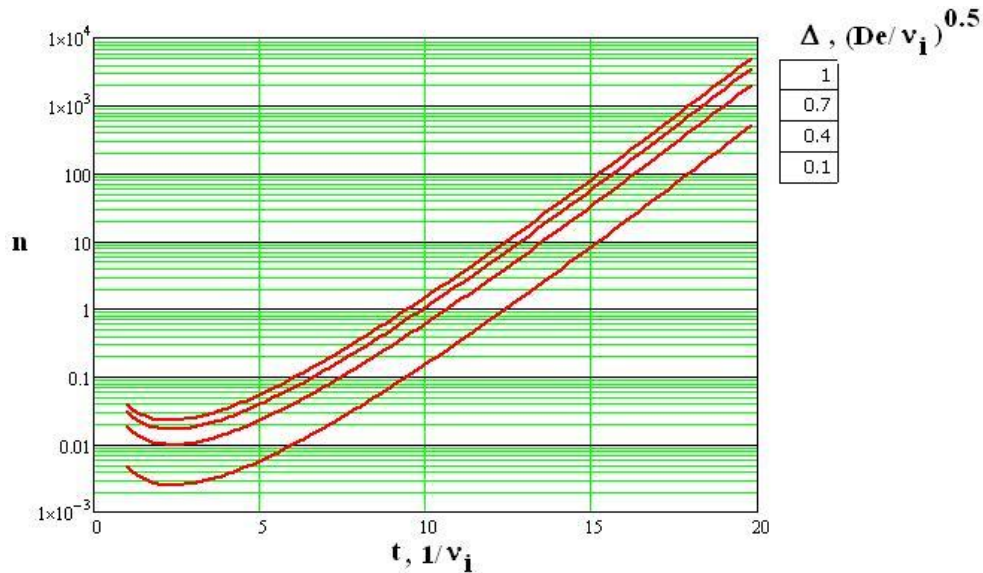


Fig.11.2. Concentration in the avalanche dependence via time at the distance $1(D_e/v_i)^{0.5}$ from the surface

11.3. Critical breakdown field in MW field calculations at middle and high gas pressures

A breakdown in the high-frequency field possesses the features requiring specification since properties of the category MW discharge essentially vary depending on pressure. Many works which are devoted to Research of the breakdown process have become classical¹². The Majority of them are carried out with reference to breakdown of gases of small and average pressure. Our researches cover also high pressures. Features of the breakdown in gases of the high pressure have required additional studying.

Here we will develop the simplified theory of a breakdown in a gas in a wide range of gas pressure.

Let's consider electron behavior in a gas in the presence of periodic electric field.

$$E = E_0 \cdot \sin \omega t \quad (11.1)$$

The equation of the individual electron movement in the electric field can be written down in a form

$$\frac{dV}{dt} + \frac{V}{\tau_{tr}} = \frac{eE_0}{m} \cdot \sin \omega t \quad (11.2)$$

Where

e, m - a charge and mass of the electron,

$1/\tau_{tr}$ - frequency of transport collisions

The second term in the left part of the equation describes electron impulse losses in transport collisions.

The equation (11.2) is the linear differential equation of 1st order. Its solution can be written down in a form

$$V = \exp\left(-\frac{t}{\tau_{tr}}\right) \cdot \int \frac{e \cdot E_0}{m} \cdot \sin \omega t \cdot \exp\left(\frac{t}{\tau_{tr}}\right) dt$$

that after integration gives an expression

$$V = \frac{eE_0\tau_{tr}}{m} \cdot \frac{\sin \omega t + \omega\tau_{tr} \cdot \cos \omega t}{1 + \omega^2\tau_{tr}^2}$$

Movement in the electric field E with a speed V is accompanied by gain of energy which is accounted for in the right part of the electron energy balance equation

$$\frac{dT_e}{dt} + \frac{T_e}{\tau_{rel}} = \frac{\mu E_0^2}{1 + \omega \tau_{tr}} \sin^2 \omega t + \omega \tau_{tr} \sin \omega t \cos \omega t \quad (11.3)$$

where

T_e – electron temperature,

τ_{rel} – electron relaxation time

$$\mu = \frac{e \tau_{tr}}{m}$$

For simplicity the gas temperature is assumed negligibly small with respect to the electron temperature. It is convenient to represent the equation (11.3) in the form

$$\frac{dT_e}{dt} + \frac{T_e}{\tau_{rel}} = \frac{\mu E_0^2}{1 + \omega \tau_{tr}} [1 - \cos 2\omega t + \omega \tau_{tr} \sin 2\omega t] \quad (11.4)$$

The equation (11.4) also can be integrated. Its solution is

$$T_e = \frac{\mu E_0^2}{2(1 + \omega \tau_{tr})} \exp\left(-\frac{t}{\tau_{rel}}\right) \int [1 - \cos 2\omega t + \omega \tau_{tr} \sin 2\omega t] \exp\left(\frac{t}{\tau_{rel}}\right) dt \quad (11.5)$$

After integration and transformation we get an expression

$$T_e = T_0 \left(1 + \frac{1}{1 + 2\omega \tau_{rel}} [1 + 2\omega \tau_{tr} \omega \tau_{rel} \cos 2\omega t + 2\omega \tau_{rel} + \omega \tau_{tr} \sin 2\omega t] \right) \quad (11.6)$$

where

$$T_0 = \frac{\mu E_0^2 \tau_{rel}}{2(1 + \omega \tau_{tr})}$$

is mean electron temperature.

Often used expression is

$$\tau_{rel} = \frac{\tau_{tr}}{\delta}, \quad \delta < 1$$

Let's designate

$$\eta = \omega \tau_{tr},$$

уравнение **Ошибка! Источник ссылки не найден.** представим в более компактном виде

$$T_e = T_0 \left(1 + \frac{1}{1 + 2\eta^2} [1 + 2\delta \eta^2 \cos 2\omega t + 2 + \delta \sin 2\omega t] \right) \quad (11.7)$$

and equation (11.7) we represent in more compact form

$$T_e = T_0 \left(1 + \frac{1}{1 + 2\eta^2} \cos 2\omega t + 2 \sin 2\omega t \right) \quad (11.8)$$

Knowing behavior of electron temperature in time, it is possible, using known dependence of total frequency of ionization on temperature $\nu_i(T_e)$ to define an average on time effective frequency of ionization

$$\nu_{ef} = \frac{\omega}{2\pi} \int_0^{2\pi} \nu_i(T_e, E_0, t) dt$$

Equality to zero of the average frequency of ionization defines a critical field of the breakdown E_{0cr}

$$\int_0^{2\pi} \nu_i(T_e, \eta, E_{0cr}, t) dt = 0 \quad (11.9)$$

As approximation of total frequency of ionization dependence on electronic temperature we use an expression

$$\nu_i = \nu_a \left(\left(\frac{T_e}{T_{cr}} \right)^{5.3} - \left(\frac{T_e}{T_{cr}} \right)^2 \right) \quad (11.10)$$

where

ν_a – attachment frequency,.

T_{cr} – critical temperature for the constant field.

First term in the right hand side corresponds to electron impact ionization, the second one – to the dissociative attachment.

In Fig.11.3 is represented a result of numerical integration of the equation(11.9), and in Fig.11.4 – the same dependence on air pressure for $\lambda=8.9$ cm

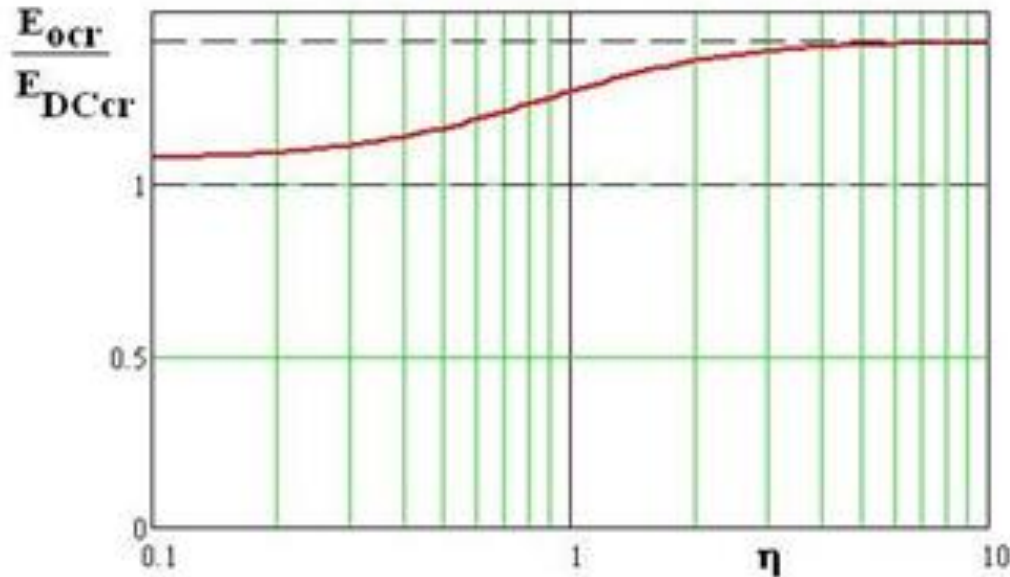


Fig.11.3. The result of numerical integration of Eq.(11.9)

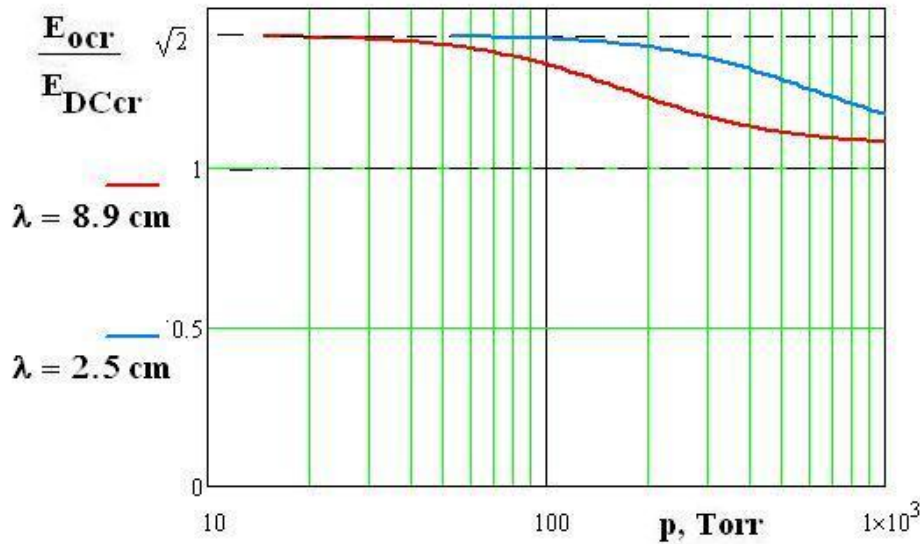


Fig.11.4. The result of numerical integration of the Eq.(11.9). E_{0cr}/E_{DCcr} via pressure dependence for air at $\lambda=8.9$ cm

From the obtained dependences follows the simple but important conclusion . At $\eta > 1$ (i.e. at $p < 100$ Torr for $\lambda = 8.9$ cm) the breakdown threshold corresponds to equality **of the effective** value of electric field and the critical value of the constant field

$$\frac{E_0}{\sqrt{2}} = E_{DCcr}, \quad \eta > 1 \quad (11.11)$$

At $\eta < 1$ (i.e. at $p > 100$ Torr for $\lambda = 8.9$ cm) the breakdown threshold corresponds to equality **of a peak** value of the electric field and the critical value of a constant field

$$E_0 = E_{DCcr}, \quad \eta < 1 \quad (11.12)$$

The equation(11.4), also as the equation (11.2) in the assumption of coefficients constancy. The equation as well as the equation was integrated in the assumption of coefficients constancy. At the same time characteristic times of scattering and a relaxation are the electron temperature functions. The value of τ_{ek} weakly varies in a range of temperatures interesting to us, so in the assumption of a constancy of time of scattering it is possible to consider the equation (11.2) integration to be justified. However the relaxation time considerably varies in a vicinity of 1-2 eV. Therefore for specification of the analysis result a numerical integration of the equation (11.4) in which the real dependences of ionization reactions by the electron impact were considered, attachment, elastic collisions, dissociation, molecular and electronic excitation calculated by known cross sections has been carried out,

$$\tau_{tr} = \tau_{tr} T_e \quad (11.13)$$

and

$$\tau_{rel} = \tau_{rel} T_e \quad (11.14)$$

In general case, the critical value of the electric field amplitude is defined by the formula (11.15)

Result of calculation of the equation (11.4) with accounting for dependences (11.13) and (11.14) calculated by known cross sections of elementary processes (elastic and inelastic collisions, dissociative attachment etc.) for the wavelength of 8.9cm is shown in **Fig.11.5**.

Transition from the amplitude to the effective value at equality is visible to the critical constant field E_{DCcr} . At pressure below 10Torr there is a transition to a mode of rare collisions (this mode does not appear in the assumption $\delta = 0$).

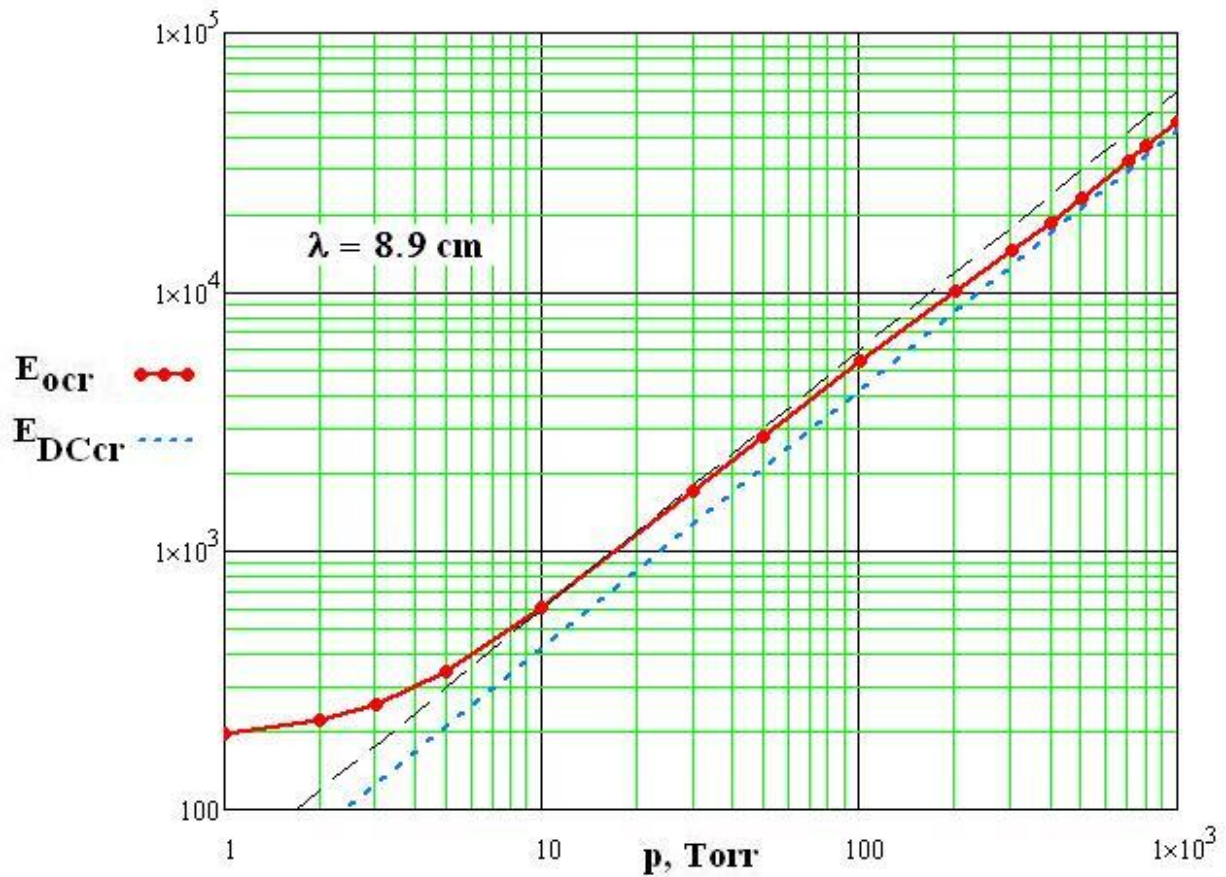


Fig.11.5. Dependence of the electric field amplitude critical value on air pressure; $\lambda = 8.9$ cm

The obtained result is physically quite transparent and does not require explanations. It was important to clarify, at what gas pressure values there is a change of the amplitude for the effective value

$$E_{cr} = E_{crDC} \sqrt{\frac{1.2 + 2 \omega \tau_{rel}^2}{1 + \omega \tau_{rel}^2} \frac{1 + \omega \tau_{tr}^2}{1 + \omega \tau_{tr}^2}} \quad (11.15)$$

in which for estimates one can accept

$$\tau_{tr} \approx \frac{1.6 \cdot 10^{-10}}{p, \text{Torr}}, s \quad (11.16)$$

$$\tau_{rel} \approx \frac{1 \cdot 10^{-8}}{p, \text{Torr}}, s \quad (11.17)$$

As to physics of the surface streamer discharge development the experiments have shown, that the electrostatic effects connected with influence of charges, induced in the dielectric by the streamer discharge, have no essential influence. Independence of behavior of the surface streamer discharge testifies to its independence on a thickness of the dielectric layer. Thus, the simplification of the streamers propagation along the dielectric surface is caused by more complex factors, such as electron photo emission from a surface under the influence of ultra-violet radiation from heads of the streamers, influence of double layers on an ambipolar diffusion and other difficultly accounted for processes.

Attracts the attention the fact that the characteristic size of cells of the streamers network in the surface discharge practically does not depend on the gas pressure in the area of streamer discharges and is proportional to length of a wavelength of radiation.

Marked results of observations will lie down in a basis of the developed model of the surface streamer discharge.

11.4. Calculations of the streamer discharge propagation velocity

At a field with amplitude smaller critical, the streamer propagation is impossible without falling of a gas density in the channel of the streamer as a result of ohmic heating induced by the MW current that is necessary for fulfillment of a condition of maintenance of ionization $E/N = (E/N)_{cr}$.

The estimation of the streamer propagation speed in the subcritical field can be carried out starting from the following simple reasoning prompted by numerical modeling.

In order the propagation takes place, it is necessary, that the field on a streamer head exceeded the critical value. It is possible, if a conductivity of the streamer already in his head has grown from small values to a value, sufficient for increase of a field to the critical value. For an estimation of this value we will use of known relations for extended ellipsoid with half axes L and a ($L \gg a$), deduced for a stationary field.

A field at an ellipsoid top A_{max} and inside it E_{in} are equal, respectively,

$$E_{max} = E_0 \frac{1 + iS}{1 + i \frac{S}{Q}} \quad (11.18)$$

$$E_{in} = E_0 \frac{1}{1 + i \frac{S}{Q}} \quad (11.19)$$

where

$$S = \frac{4\pi\sigma}{\omega} \quad (11.20)$$

E_0 – an applied field ;

ω – a circular frequency of MW field,

σ – a conductivity;

Q – a form factor.

Q for a strongly extended ellipsoid is described by an approximate relation

$$Q \approx \frac{2L}{a \cdot \ln\left(\frac{L}{2a}\right)} \quad (11.21)$$

where

L – is a large half axis of the ellipsoid;

$a \ll L$ – a curvature radius at the ellipsoid top;

В случае идеальной проводимости ($S = \infty$)

$$\frac{E_{max}}{E_0} = Q \quad (11.22)$$

Application of these relations to the case of MW fields is admissible, if the size of the streamer does not reach resonant value and the conductivity has a value smaller than those at which the skin-effect appears.

As a field in the streamer is smaller than the critical one, then for maintenance of the ionized conditions with corresponding falling of the gas concentration by E_{cr}/E_0 times heating of the streamer is necessary for fulfillment of condition $E_{in}/N = (E/N)_{cr}$.

On the streamer axis in his head it is possible to write the equation of energy conservation in the assumption of isobaricity and isothermicity in the form

$$\frac{1}{T} \cdot \frac{dT}{dt} = \frac{\sigma \cdot t \cdot E \cdot t^2}{C_p p} \quad (11.23)$$

where

C_p – specific heat capacity at constant pressure,

T – gas temperature

Equation integration we undertake at the assumption, that the electric field within a zone of heating varies a little and is near to the critical value for undisturbed gas, and conductivity grows with a constant increment

$$\sigma \cdot t = \frac{\omega}{4\pi} Q \exp \nu_i t \quad (11.24)$$

After integration and insertion of (11.21) we get

$$\ln\left(\frac{T}{T_0}\right) = \ln\left(\frac{E_{cr}}{E_{in}}\right) = \frac{E_{cr}^2}{C_p p} \cdot \frac{L}{2\lambda \nu_i} \cdot \frac{c}{\ln\left(\frac{L}{2a}\right)} \quad (11.25)$$

c – a light velocity;

λ – a wavelength of MW field;

From here follows an estimate of the ionization frequency in the streamer head

$$\nu_i = \frac{E_{cr}^2}{C_p p} \cdot \frac{L}{2\lambda} \cdot \frac{c}{\ln\left(\frac{L}{2a}\right) \cdot \ln\left(\frac{E_{cr}}{E_{in}}\right)} \quad (11.26)$$

For a velocity V and depth of the ionization front h the following relations are valid in known assumptions

$$V = 2\sqrt{D_e \nu_i} \quad (11.27)$$

$$h = 2\sqrt{\frac{D_e}{\nu_i}} \quad (11.28)$$

$$h = 4 \frac{D_e}{V} \quad (11.29)$$

D_e – is a coefficient of free electron diffusion .

Assuming $a=h$, $S=Q$, $L=\lambda/4$, $E_{in}=E_0$ and inserting (11.27) to (11.25), we get the transcendent equation for unknown V

$$V \cdot \ln\left(\frac{LV}{8D_e}\right) = 2 \frac{E_{cr}^2}{C_p p} \cdot \frac{L}{2\lambda} \cdot \frac{c}{\ln\left(\frac{E_{cr}}{E_0}\right)} \quad (11.30)$$

The equation (11.30) is solved numerically using estimate relations for a coefficient of the electron diffusion

$$D_e = \frac{10^6}{p_{Torr}}, \quad \text{cm}^2/\text{s} \quad (11.31)$$

and the critical field

$$E_{cr} \lambda, p_{Torr} = 33 p_{Torr} \sqrt{\frac{1.25 + 2 \omega \tau_{rel}^2}{1 + \omega \tau_{rel}^2} 1 + \omega \tau_{tr}^2}, \quad \text{V/cm} \quad (11.32)$$

where time of electron transport collisions and a relaxation time are described by equations

$$\omega \tau_{tr} = \frac{30}{\lambda_{[cm]} p_{[Torr]}} \quad (11.33)$$

$$\omega \tau_{rel} = \frac{\omega \tau_{tr}}{\delta}, \quad \delta = 0.03 \quad (11.34)$$

For rude estimate a logarithm in the left hand side of the equation (11.30) can be changed for its typical value

$$\ln \left(\frac{LV}{8D_e} \right) \approx \Lambda \quad (11.35)$$

and lead the equation (11.30) to an explicit form convenient for estimates

$$V \approx 2 \frac{E_{cr}^2}{C_p p} \cdot \frac{L}{2\lambda\Lambda} \cdot \frac{c}{\ln \left(\frac{E_{cr}}{E_0} \right)} \quad (11.36)$$

Values given by an expression (11.36) can differ from solutions of the equation (11.30) up to two times.

The formula (11.36) specifies a weakness of the subcritical discharge propagation velocity dependence on degree of a field undercriticality if the field is not near to the critical to value. In the latter case the streamer speed sharply increases, that corresponds to transition to a mode of an over critical discharge with its high values of propagation speed.

The propagation speed of the discharge front is smaller than a speed of a streamer development. The streamer, having reached the resonant size $\lambda/4$ in a field direction, generates a streamer of a following echelon at a distance $\sim \lambda/8$. In a flat case the discharge front speed can be estimated as $V/2$. In case of three-dimensional distribution (a volumetric streamer discharge) the propagation speed decreases by $2^{1/2}$

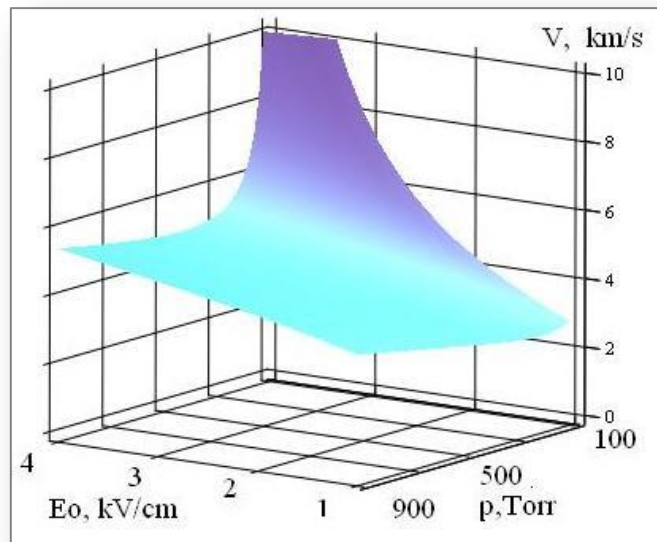


Fig.11.6. Surface discharge front speed dependence on pressure and the electric field amplitude E_0

So, the discharge front speed towards to radiation is estimated by a relation

$$V_{fr} \approx V \cdot 2^{n/2} \quad (11.37)$$

where V is defined by the equation or the approximation formula, and $n=2$ or 3 for the surface or the volumetric discharge, respectively.

In Fig.11.6 and Fig.11.7 are represented dependences of the surface discharge front speed on pressure and amplitude of the electric field or the under criticality parameter E_0/E_{cr} respectively, the equations being the solution of the equation.

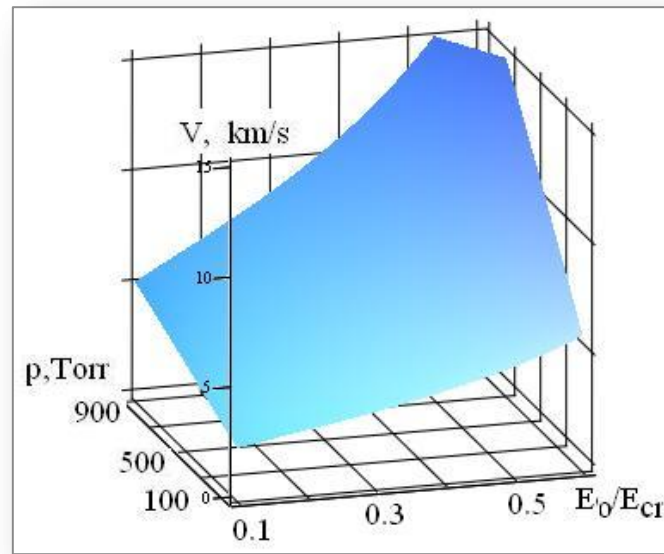


Fig.11.7. Surface discharge front speed dependence on pressure and the undercriticality parameter E_0/E_{cr}

The used simplified approach based on experience of numerical modeling, does not apply for the strict description of the phenomenon. However, the equation (11.30) gives values of the propagation speed quite close to the observed, that proves a choice of defining factors in the course of the streamer propagation.

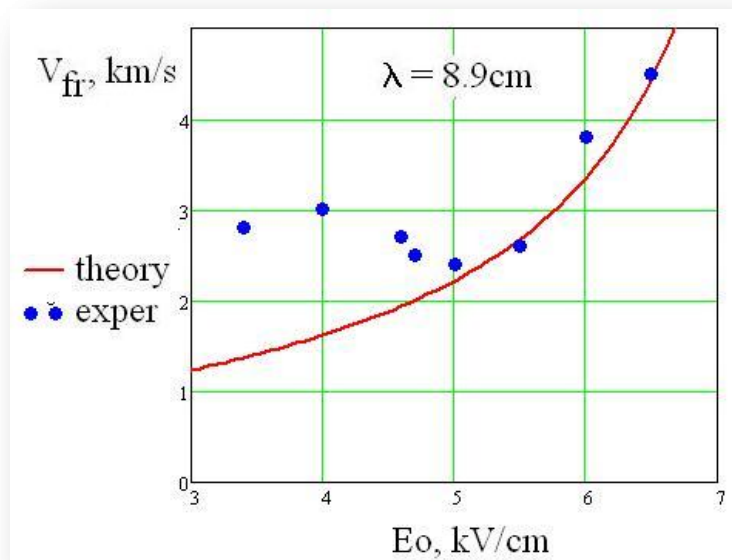


Fig.11.8. Dependence of the streamer propagation speed in the volumetric discharge on the electric field amplitude at constant pressure, $p=200\text{Torr}$, $\lambda = 8.5\text{cm}$. An estimation (6.7) - a continuous red line, measurements - dashed line with points

In Fig.11.8 an estimation of the subcritical discharge streamer propagation speed (11.36) with the account for (11.37), the case $n=3$ (designated by a continuous red line), is compared with results of measurements [13] for the volumetric streamer discharge at $p=200\text{Torr}$, $\lambda = 8.9\text{cm}$ (points). It is possible

to see that the measured values though lay a little above the estimated one give the similar general course of curves.

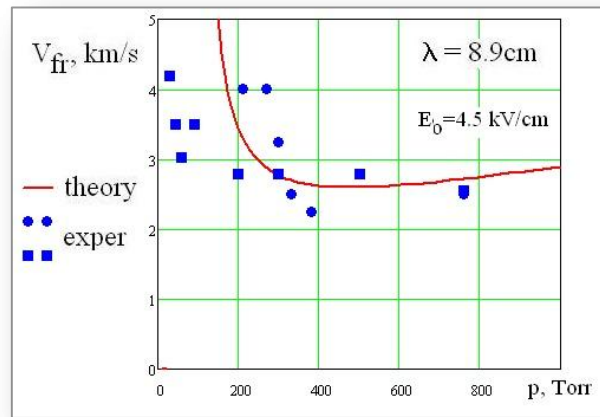


Fig.11.9. Comparison of the solution (11.30) for $n=2$ with the values measured in the case of the longitudinal streamer surface discharge at the wavelength of 8.9cm

In Fig.11.9 a solution of (11.30) with use of (11.37) for $n=2$ is compared with the values measured in the case of the longitudinal streamer surface discharge at the wavelength of radiation 8.9cm. By circles and small squares measurements of two various series in identical conditions on surfaces of different dielectric materials (**Table 7.1** and **Table 7.2**) are designated. In **Fig.11.10** the same comparison is carried out for the longitudinal surface discharge in radiation with the wavelength of 2.5cm. An agreement between the theoretical dependence an experimental values is possible to recognize quite satisfactory.

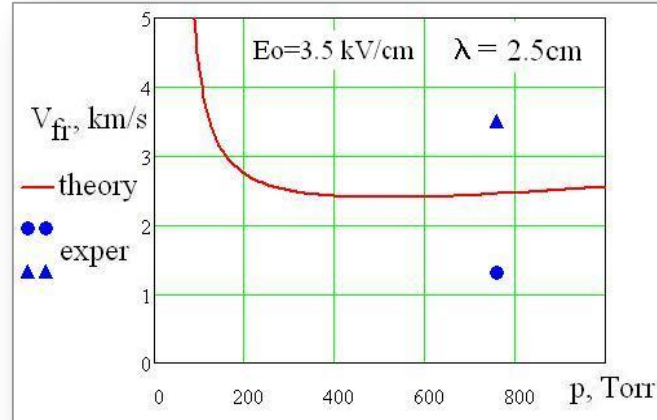


Fig.11.10. Comparison of the solution (11.30) with use of (11.37) for $n=2$ with the values measured in the case of the longitudinal streamer surface discharge at the wavelength 2.5cm.

Leaning against the developed scheme of calculation, it is possible to obtain estimations for other important parameters. In particular, using relations (11.29), (11.31) and (11.30) (or(11.36)), it is possible to obtain an expression for a streamer radius. The border between the attached and developed streamer discharge in (p-E) diagram can be obtained from a condition

$$\frac{E_{cr}}{E_0} = Q \ a, L \quad (11.38)$$

where $L = \lambda/4$ and $a=h$, defined by formulas (11.28) and (11.29). A comparison of theoretical dependences and measurements is carried out in **Fig.11.11**. A coincidence is also good.

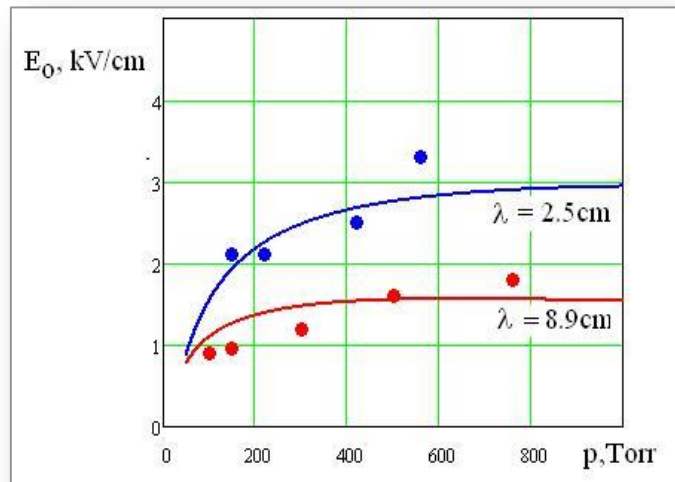


Fig.11.11. A border between the attached and developed forms of discharges. Theory - solid lines, points – measurement data

11.5. Determination of electrostatic effects influence on behavior of the surface MW discharge

All experiments executed under the program of the present Project are carried out at placing of dielectrics in the field of the quasi-optical EM beam, namely this situation is analyzed in the section 11.5a. However, the question of the surface discharges nature arises and in other typical cases, in particular, at occurrence of the streamer surface discharge on a surface of the radiating dielectric aerial. Section 11.5b is devoted to researches of this case.

11.5a. Influence of the induced surface charge on a streamer propagation at MW wave falling on a dielectric surface

As the reasons causing primary propagation of the discharge over a dielectric surface electrostatic effects and physical and chemical surface processes in the presence of the discharge were considered.

Experimental researches have shown, that the material sort of the dielectric does not influence properties of the surface discharge from what follows, that physical and chemical surface processes are not the factor defining primary propagation of a streamer over a surface.

In this connection a theoretical research of features of electromagnetic field distribution near a streamer in the presence of a dielectric layer has been undertaken.

The increase in electric field around a streamer head at the expense of inducing of charges and currents in the dielectric at a close arrangement of the streamer over a surface could be one of the reasons causing primary propagation of the streamer along a surface of the dielectric. For check of this factor importance an electrodynamic calculation has been carried out

This effect was investigated numerically in modeling statement (the streamer was simulated by a metal rod as it is shown in a **Fig.11.12**).

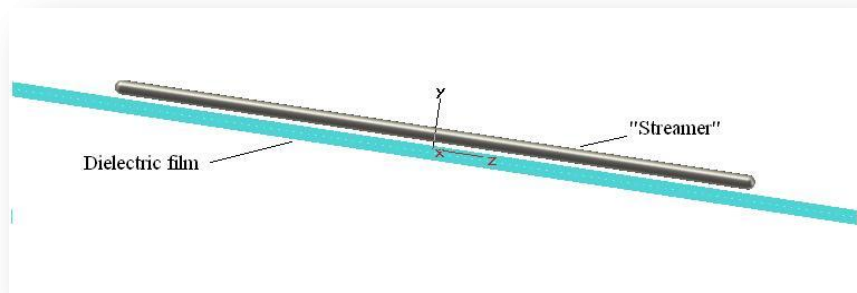


Fig.11.12. «Streamer» over a dielectric film

Calculations have shown that a field increase on the electrostatic effect really occurs even at a small thickness of a film. In **Fig.11.13** the field distribution in a vicinity of a head of the "streamer" located on a thick dielectric layer is shown. It is seen that the large field is concentrated in the area between a surface of a film and a "streamer" head.

The increase value strongly depends on a dielectric permeability of a film. As it is seen in **Fig.11.14** the amplitude increases considerably at a dielectric permeability ϵ value greater than 10 and limits to 2 at $\epsilon > 100$.

Since in experiments the streamer propagation along a surface was observed at $\epsilon = 2 \div 4$, and the increase in the field amplitude of a streamer head near a dielectric surface with a dielectric permeability $\epsilon \sim 2-4$ (typical values for used materials) does not exceed 10-15% for thick dielectric layers and is very small for thin films, so it is necessary to accept that the increase in a field amplitude in a streamer head in itself plays an essential role in the course of the discharge propagation along a dielectric surface. (It is in full agreement with results of observations and agrees with the conclusion made above that presence of a dielectric surface does not interfere in a breakdown process, but actively influences a streamer propagation along a dielectric surface).

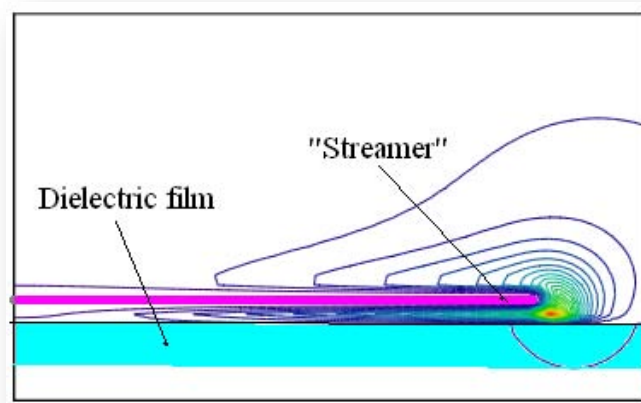


Fig.11.13. Electric field amplitude distribution in the vicinity of the "streamer" head place over a dielectric film

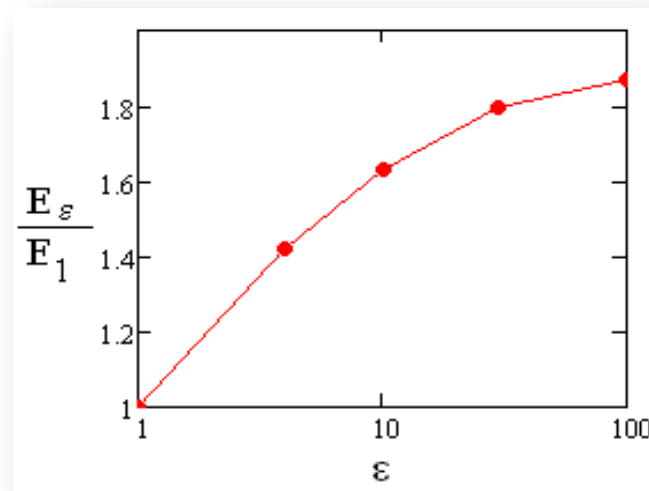


Fig.11.14. Electric field growth dependence in the vicinity of the "streamer" head placed on the dielectric surface with respect to its dielectric permeability

Probably, an influence of electrostatic effect is revealed not in the amplitude increase in the maximum, but in its displacement in the side of a dielectric. This displacement also defines primary development of a streamer along a surface.

In this connection more detailed calculations have been carried out.

At calculations the special attention has been given to the distribution of the electric field amplitude in vicinity of a head of the streamer located along a surface of a dielectric layer at a distance, much smaller its length and comparable with its diameter as it is observed in experiments. At calculations the streamer was simulated by ideally conducting thin cylinder. The problem statement is shown in **Fig.11.15**.

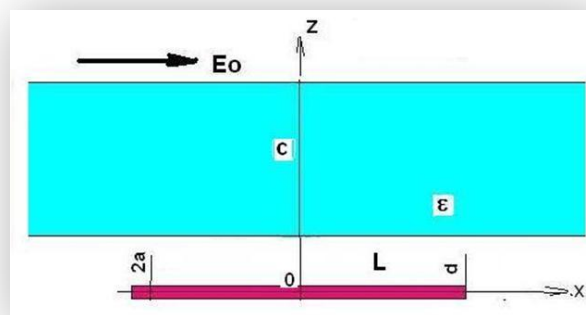


Fig.11.15. Problem statement about a distribution of electric field amplitude near the thin conductor located along a dielectric layer of a small thickness at a small distance from it

If the length of the cylinder is less than a half length of a radiation wave then the calculation can be carried out in the static approach, using the known solution for a potential of a point charge over a dielectric layer of a final thickness.

$$\phi(r, z) = \begin{cases} \frac{1}{\sqrt{r^2 + z^2}} + \int_0^\infty A_1(\kappa) J_0(\kappa r) \exp(-\kappa z) d\kappa, & z < d \\ \int_0^\infty B_1(\kappa) J_0(\kappa r) \exp(-\kappa z) d\kappa + \int_0^\infty B_2(\kappa) J_0(\kappa r) \exp(\kappa z) d\kappa, & d < z < d + c \\ \int_0^\infty A_2(\kappa) J_0(\kappa r) \exp(-\kappa z) d\kappa, & d + c < z \end{cases} \quad (11.39)$$

where

$$\begin{aligned} A_1(\kappa) &= \beta \frac{\exp(-2\kappa b) - \exp(-2\kappa d)}{1 - \beta^2 \exp(-2\kappa c)} \\ A_2(\kappa) &= \frac{1 - \beta^2}{1 - \beta^2 \exp(-2\kappa c)} \\ B_1(\kappa) &= \frac{1 - \beta}{1 - \beta^2 \exp(-2\kappa c)} \\ B_2(\kappa) &= \beta \frac{1 - \beta \exp(-2\kappa b)}{1 - \beta^2 \exp(-2\kappa c)} \\ \beta &= \frac{\varepsilon - 1}{\varepsilon + 1} \\ b &= c + d \end{aligned}$$

c – a thickness of the dielectric layer,

d – a distance between the conductor axis and the layer surface,

ε – a dielectric permeability of the layer.

Charge distribution in the conductor with a half length L and linear conductivity σ , located under the dielectric layer along the electric field E_0 , was determined with a help of a numerical solution of the integro-differential equation (11.40)

$$\frac{\partial}{\partial t} q(x, t) = \frac{\partial}{\partial x} \sigma(x) \frac{\partial}{\partial x} \int_{-L}^L q(x, t) \phi(\sqrt{x - x_1^2 + a^2}) dx_1 \quad (11.40)$$

a – is the conductor radius ($a < d$).

The steady solution obtained in the calculation has turned out to be close to the known analytical solution for a conductor in a static electric field in free space

$$q(x) = \begin{cases} \frac{E_0 x}{\ln \left(4 \frac{|L^2 - x^2| + a^2}{a^2} \right) - 1}, & |x| < L \\ 0, & |x| > L \end{cases} \quad (11.41)$$

In Fig.11.16 we compare both solutions.

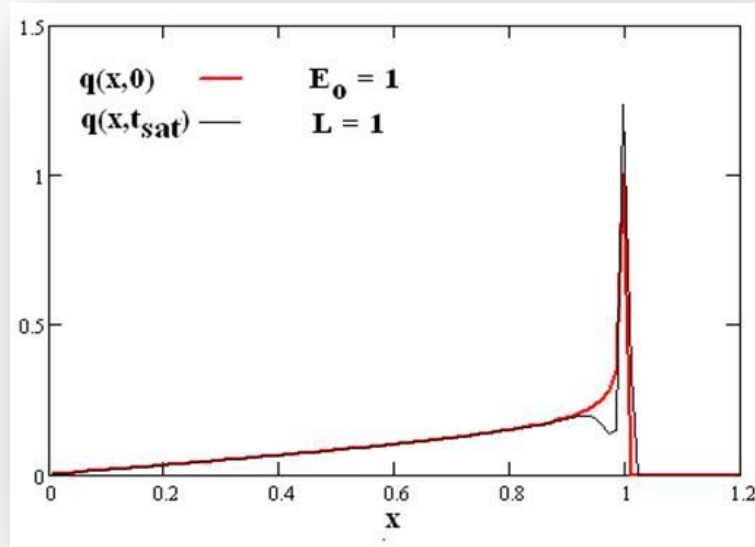


Fig.11.16. Charge distribution along a conductor of $2L$ in length in the field E_0 . Red curve – is the solution (11.41), black curve - is the solution of the equation (11.40)

The obtained distribution of a charge allows to calculate the electric field distribution by means of relations

$$\Phi_{x,z} = \int_{-L}^L q(x_1) \phi \sqrt{x-x_1^2+a^2}, z dx_1 \quad (11.42)$$

$$\vec{E} = -\nabla \Phi_{x,z} + \vec{E}_0 \quad (11.43)$$

The distributions of the electric field absolute value calculated in the static approach for various thickness and permeability of the layer are shown in Fig.11.17.

In **Fig.11.18** a dependence of the value characterizing displacement of the field maximum via a thickness and permeability of the field is represented. It can be seen, that the displacement is essential, if the thickness of the dielectric layer is greater than a distance from an axis of a streamer to a surface, and permeability $\epsilon > 2$.

At the length of the conductor (the streamer) close or equal to the half length of a wave for determination of the amplitude distribution of the electric field the calculations in electrodynamic approach on the basis of Maxwell equations are necessary. Such calculations have been carried out by means of program CST MW Suite Studio. In **Fig.11.18** the example of the electrodynamic calculation for a conductor of resonant length is represented. Calculation parameters are: wavelength of MW radiation $\lambda = 11.6\text{cm}$, $2L=5\text{cm}$, $2a=0.2\text{cm}$, $d=0.2\text{cm}$, a thickness of the dielectric $c=0.1\text{cm}$, $\epsilon = 4$. Wave of MW radiation propagates normally to the film surface (in **Fig.11.18** - from below upwards), the wave electric field is focused along the conductor.

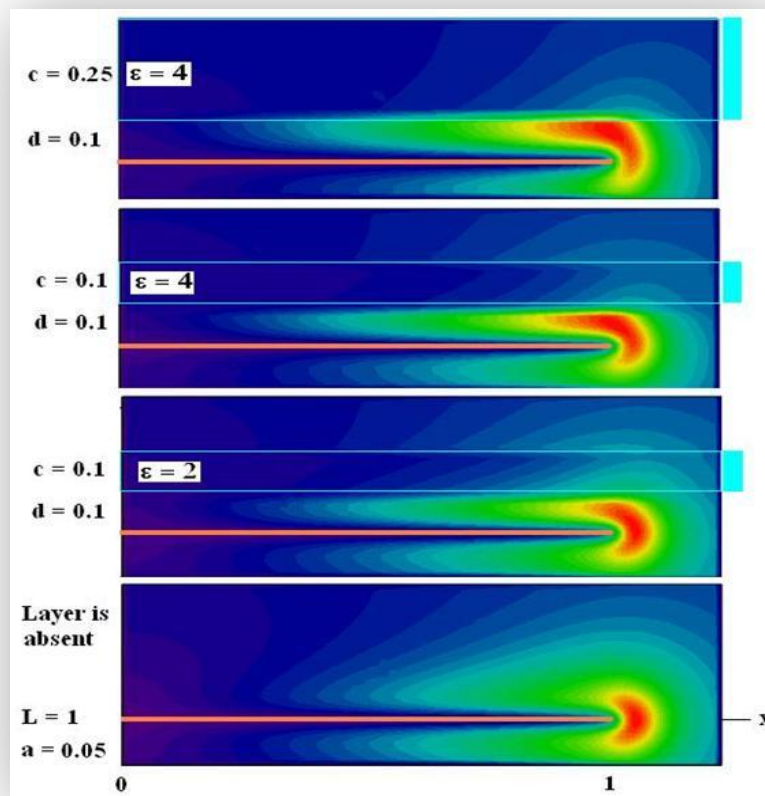


Fig.11.17. The distributions of the electric field absolute value calculated in the static approach for various thickness and permeability of the layer. Red color corresponds to the area of large values of the electric field absolute value.

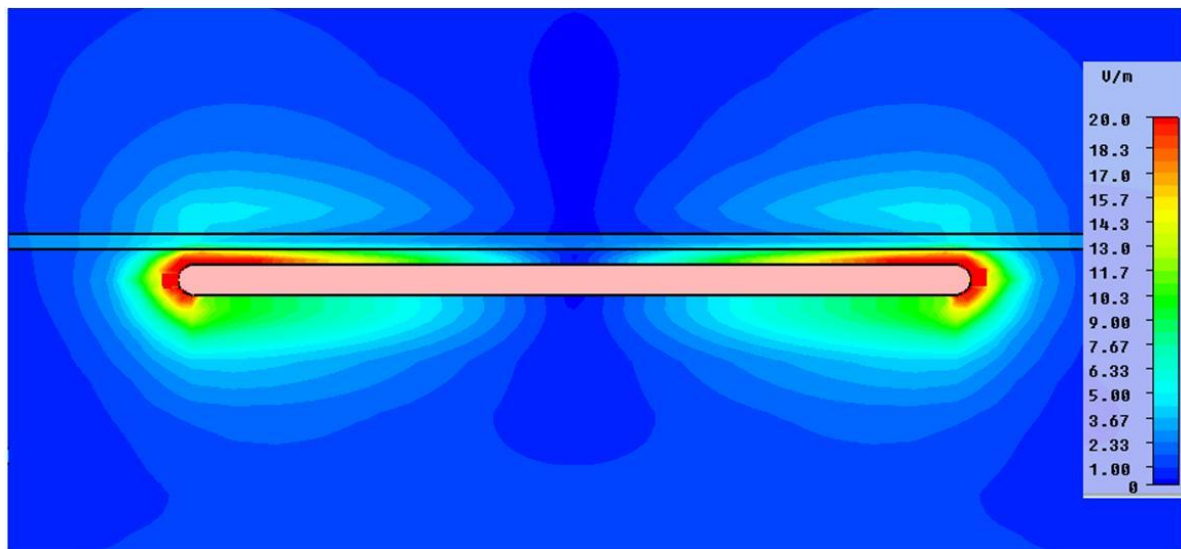


Fig.11.18. Distribution of the electric field amplitude round the conductor of resonant length located under a thin dielectric film with $\epsilon = 4$

The calculations executed both at electrostatic and at electrodynamic approaches, have shown, that presence of a dielectric layer displaces a maximum of the amplitude in the area of a streamer head to a surface (not changing essentially amplitudes in the maximum). In **Fig.11.19** a dependence of the value characterizing the displacement of the maximum of the field on a

thickness and permeability of the field is represented. It can be seen that the displacement is essential, if the thickness of the dielectric layer is greater than the distance from the axis of the streamer to the surface, and the permeability is $\epsilon > 2$.

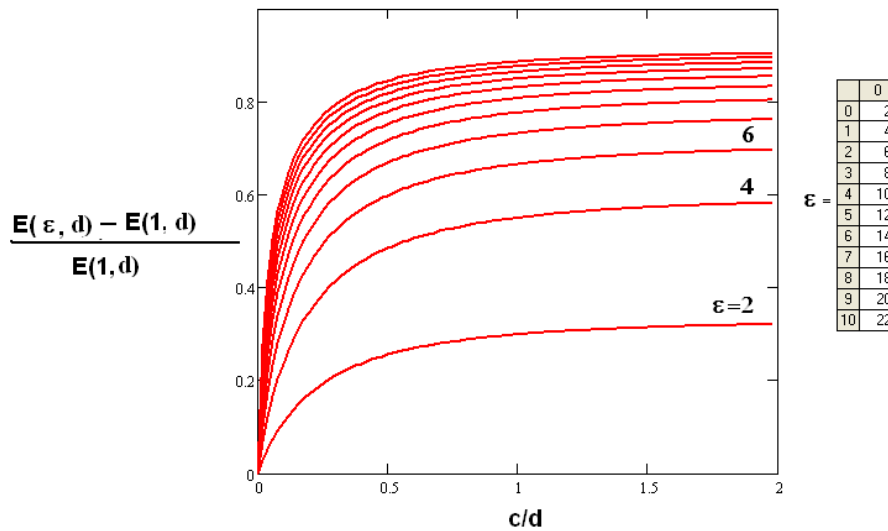


Fig.11.19. A dependence of the parameter characterizing a displacement of the electric field maximum at a head of the streamer towards a surface on a thickness and permeability of the layer

Executed earlier numerical modeling of initiated streamer discharge propagation in the volume (at absence of a surface) has shown, that the streamer develops in a direction of the maximum of the field amplitude defined by the sum of a primary field and a field of charges, created by currents in streamer channels, and maximal in the streamer head. The carried out research has shown that at presence of the dielectric the charges induced in the dielectric move a maximum of the electric field amplitude closer to the dielectric surface. Thereof the streamer, supporting the tendency to propagate in the direction of the field maximum, continuously slides over the surface. Since the arising asymmetry of the field distribution does not depend on the undercriticality degree then the propagation over a surface is observed in all area of subcritical discharges existence.

Thus, the electrodynamic interaction of a streamer with the dielectric is a principal cause of the streamer discharge propagation along a surface.

It is possible to state, that the electrostatic factor is defining also for DC surface discharges.

At the same time it is impossible to exclude some influence of the physical and chemical factors revealed on a dielectric surface at discharge propagation.

As the factor stimulating distribution along a surface, it is possible to consider an ionization of molecules of air adsorbed on a dielectric surface under the influence of deceleration UV radiation from the area of a streamer head where the electron temperature is sufficiently high.

An emission of electret electrons can be the possible factor of stimulation also. Dielectric polymeric materials are attributed to the electret category for which external influences are the reason of occurrence of the surface charges caused both by polarization, and electron emission. Electrets can emit up to 10^{10-12} electrons from 1 cm^2 of a surface. For electron emission from a surface of a dielectric film it can appear to be quite sufficient not only ultra-violet radiation, but also hot electrons and the ions reaching the surface in a process of ambipolar diffusion. Additional emission electrons from the surface accelerate a process of a streamer propagation, so far as the propagation occurs along the surface. The factor of the electret emission does not depend on a dielectric surface orientation concerning a radiation direction.

To a greater or lesser extent mentioned factors influence the propagation process. Their specific role as well as other unknown factors, can be revealed during more detailed and labor-consuming researches.

However, the most probable factor defining the primary propagation of the streamer discharge along a dielectric surface is the displacement of the electric field maximum concerning the streamer head towards the surface because of the influence of charges induced on the dielectric surface. The effect should affect at a thickness of a dielectric layer exceeding a distance between a streamer and a dielectric approximately equal to the streamer radius.

11.5b. Influence of the induced surface charge on a streamer propagation over a surface of radiating dielectric antenna

The analysis of experiments conditions with the streamer discharge on a surface of the dielectric aerial is carried out and numerical modeling of electromagnetic processes in a vicinity of the dielectric aerial in the presence of discharge "streamers" is carried out.

The analysis of experiments conditions with the streamer discharge on a surface of the dielectric aerial is carried out and numerical modeling of electromagnetic processes in a vicinity of the dielectric aerial in the presence of discharge "streamers" is carried out.

Earlier it has been shown¹⁴, that the principal cause of the propagation of the streamer discharge initiated on a surface of a dielectric, exclusively over this surface, is the electrodynamic interaction. This conclusion has been made on the basis of experiments and calculations with reference to the dielectrics, placed in freely propagating MW radiation. However, surface streamer discharges can appear in the conditions which essentially different from the described above. In particular, the strongly pronounced streamer discharge at air pressure of an atmospheric order is observed on a surface of the dielectric aerial used in experiences of V.M.Shibkov¹⁵. In this installation working at frequency of 12.5GHz, the dielectric aerial is the continuation of the waveguide excited on the basic mode H_{10} . Its transversal cross-section copies a profile of the waveguide internal section. In **Fig.11.20** one can see the simplified design of a unit accepted to calculation a waveguide-aerial, it corresponds to the real, and the calculated distributions of the electric field amplitude in various sections are shown. One can see that in the aerial the mode of a running wave is realized. The electric field amplitude in the dielectric aerial is maximal on a surface of its wide sides and is small on a surface of the narrow ones. Out of a body of the aerial the field exponentially quickly decreases with removal from the surface.

The discharge is initiated on a joint of a waveguide with an open surface of wide sides of the aerial where the electric field amplitude accepts the maximum value exceeding the critical, and in the form of thin discharge channels propagates along the aerial over its surface with a speed of some km/s. The typical kind of the discharge is shown in a photo of **Fig.11.21** borrowed from the reference [17]. The photo borders approximately coincide with a projection of a wide side of the aerial. The structure of conducting channels, forming on the aerial surface, is different from the structure formed on a surface of the dielectric in the field of a free electromagnetic wave (see **Fig.2**). If in case of the surface discharge in a free wave the streamers propagate mainly transversally a direction of a wave propagation along the electric field, moving ahead towards the radiation by formation of resonant conditions and branching¹⁶, the streamers on the aerial surface propagate almost rectilinearly in the direction of the wave propagation. The branching only increases a density of a longitudinal streamers network.

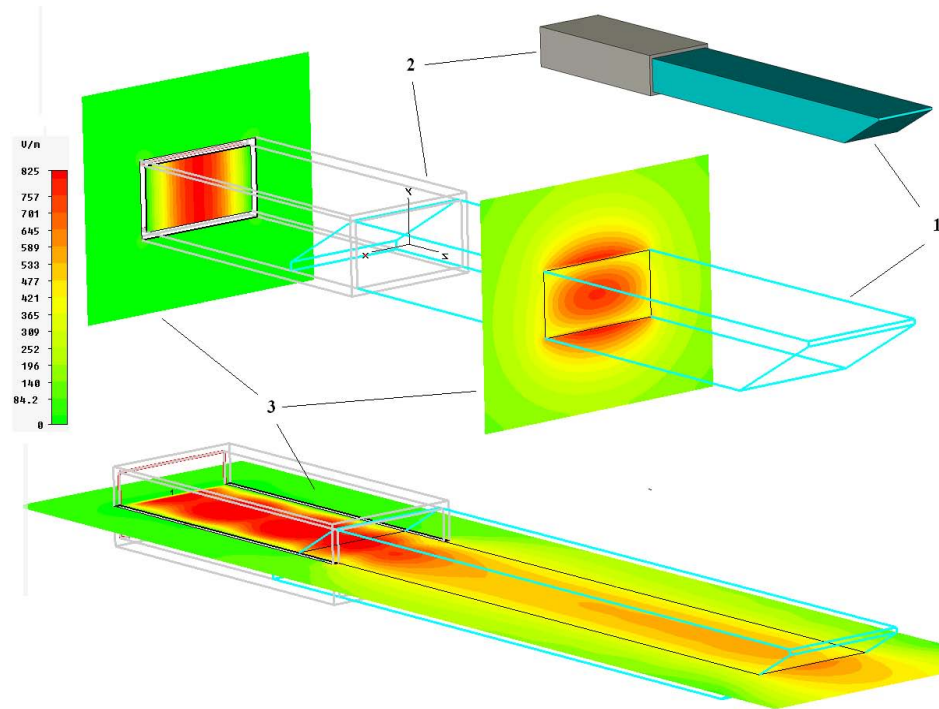


Fig. 11.20. The simplified design of the unit a wave guide-aerial accepted to calculation, corresponding to the real, and the calculated distributions of the electric field amplitude in various sections, 1 - the dielectric aerial, 2 - a waveguide, 3 - distributions of the electric field amplitude in various sections

In this connection the calculation of an electromagnetic field distribution in the system with the discharge has been carried out. The discharge was modeled by well conducting thin rods located over wide sides of the dielectric aerial as it is shown in **Fig.11.21**.

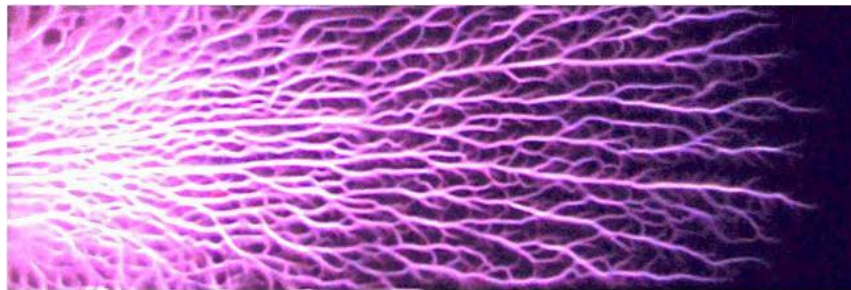


Fig.11.21. The streamer discharge on a surface of the dielectric antenna. Pulse duration is $10\mu\text{s}$, generator power - 70kW



Fig.11.22. Systems with a discharge model: 1 – a waveguide, 2 - antenna, 3 – thin rods simulating the streamer discharge.

The result of the calculation is shown in **Fig.11.23**. One can see that the discharge is the wave guide continuation, keeping the field structure (with shortening of the wavelength because of the dielectric influence).

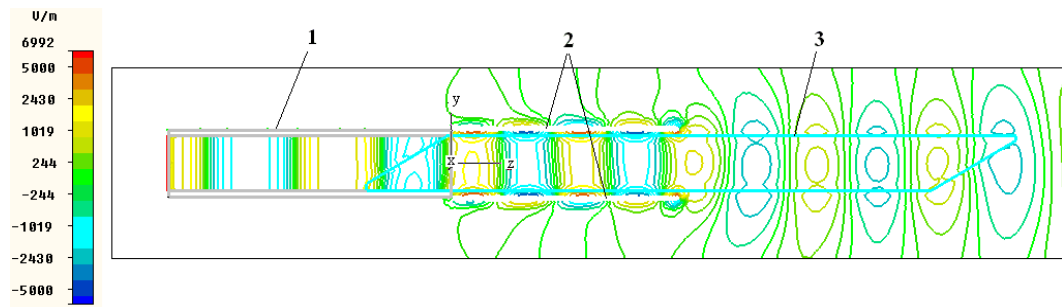


Fig. 11.23. Instant distribution of the electric field value in the system with the discharge model in a plane $x=0$: a 1-waveguide, 2-model of the streamer discharge, 3 - the aerial

Thus, the maximum of a field connected with a joint of a waveguide with a free surface of the aerial, a head of streamers bear with themselves almost independently of length of the propagation L that demonstrates **Fig.11.24**.

This first basic difference of the propagation mechanism: there is no necessity for the streamer system to be in an electrodynamic resonance with MW field during each moment of time for maintenance of the field over criticality on a head of streamers. On the other hand streamers cannot deviate from an aerial surface since the field is large only near the aerial.

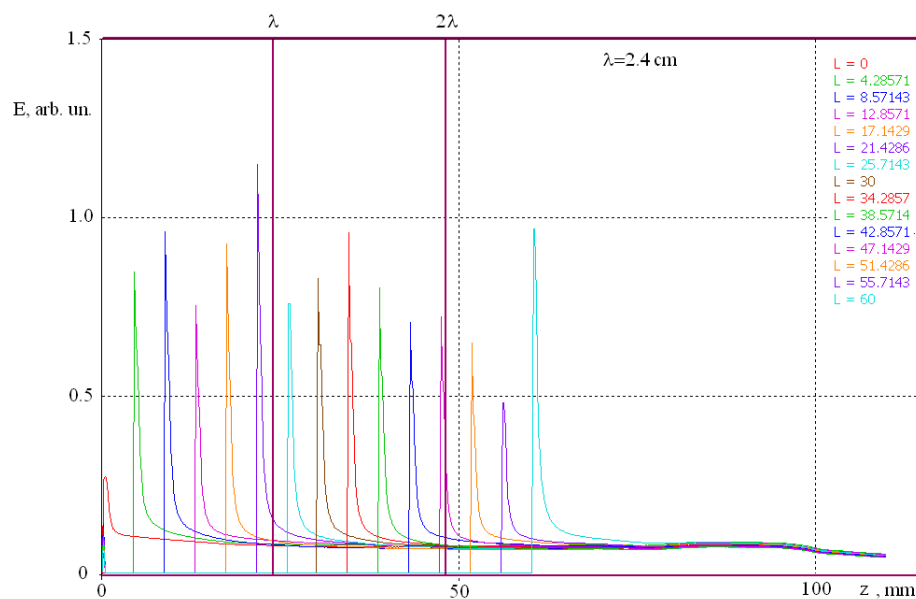


Fig. 11.24. A distribution of amplitude along an axis of one of the "streamers" at their various length L

However the factor essential for the surface discharges in the free field (displacement of a maximum of a field near the streamer head to the side of a dielectric), plays definite part also in the case of propagation over a surface of the dielectric aerial. In **Fig.11.25** one can see the distribution of the electric field amplitude near a head of one of the "streamers", obtained in the same calculation.

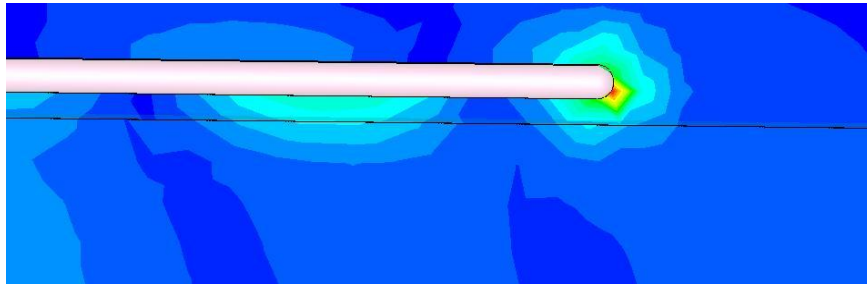


Fig.11.25. A distribution of the electric field amplitude near a head of one of the "streamers" in a plane $x=0$. A black line - a border of the dielectric aerial

The field maximum is displaced towards a surface of the dielectric aerial. The streamer, sprouting into the large field area, is compelled to slide along the surface.

Thus, also in this case a principal cause of the propagation of the initiated streamer discharge along a surface of a dielectric is the electrodynamic interaction of the streamer with the dielectric. Physical and chemical processes on a surface at presence of the streamer discharge play a supporting role.

It is possible to assume, that the electrostatic factor is defining also for DC surface discharges.

Results

During researches, on the type belonging to fundamental, executed in full agreement with the Plan of Works 3784p [EOAR 0777011] (the Attachment I), following results are obtained:

- ❖ the Electric discharge on a surface of a dielectric material (further dielectric) can be initiated in the field of MW radiation with an amplitude considerably smaller than the critical value.
- ❖ Presence of a dielectric in the field of MW radiation though brings a disturbance in a distribution of an electromagnetic field, does not influence a value of a breakdown amplitude of the electric field on a surface of the dielectric.
- ❖ The area of existence of purely surface MW discharge coincides with the area of existence of the volumetric subcritical discharge at placing of the initiator on a shady side of a dielectric plate and somewhat reduced from the side of an overcriticality border in with turn of a plate with the initiator towards the radiation.
- ❖ Presence of a dielectric does not influence the border dividing a subcritical and a deeply subcritical discharges.
- ❖ Presence of a dielectric does not bring a limitation on initiation possibility of the discharge in a subcritical field.
- ❖ The surface discharge is the streamer one and a transition into the diffusion form occurs at low pressure on the border of over criticality with the transition into the volumetric overcritical discharge.
- ❖ Streamers growth velocity of the surface discharge is the same as the streamers growth velocity in the volumetric discharge; a front speed of the streamer network of the surface discharge is somewhat higher (no more than by 2 times) than the front speed of the streamers network of the volumetric discharge category with other things being equal.
- ❖ Properties of the surface discharge remain on surfaces, as with positive, so with negative curvatures.
- ❖ The surface discharge is insensitive to a value of air humidity and presence of aerosols, both in motionless air, and in its high-speed stream.

- ❖ The increase in wettability of a surface of dielectrics after the influence of the streamer surface discharge is revealed.
- ❖ The surface discharge possesses the same ability to initiate a combustion of propane-air mixture also as the volumetric subcritical discharge.
- ❖ The surface discharge possesses smaller absorbing ability, than the volumetric one with other things being equal.
- ❖ Properties of the surface discharge are not sensitive to a dielectric material sort at a thickness of a layer greater than 100 microns.
- ❖ The principal cause of primary propagation of the streamer subcritical discharge on a surface of a dielectric is an influence of a dielectric layer on a distribution of an electromagnetic field in a vicinity of a streamer head is revealed.

Conclusions

The carried out research has advanced physics of the surface discharges and has revealed their properties, important for a number of applications.

Research of surface discharges is expedient for continuing with reference to development of the subcritical initiated discharges on dielectric threads and grids.

References

- ¹ Project ISTC #3784p (077011). Annual technical report, 2008 (1st year).
- ² L.P.Grachev, I.I.Esakov, K.V. Khodataev, V.V. Tsyplov High frequency air breakdown in presence of the metallic ball. //Fizika Plasmy, 1992, V.18, N.3, P. 411-415.
- ³ s.Popovic, L.Vuskovic, I.I.Esakov, L.P.Grachev and K.V.Khodataev. *Subcritical microwave streamer discharge at the surface of a polimer foil*. //Appl. Phys. Letters, v.81, Nu.11, pp.1964-1965.
- ⁴ Kirill V. Khodataev. *Microwave breakdown threshold at low and high pressure*. 47th AIAA Aerospace Sciences Meeting and Exhibition. 5-8 January 2009, Orlando, Florida. Paper AIAA 2009-1410.
- ⁵ Annual Technical Report on ISTC Project No. #3784p (077011), 2-nd year, (2009).
- ⁶ Final Technical Report on ISTC Project No. 2820p (027007). (2006)
- ⁷ Kirill V. Khodataev. *The physical basis of the high ability of the streamer CBQ discharge to a resonant absorption of CBQ radiation*. 42nd AIAA Aerospace Sciences Meeting 5-8 January 2004, Reno, NV. Paper AIAA-2004-0180
- ⁸ K.Khodataev. *Electrodynamics of the undercritical microwave discharges*. Proc. of 6th Workshop on Magnetoplasma Aerodynamics for Aerospace Applications. May 24-27, 2005. Institute of High Temperatures RAS, Moscow, Russia
- ⁹ I.I.Esakov, L.P.Grachev, K.V.Khodataev. *Parameters of plasma in the resonant channel microwave streamer discharge of high pressure*. //Proc. of The 2nd Workshop on Magnetoplasma Aerodynamics in Aerospace Applications. 5-7 April 2000, Moscow, Russia, pp. 154-162.
- ¹⁰ Kirill V. Khodataev. *Microwave breakdown threshold at low and high pressure*. 47th AIAA Aerospace Sciences Meeting and Exhibition. 5-8 January 2009, Orlando, Florida. Paper AIAA 2009-1410
- ¹¹ V.P.Korobeynikov. *Theory of a point explosion*. M. "Nauka". 1985. pp. 79, 87.
- ¹² A.D.MacDonald. *Microwave Breakdown in Gases*. New York. 1965.

- ¹³ L.P. Grachev, I.I. Esakov, G.I. Mishin, K.V. Khodataev. A front velocity of the stimulated MW discharge in the wave beam. //Zurnal Tekhnicheskoi Fiziki, 1995, V.65, N.5, P.21-30
- ¹⁴ Kirill V. Khodataev. *The Nature of Surface CB_Q Discharges*. 48th AIAA Aerospace Sciences Meeting and Exhibition. 4-8 January 2010, Orlando, Florida. Paper AIAA 2010-1378.
- ¹⁵ Valeriy M. Shibkov, Andrey F. Aleksandrov, Lidia V. Shibkova, Andrey A. Karachev, and Romans. Konstantinovskij. 48th AIAA Aerospace Sciences Meeting Including the New Horizons Forum and Aerospace Exposition. 4 - 7 January 2010, Orlando, Florida. Paper AIAA 2010-265
- ¹⁶ Kirill V. Khodataev. *Propagation of Microwave Subcritical Streamer Discharge Against Radiation by Branching and Looping*. 46th AIAA Aerospace Sciences Meeting 7-10 January 2008, Reno, NV, USA. Paper AIAA-2008-1405

Comments

No comments

Attachments

Attachment 1:	The list of the published papers and reports
1	Annual Technical Report on ISTC Project No. #3784p (077011), 1-st year, (2008).
2	Annual Technical Report on ISTC Project No. #3784p (077011), 2-nd year, (2009).
3	I. Esakov, L. P.Grachev, K.V. Khodataev, V. L. Bychkov, D.M.Van Wie. <i>Surface Discharge in a Microwave Beam</i> . IEEE Transactions on Plasma Science, Vol.35, No.6, December 2007. P.1658-1663
4	Konstantin V. Alexandrov, Eugeny B. Alfeev, Lev P. Grachev, Igor I Esakov, Alexei I. Khomenko, Kirill V. Khodataev, Vyacheclav A. Vinigradov. <i>Experimental investigation of a surface discharge in focused beam of microwave radiation at wavelength of 2.5cm and 8.9cm</i> . 47 th AIAA Aerospace Sciences Meeting and Exhibition. 5-8 January 2009, Orlando, Florida. Paper AIAA 2009-845.
5	Kirill V. Khodataev. <i>Microwave breakdown threshold at low and high pressure</i> . 47 th AIAA Aerospace Sciences Meeting and Exhibition. 5-8 January 2009, Orlando, Florida. Paper AIAA 2009-1410
6	Konstantin V. Alexandrov, Eugeny B. Alfeev, Lev P. Grachev, Igor I Esakov, Alexei I. Khomenko and Kirill V. Khodataev. <i>Experimental study of surface-volumetric discharge transition at various polarization and angle of falling of microwave radiation</i> . 48 th AIAA Aerospace Sciences Meeting and Exhibition. 4-8 January 2010, Orlando, Florida. Paper AIAA 2010-1193
7	Kirill V. Khodataev. <i>The Nature of Surface CB₄ Discharges</i> . 48th AIAA Aerospace Sciences Meeting and Exhibition. 4-8 January 2010, Orlando, Florida. Paper AIAA 2010-1378
Attachment 2:	The list of presentations at conferences and meetings
	The published reports 3-7 subsystems of the Appendix 1 have been presented at corresponding conferences and meetings
Attachment 3:	The information on patents and copyrights (to list and describe patents and copyrights which were or can be received as a result of project performance)
	Patents and copyrights are not present